Norwegian University of Life Sciences

Master's Thesis 2019 30 ECTS
REALTEK

Modeling and optimization of pyrolysis reactors

Carl Wilhelm Støren Aschjem
Energi og Miljøfysikk

Preface

I would like to thank my supervisor prof. Jorge Mario Marchetti and co-supervisor dr. Heidi Samuelsen Nygård at the department of REALTEK on NMBU for providing both academic and linguistic knowledge during my work with this thesis. Your constructive feedback has been motivating and resulted in a better thesis.

I am also thankful for my dad who has proof-read my thesis and my son for being patient during the writing process.

Carl Wilhelm Støren Aschjem

Ås, Mai 2019

Abstract

Biomass has been used as an energy source since ancient times but have the last centenary been replaced by fossil alternatives. This is causing of climate changes and emptying oil reservoirs. Concerns around the negative effects of fossil fuels has resulted in new interest around biomass and other renewable energy sources. In Norway it will be forbidden to use fossil fuels for heating purposes by 2020, this in combination with economic incentives for installation of renewable alternatives from the government has resulted in a growth of wood firing heat systems around the country. On farms, where the heat demand is highly dependent on season, big boilers are often installed to meet the demand at the most critical conditions like cold winters or when drying the agricultural yields.

The goal of this study is to investigate pyrolysis reactors as an alternative to wood burners. The pyrolysis process yields gas, pyrolysis oil, char and heat dependent on the operational conditions. This is done by using mathematical models to investigate the conditions that produces the most and least heat and analyze the dominant yields under these conditions.

Two mathematical models are investigated. One is describing a slow pyrolysis auger reactor and the other is describing a fast pyrolysis reactor where a hot inert gas is used to heat the feedstock. Both models are solving the heat equation with a kinetic scheme implemented. The kinetics are solved using a finite rate scheme for both models and the heat equation is simplified into 2 spatial dimensions for the slow pyrolysis auger model and 1 spatial dimension for the fast pyrolysis model.

Features added to the models which is uncommon for pyrolysis models are simulations of moist feedstock and a calculation of the time volatiles stay hot and keeps decomposing inside the reactor.

The fast pyrolysis reactor model predicts an overall low released heat which is decreasing with temperature. This reactor does not stand as a valid alternative to a wood burner.

The slow pyrolysis auger reactor predicts the lowest energy released pr. unit time at low temperatures where char and pyrolysis oil are the main yields. In the scenario where the highest energy released pr. unit time is preferred, gas is the main yield. The slow pyrolysis reactor has the highest time consumption and char yield on the cost of pyrolysis oil, but also a much higher amount of released heat pr. unit time as a result of the construction of the reactor. These findings tell that under low energy demand, pyrolysis oil and char can be produced and at high energy demands, gas is the main yield. This kind of reactor may be a valid option to wood burners.

For the highest possible oil yield, this work predicts that temperatures around 1100K, low cooldown time of volatiles and fast pyrolysis is the preferred configuration. The highest possible char yield is obtained by low temperatures, high volatile cooldown times and slow pyrolysis. For a high gas yield, high temperature, fast pyrolysis and long cooldown time of volatiles is preferred.

The effect of moist is shown to have a negligible effect on the yields at a dry feedstock basis, but a huge impact on the energy consumption. The cooldown time for volatiles are shown to be the main effect of pyrolysis oil and gas yields at temperatures above 800K. Longer cooldown times results in a higher amount of oil cracked into mainly gas and a small fraction of char.

Sammendrag

Biomasse har blitt brukt som energikilde siden oldtiden, men har det siste århundre blitt erstattet med fossile alternativer. Dette forårsaker klimaendringer og tømming av oljereservoar. Bekymringer knyttet til de negative effektene rundt bruk av fossile energikilder har resultert i ny interesse rundt biomasse og andre fornybare energikilder. I Norge vil det bli forbudt å bruke fossil olje som energikilde innen 2020, dette i kombinasjon med økonomiske insentiver for installasjon av fornybare alternativer fra staten har resultert i en vekst av vedfyringssystemer rundt om i landet. På gårdsbruk, hvor behovet for varme avhenger mye av sesong blir det ofte installert store fyringsanlegg for å dekke behovet de få ukene i året hvor det er kaldest eller et behov for å tørke avlinger.

Målet med denne oppgaven er å undersøke pyrolysereaktorer som et alternativ til vedfyringsanlegg. Pyrolyseprosessen gir gass, pyrolyseolje, kull og varme avhengig av driftsforholdene. Undersøkelsen gjøres ved å bruke matematiske modeller til å forutsi hvilke driftsbetingelser som gir mest og minst varme, samt hvilket produkt som produseres av prosessen under disse driftsbetingelsene.

To matematiske modeller er undersøkt. Den ene skal beskrive en langsom augerreaktor og den andre en hurtig pyrolysereaktor hvor en varm inert gass brukes for å varme biomassen. Begge modellene løser varmelikningen med en kinetisk algoritme implementert. Kinetikken løses ved bruk av en 'finite rate' fremgangsmåte og varmelikningen er forenklet til en dimensjon for den hurtige pyrolysereaktoren og to dimensjoner for den langsomme augerreaktoren.

Nye beregninger lagt til modellen som er uvanlig for pyrolysemodeller simulering av fuktig biomasse og tiden det fra gassene blir produsert i reaktoren til de blir kjølt ned.

Den raske reaktormodellen forutsier en generell lav frigjort varme som avtar med temperaturen. Denne reaktoren står ikke som et gyldig alternativ til en vedbrenner.

Den langsomme reaktormodellen forutsier mer frigjort varme pr. tidsenhet som stiger ved høyere driftstemperatur. Ved lav driftstemperatur er biokull og pyrolyseolje de mest produserte produktene. Ved høyere driftstemperatur vil mer varme frigjøres og en størst andel gass vil bli produsert. Disse funnene forteller at ved lavt behov for varme kan biokull og olje produseres. Dersom varmebehovet stiger kan gass produseres. Denne typen reaktor kan være et alternativ til en vedbrenner.

For høyest mulig utbytte av pyrolyseolje forutsier modellene at temperaturer rund 1100K, rask nedkjøling av de produserte gassene og rask pyrolyse som de beste driftsbetingelsene. For høyest mulig utbytte av biokull er lav temperatur, lang nedkjølingstid for produserte gasser og langsom pyrolyse foretrukket. Gass blir produsert i størst grad ved høye temperaturer, lang nedkjølingstid for de produserte gassene og rask pyrolyse.

Fukt i biomassen er vist å ikke påvirke hva som blir produsert nevneverdig, men det har en stor effekt på energiforbruket. Avkjølingstiden for de produserte gassene er vist å være den viktigste enkeltfaktoren for pyrolyseolje og gassutbytte ved temperaturer over 800K. Lengre nedkjølingstid resulterte i høyere nedbryting av pyrolyseolje til hovedsakelig gass og små mengder biokull.

Table of content

Preface 2

Abstract 3

Sammendrag 4

Table of figures 7

Nomenclature 9

1. Motivation 10

1.1 Aim of the study 10

2. Literature overview 12

2.1 Biomass 12

2.2 Pyrolysis of biomass: 14

2.2.1 Energy consumption and efficiency of reactors 14

2.3 Pyrolysis reactors 15

2.3.1 Fixed bed reactors 15

2.3.2 Fluidized bed reactors 17

2.3.3 Auger reactor 18

3. Kinetic models 20

3.1 Kinetic model 1 20

3.1.1 Mass conservation 21

3.1.2 Rate of changes 26

3.1.3 Heat of reaction 27

3.2 Kinetic model 2 28

3.2.1 Mass conservation 28

3.2.2 Heat of reaction 30

4. Reactor models 32

4.1 Reactor 1 32

4.1.1 Heat conduction 32

4.2 Reactor 2. 36

4.2.1 Internal nodes 36

4.3 The thermal values 38

4.3.1 Thermal conductivity 38

4.3.2 Heat capacity 38

4.3.3 Effective density 38

4.4 Energy analysis 38

4.4.1 Energy consumption 38

4.4.2 Released heat 39

5. Results 40
5.1 Model 1, kinetics 2. 42
5.1.1 Time consumption 42
5.1.2 Yields 43
5.1.3 Energy consumption: 45
5.1.4 Released heat: 47
5.2 Model 2, kinetics 2 50
5.2.1 Time consumption: 51
5.2.2 Yields 51
5.2.3 Energy consumption: 53
5.2.4 Released heat: 55
6. Discussion 58
6.1 Reactor model 1: 58
6.1.1 Time consumed and moist 58
6.1.2 Yields and energy 58
6.2 Reactor model 1, kinetics 2 59
6.2.1 Time consumed and moist 59
6.2.2 Yields and energy 59
6.3 Comparing the models 60
7. Conclusion 62
7.1 Further work 62
References 64
Appendix A, scheme for heat equation 68
A.1 Scheme for 1D heat equation 68
A.2 Scheme for 2D heat equation 69
A.3 Scheme for kinetic models. 73
Appendix B. Raw data results. 75
B.1 Results reactor model 1, kinetics 2 75
B.2 Results reactor model 2, kinetics 2 78

Table of figures

Fig. 2-1: Simplified representation of the fixed bed reactor. Based on the Pyrolysis GMBH reactor[28] 15
Fig. 2-2: A representation of a BFB reactor. Drawn using the software SketchUp [32] 17
Fig. 2-3: A representation of a CFB reactor. Drawn using the software SketchUp [32]. 18
Fig. 2-4: A representation of a SPA reactor. Drawn using the software SketchUp [32] 18
Fig. 2-5: PYREG's reactor scheme adapted from the German website eliquostulz[36] Pictures adapted from PYREGS's website [37]. (Picture reprinted with permission from PYREG GmbH[38]) 19
Fig. 2-6: Illustration of an FPA reactor. Drawn using the software SketchUp [32].....19
Fig. 3-1: Representation of kinetic model 1.....20
Fig. 3-2: Mass fraction as a function of temperature for different feedstocks. Adapted and reprinted with permission from Jankovic et. al[41].....21
Fig. 3-3: Sigmoid curve in the interval [-6,6]. Eq. (3.3) 22
Fig. 3-4: Water content as a function of temperature. Eq. (3.5) in the interval 298K to 423K with ρ^*_w =1 and 0.5. 23
Fig. 3-5: Representation of volume before and after some of the solid has decomposed into gas.....24
Fig. 3-6: Illustration of β's and ε's impact on the volatile volume. $V_{volatile}$ is the volume of the volatiles and V_{solid} is the volume if the solid mass. 26
Fig. 3-7: Illustration of the kinetic model 2.....28
Fig. 3-8: Illustration of eq. (3.34) at *time = t_0 + time volatiles spend inside reactor*. 30
Fig. 4-1: Representation of a single particle inside a fast pyrolysis reactor with a heat conducting medium. It is assumed that the heat will be conducted symmetric from all spatial directions towards the center of the particle. The lines a, b and c represent lines where the heat will be equally distributed.....32
Fig. 4-2: The center node receives 2 times the heat from node 1 due to the symmetry at the center 1<->0<->1. 34
Fig. 4-3: Illustration of surface node in the 1D heat equation. Completely insulated boundary with a heat flux to the surface node.....34
Fig. 4-4: Representation of the slow pyrolysis auger reactor and representation of assumed geometry for the feedstock inside the reactor.....36
Fig. 4-5: Cylindrical wedge cut in 10 and 100 along the length. 36
Fig. 4-6: Representation of surface point for the cut cylindrical wedge with two sides that receives heat from the surroundings. 37
Fig. 5-1: Seconds until 0.1% biomass left as a function of temperature in the range 700K to 1350K. Three different moist contents are plotted. The plot is for virgin feedstock and with no losses. 42
Fig. 5-2: Final yields as a % of dry feedstock weight at temperatures between 700 to 1350K. Cooldown time for the volatiles are set to 0.001s. 43
Fig. 5-3: Final yields as a % of dry feedstock weight at temperatures between 700 to 1350K. Cooldown time for the volatiles are set to 1.005s. 43
Fig. 5-4: Final yields as a % of dry feedstock weight at temperatures between 700 to 1350K. Cooldown time for the volatiles are set to 1.005s. Dashed line represents moist feedstock and solid line represents dry feedstock. 44
Fig. 5-5: Energy consumed as a function of temperature with three different moist values. Volatile cooldown time is set to 0.001s. The results are shown pr. cubic meter virgin feedstock. 45
Fig. 5-6: Comparison energy consumed by the pyrolysis process and energy needed to heat the feedstock.The plot shows energy consumed as a function of temperature. The cooldown time of volatiles is set to 0.001s and the moist is set to 0%. 46
Fig. 5-7: Energy consumed by the pyrolysis process as a function of temperature. The results are shown pr. cubic meter virgin feedstock. The cooldown time of volatiles is set to 0.001s and the moist is set to 0%. 46

Fig. 5-8: Energy consumed by the pyrolysis process as a function of temperature. The results are shown pr. cubic meter virgin feedstock. The cooldown time of volatiles is set to 0.001s and the moist is set to 25%. 47
Fig. 5-9: Released heat as a function of temperature with μt = 0.007/s and μo= 0.05. both factors contribute equal at 1200K. The feedstock feed is set to 0.019kg/s and moist = 0.....48
Fig. 5-10: Total consumed energy as a function of percent consumed energy of total energy in feedstock plotted against temperature. μt = 0.007/s and μo= 0.05, both factors contribute equal at 1200K. 48
Fig. 5-11: Total consumed energy pr. kg virgin feedstock plotted against temperature. μt = 0.007/s and μo= 0.05, both factors contribute equal at 1200K. 49
Fig. 5-12: Seconds until 0.1% biomass left as a function of temperature in the range 700K to 1350K. Three different moist contents are plotted. The plot is for virgin feedstock and with no losses.....51
Fig. 5-13: Final yields as a percent of dry feedstock weight at temperatures between 700 to 1350K. Cooldown time for the volatiles are set to 0.001s.....51
Fig. 5-14: Final yields as a % of dry feedstock weight at temperatures between 700 to 1350K. Cooldown time for the volatiles are set to 1.005s.....52
Fig. 5-15: Final yields as a % of dry feedstock weight at temperatures between 700 to 1350K. Cooldown time for the volatiles are set to 1.005s. Dashed line represents feedstock with 30% moist and solid line represents dry feedstock. 52
Fig. 5-16: Energy consumed as a function of temperature with three different moist values. The results are shown pr. cubic meter virgin feedstock. 53
Fig. 5-17: Energy consumed as a function of temperature. The moist is 0% and the results are shown pr. cubic meter virgin feedstock.....53
Fig. 5-18: Energy consumed by the pyrolysis process as a function of temperature. The results are shown pr. cubic meter virgin feedstock. 54
Fig. 5-19: Energy consumed by the pyrolysis process as a function of temperature. The results are shown pr. cubic meter virgin feedstock and with three different values of moist. 54
Fig. 5-20: Released heat pr. unit time as a function of temperature with μt = 0, 0.001 and 0.008 and μo = 6,5,0. The plot is describing energy released with a feedstock feed of 0.019kg/s dry feedstock. 55
Fig. 5-21: Released heat pr. unit time as a function of temperature with μt = 0, 0.001 and 0.008 and μo = 6,5 and 0. The plot is describing energy consumed pr. cubic meter dry feedstock with a feedstock feed of 0.019kg/s. 56
Fig. 5-22: Released heat pr. unit time as a function of temperature with μt = 0.001 and μo =5. Feeding rate is 0.019kg/s. The plot shows three different values for moist. 56

Nomenclature

A	Pre-exponential constant [s^{-1}]
C_p	Constant pressure heat capacity [kJ/kg*K]
$\overline{C_p}$	Effective constant pressure heat capacity [kJ/kg*K]
d	Diameter [m]
E	Activation energy [J/kg*K]
E_{heat}	Energy consumed by heating the feedstock [J]
E_{out}	Energy released by the process [J]
$E_{pyrolysis}$	Energy consumed by decomposition of the feedstock [J]
E_{total}	Total consumed energy [J]
h	Overall heat transfer coefficient [W/m^2*K]
k	Reaction rate
q	Rate of temperature change due to heat added/produced [K/s]
q'	Energy added to the control volume [J/m^3].
R	Universal gas constant [J/mol*K]
t	Time [s]
T	Temperature [K]
T_{inf}	Ambient temperature [K]
V	Volume [m^3]
X, Y, Z	Spatial directions []
x, y, z	Location in spatial grid []

Abbreviations

BFB	Bubbling Fluidized bed
CFB	Circulating fluidized bed
CHP	Combined heat and power
FPA	Fast pyrolysis auger
PPM	Parts Per Million
SPA	Slow pyrolysis auger

Superscripts

*	initial
out	Leaving the control volume

Greek letters

β	Volume factor []
γ	Arbitrary value calculated with moist feedstock
$\hat{\gamma}$	Arbitrary value corrected to dry mass.
ε	Porosity []
Δh	Heat of reaction [J/kg*K]
Δt	Length of time step [s]
$\Delta x, y$	Length of spatial step [m]
μ_o	Overall heat loss efficiency []
μ_t	Time dependent heat loss efficiency [s^{-1}]
ρ	Density [kg/m^3]
ρ'	Relative density [kg/m^3]
$\bar{\rho}$	Effective density [kg/m^3]
σ	Thermal conductivity [W/m*K]
σ'	Effective contact conductivity [W/m*K]
$\bar{\sigma}$	Effective thermal conductivity [W/m*K]

Subscripts

bulk	Bulk material
c	Char
c2	Secondary char reaction
end	Last step
f	Virgin feedstock
g	gas
g2	Secondary gas reaction
i	Components virgin feedstock, gas, pyrolysis oil, intermediate solid or char
is	Intermediate solid
j	Step j in Y direction
l	Step l in X direction
n	Step n in time
o	Pyrolysis oil
out	From outside the control volume
Pure solid	All matter is pure solid
reaction	From reaction
solids	All solid matter
tot	All matter
vap	Water vapor
vi	Time before volatiles gets cooled down
w	Liquid water
0	Initial

1. Motivation

Since the industrial revolution the global energy and fossil fuel consumption have been steadily increasing [1] on the cost of higher concentration of greenhouse gases in the atmosphere and decreasing oil reservoirs. According to the National Oceanic and Atmospheric administration, the CO_2 concentration has gone from *396 ppm* in 2014 to *406 ppm* in 2018[2]. An estimate done in 2018 predicts that the oil in most countries will be consumed within a 50 year period[3], this is an estimate with lots of assumptions and uncertainty, nevertheless it stresses that the oil reserves are limited. The consequences will be ever raising fossil fuel prices and the consensus in the climate-change resource community is that higher levels of greenhouse gases cause climate changes[4]. As a result, both the political and academic interest in renewable energy researches have been increasing the recent years.

Through a process called pyrolysis with biomass as feedstock four major components are obtained; pyrolysis oil, gas, biochar and heat. Some parts of the biochar are very stable forms of carbon and research has shown that it can stay in the soil for thousands of years without degrading[5]. Under certain conditions, biochar could also contribute positively to the agricultural yields[6] without any negative effects[7]. The gas, pyrolysis oil and heat are good renewable alternatives to fossil fuels.

Through the Paris agreement in 2015, Norway sat a goal to reduce the emissions by 40% in the land sector within 2030[8]. After the agreement, SINTEF made a report on how to reduce the agriculture emissions in Norway and concluded that if $10^6 m^3$ of agricultural and forestry waste was turned into char and spread on the soil, this alone would reduce the current emissions in the sector with just below 50%[9]. On a global scale, the measure can in theory reduce todays man made emission with 12%[10].

In Norway, there has been an increase in wood chip heating systems on farms the past years due to restrictions in use of fossil energy, it will be forbidden to use fossil oil for heating in 2020. Also, there are economic incentives from the government to invest in renewable heating solutions.[11]

The change in seasonal energy demand often result in big burners to meet the requirements under the most critical conditions, especially if there is need for heat to dry grains, hay or other products. These big burners will only be used at full capacity for a few weeks a year which not is an effective use of the installed facility.[12] Another option could be installation of a pyrolysis reactor. These reactors can be run on a variety of biomass and changes done to the operational conditions can possibly affect the output to meet the required energy demand or produce a certain product if the energy demand changes.

1.1 Aim of the study

The aim of this study is to construct a mathematical model of two pyrolysis reactors, a slow and a fast to investigate how different operational conditions affect the released heat and yields of the process. The effect of moist feedstock and cooldown time for the volatiles will also be investigated.

2. Literature overview

2.1 Biomass

Biomass is a collective term used for all living or recent living organic matter and is in theory solar energy converted into chemical energy through the photosynthesis process, just as fossil fuels. The main difference is the short carbon cycle. For biomass, the carbon cycle can last from less than a year up to a couple of hundred, for fossil fuels the cycle last for millions of years. If fossil fuels could be used sustainably in the same rate as it is generated this would also be a renewable resource, however, that is unfortunately not the case[13].

In the case of this study biomass from plants will be the matter of interest. Plants synthesizes CO_2 from the surrounding air into glucose and oxygen by the following reaction:

$$energy + \ 6CO_2 + 6H_2O \rightarrow C_6H_{12}O_6 + 6O_2 \quad (2.1)$$

Then by internal reformations into several other components. The three main components are cellulose, hemicellulose and lignin. Cellulose is molecules consisting of several thousand glucose molecules, hemicellulose and lignin is more complex and consist of a various amount of sugars and sugar acids. The structure and content of molecules in lignin and hemicellulose is strongly dependent on the species and growth conditions of the plant.[14]

$$Cellulose\colon \ (C_6H_{10}O_5)_n \quad (2.2)$$

Farm products, such as corn, grains and sugar beets have a high amount of cellulose and/or hemicellulose and are good for ethanol production. Plants with high amounts of oils such as rape seed, soybean, sunflower seed etc. are good for biodiesel production and plants with a high amount of lignin such as straw, husk, wood etc. are good for production of ethanol, bioliquid and gas.[15]

Glucose, cellulose and fat rich biomass are commonly used for human or animal food. Using such biomass for energy purposes would lead to less food for higher prices. This could cause problems, especially in development countries where the poverty is more widespread. Such biofuels are often categorized as a 1. generation biofuel. In this study, lignocellulose biomass is the biomass of interest, this does not directly compete with food reserves and are often considered as waste. The resultant biofuel is categorized as a 2. Generation biofuel.[16] Values for some biomasses are presented in Table 2-1 and 2-2

Table 2-1: Lignin, cellulose, hemicellulose and chemical characteristics of selected biomass. Adapted and reprinted with permission from IntechOpen[17]

Feedstock	Ligning(%)	Cellulose(%)	Hemicellulose(%)	Carbon(%)	Hydrogen(%)	Oxygen(%)	Ash(%)
Wood	25-30	35-50	20-30	51.6	6.3	41.5	1
Switchgrass	5-20	30-50	10-40	44.77	5.79	49.13	4.30
Barley Straw	14-15	31-34	24-29	45.7	6.1	38.2	6
Wheat Straw	15-20	33-40	20-25	48.5	5.5	39.0	4

Table 2-2: Higher heating value (HHV) and lower heating value (LHV) for some biomasses.

Feedstock	HHV [MJ/kg]	LHV [MJ/kg]	Ref.
Maple wood	20.0	18.36	Phyllis2[18]
Switchgrass	18-20	16-18	Phyllis2[18]
Barley Straw	18.15	17.4	Phyllis2[18]
Wheat Straw	18.2	17.72	Phyllis2[18]
Char	28.3	-	Atsonios et.al[19]

The LHV is describing the energy released when 1kg of dry feedstock is burned and the water that results from the reaction does not condense. The HHV includes the energy released when the water condenses.[13]

2.2 Pyrolysis of biomass:

Pyrolysis is a process where the feedstock is heated to about 700K or above without presence of an oxidizing agent. At these temperatures the biomass decomposes, and new components are formed. The main products of the process are solids, gas and pyrolysis oil. The yields and composition is dependent on several factors, such as feedstock, temperature, heating rate, particle size and more.[20]

Pyrolysis is typically categorized into three categories: Slow, fast and flash pyrolysis. The processes and some typical yields are categorized in Table 2-3.

Table 2-3: Typical values for the different pyrolysis processes. Adapted and reprinted with permission from IntechOpen[17]

Pyrolysis Process	Solid Residence time (s)	Heating Rate (K/s)	Particle Size (mm)	Temperature (K)	Product Yield (%)		
					Pyrolysis Oil	Char	Gas
Slow	450-500	0.1-1	5-50	800-1200	30	35	35
Fast	0.5-10	10-200	<1	1100-1500	50	20	30
Flash	<0.5	>1000	<0.2	1300-1570	75	12	13

Slow pyrolysis is pyrolysis where the feedstock is heated at a slow rate and usually to a temperature around 800 to 1200K. When using big particles in the reactor, this is accomplished inside the particle as the outer layer works as a heat insulator. This could also be accomplished by constructing the reactor in a way that heats the biomass slowly.[21] The main yield under this conditions is char[22]. Char or biochar may be the most ancient fuel used by mankind. Before the discovery of coal, this was used to heat and extract metals[15].

In fast pyrolysis, the biomass is heated rapidly, often to temperatures above the slow pyrolysis reaction. If the residence time of solids and volatiles are low, the main yield is oily liquids. As the temperatures raises the process favorizes gas over pyrolysis oil[22]. The earliest known use of this technique is recorded back to ancient Egyptian times where the oily residues were used to preserve boats[23].

Flash pyrolysis is a promising method for pyrolysis oil production. The pyrolysis oil yields can be as high as 75% [24]. The process can in short terms be explained by even faster heating rate than fast pyrolysis and shorter residence time of the feedstock.

2.2.1 Energy consumption and efficiency of reactors

In every process that converts energy from one form to another, there will be losses. For the pyrolysis process, losses can be categorized into three groups[25].

(i) Heat loss due to conduction and emission from the reactor walls.
(ii) Heat loss due to energy recycling from the hot yields.
(iii) Heat loss due to energy recycling from the heat conducting medium.

A last group can be added which is the energy consumed by reactions in the feedstock[26], however these losses will by the laws of thermodynamics either be released as heat inside the reactor or when the yields are used in the future.

In modern slow pyrolysis reactors, the heat lost to the surroundings are often utilized and used as a heat energy source[27]. For fast pyrolysis reactors the heat lost to the surroundings are considerate as waste[19]

Jaroenkhasemmeesuk et. al[25] did a technical review of a fixed bed pyrolysis system and found that the heat lost through (i) and (ii) was about 31.5% and the heat lost through (iii) was about 30.5%. The rest is stored

in the product yields. Further they observed that the temperature is highest where the heat transferring medium are inserted to the reactor and decreasing along the way. This is due to energy consumed inside the reactor.

2.3 Pyrolysis reactors

Various types of pyrolysis reactors have been constructed. Some are already being operated, and others are still in the test phase. Each reactor has different advantages and limitations which are listed in Table 2-4.

2.3.1 Fixed bed reactors

The fixed bed reactor can either be a reactor where the biomass is falling through a pipe with an inert gas flowing the opposite direction (countercurrent), or the biomass can be in a fixed position with the hot inert gas flowing through (concurrent). An example of a fixed bed pyrolysis reactor producer is the Swiss company 'Pyrolysis GMBH'. The reactor is countercurrent and according to the producer it has an approximate capacity of 100kg biomass per hour and the yields are about 50% char, 10% pyrolysis oil, 30% gas and 10% losses.[28]

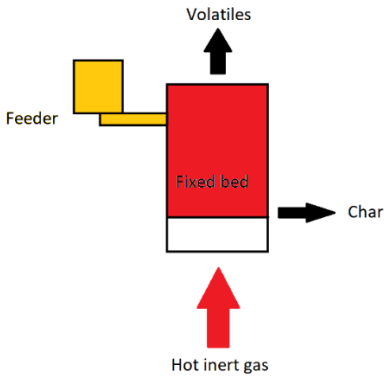

Fig. 2-1: Simplified representation of the fixed bed reactor. Based on the Pyrolysis GMBH reactor[28]

Table 2-4: Advantages, disadvantages and pyrolysis oil yields for different pyrolysis reactors. Adapted and reprinted with permission from IntechOpen[17]

Reactor type	Advantages	Limitations	Oil Yield
Fixed bed	- Simple design - Reliable - Biomass size independent	- Long solid residence time - Difficult to remove char	35-50%
Bubbling fluidized bed	- Simple design - Easy operation - Suitable for large scale	- Small particle size is needed	70-75%
Circulating fluidized bed	- Well understood technology - Good heat control - Large particle size can be used	- Small scale - Complex hydrodynamics - Fine char particles	70-75%
Rotating cone	- No carrier gas required - Less wear	- Complex process - Small particles - Small scale	65%
Vacuum	- Produces clean oil - Can process larger particles of 3-5 cm - No carrier gas required - Lower temperature required - Easier liquid condensation	- Slow process - Solid residence time to high - Require large scale equipment - Poor heat and mass transfer rate - Generates more water	35-50%
Ablative	- Inert gas is not required - Large particle size can be processed	- Reactor is costly - Low reaction rate	70%
Auger	- Compact - No carrier gas required - Lower process temperature	- Moving parts in hot zone - Heat transfer only suitable in small scale	30-50%
PyRos	- Compact and low cost - High heat transfer - Short gas residence time	- Complex design - High impurities in oil - High temperature required	70-75%
Plasma	- High energy density - High temperature - Very good temperature control	- High electrical power consumption - High operating cost - Small particles required	30-40%
Microwave	- Compact - High heating rate - Can handle big particles - High temperature	- High electrical power consumption - High operating cost	60-70%
Solar	- Use renewable energy - High heating rate	- High cost - Weather dependent	40-60%

2.3.2 Fluidized bed reactors

The fluidized bed reactor has much in common with the fixed bed reactor. The main difference is that a fluidizing medium is used inside the reactor for better heat transfer. The fluidizing medium can either consist of a fluid, like molten salt[29], or a small particle solid mass, like sand. Heat can be added through the walls of the reactor, with the fluidizing gas or through heating of the fluidizing medium.[20]

There are mainly two types of fluidized bed reactors.

(I) **Bubbling fluidized bed (BFB)**, where the char, oil and gas are removed from the fluid bed by the fluidizing gas. The char is removed with a cyclone and the gaseous components are threated in a condenser. This type of reactor needs very small feedstock particles to get the required heating rate[30]. A big scale commercial BFB reactor was running for a few years in West Lorne located in Canada and was operated by 'DynaMotive Energy Systems Corp'. The reactor is currently not running[31]. Atsonios et.al[19] did an energy balance study on a BFB reactor systems. They concluded that only 0.5% of the total energy in the feedstock was lost to the surroundings.

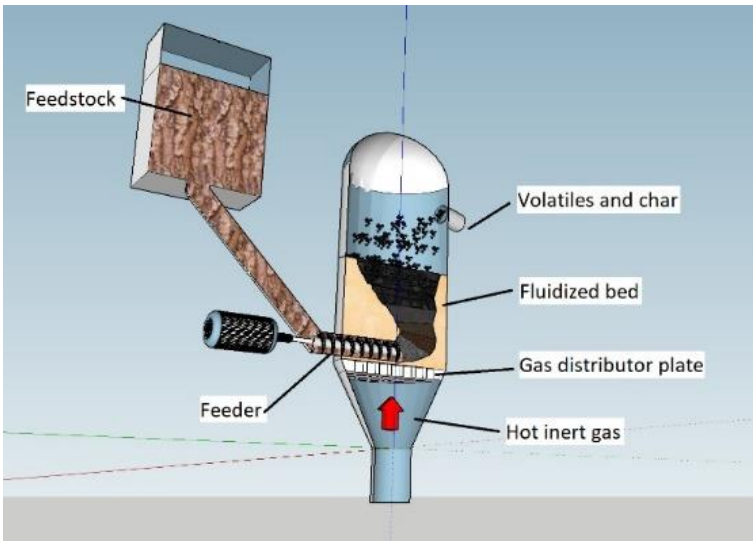

Fig. 2-2: A representation of a BFB reactor. Drawn using the software SketchUp [32]

(II) **Circulating fluidized bed (CFB)**, where the gas and oil is removed by the fluidizing gas and the char is removed by removal of bed medium. When the bed medium is removed, the char and fluidizing medium needs to be separated. This is often solved by combustion of the char, which heats the fluidizing medium and the heated fluidized medium is then re-added to the reactor along with fresh biomass. An example of a big scale CFB reactor is the Joensuu CHP (Combined Heat and Power) plant located in Finland. The reactor is manufactured by Valmet[33] and operated by Fortum[34].

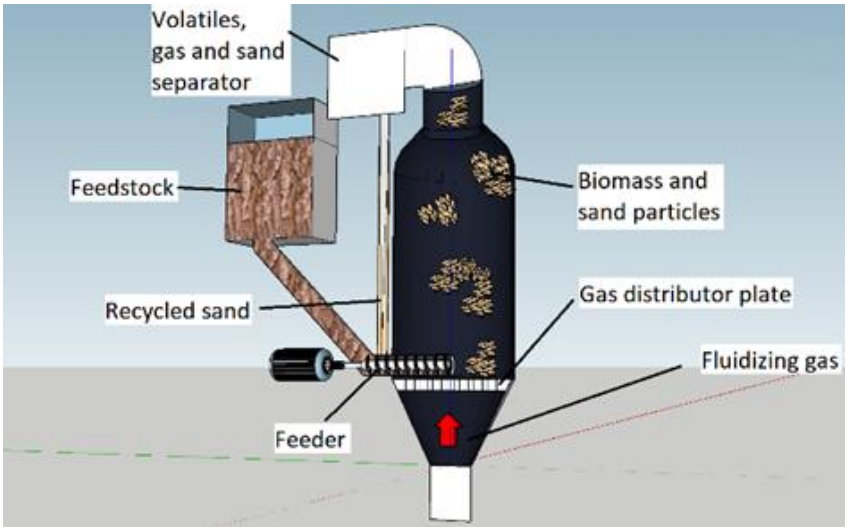

Fig. 2-3: A representation of a CFB reactor. Drawn using the software SketchUp [32].

2.3.3 Auger reactor

This type of reactor differs from the previous ones, instead of a gas as the transporter of solids, one or more augers are used. The biomass is fed into a heated pipe without any oxidizing medium and screwed through. The heat is conducted from the pipe to the biomass. There are two types of such reactors.

(I) **Slow pyrolysis auger reactor (SPA)**, which uses pure biomass in the auger. These reactors don't utilize the pyrolysis oil and burns it in the gas phase. The yields are heat energy and char. An example of a manufacturer is the German company Biomacon. One such reactor is operated by the Norwegian municipality Sandnes[35]. According to Gjerseth[27], director for environment and renovation in Sandnes municipality, the reactor has an output of 50-100kW and has a yield of 20 %wt. char. The feedstock is in the reactor for about 2 hours with operational temperature in the range 800K-1000K. The char yield is stated to be 13.8kg/hour at full capacity.

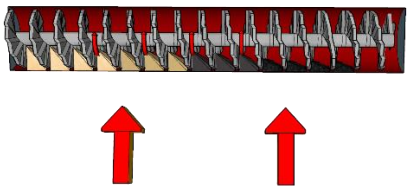

Fig. 2-4: A representation of a SPA reactor. Drawn using the software SketchUp [32]

Another manufacturer of a SPA reactor is the German company PYREG. A representation of their reactor system is shown in Fig. 2-5.

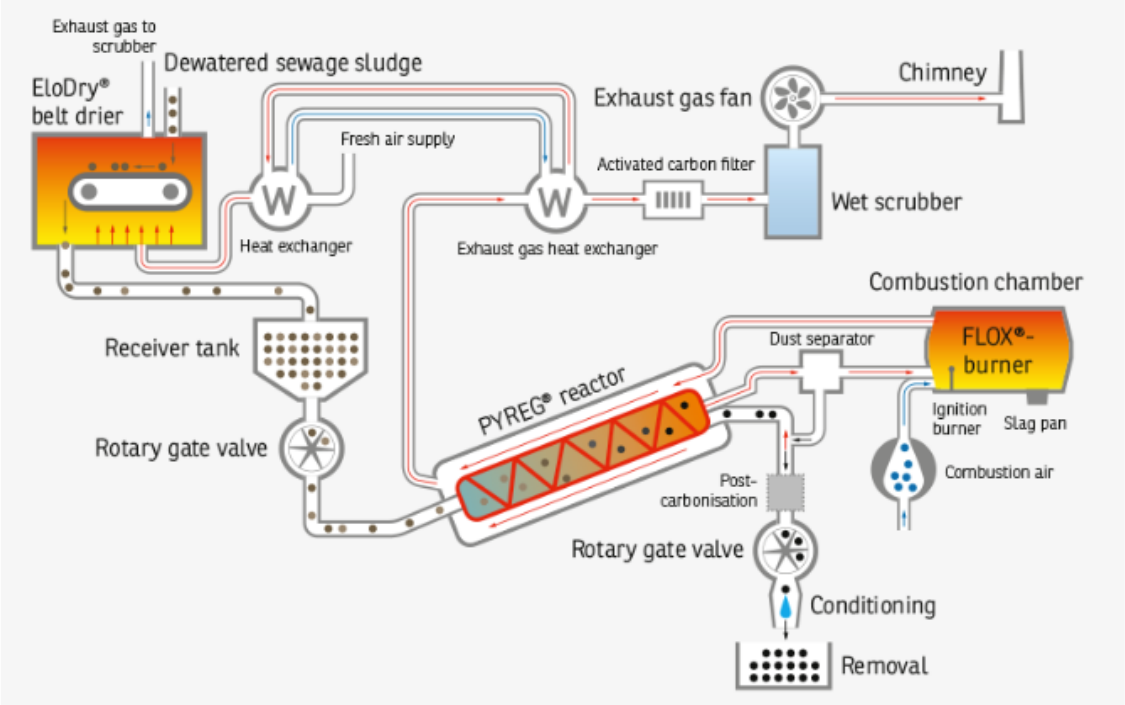

Fig. 2-5: PYREG's reactor scheme adapted from the German website eliquostulz[36] Pictures adapted from PYREGS's website [37]. (Picture reprinted with permission from PYREG GmbH[38])

(II) **Fast/medium pyrolysis auger reactor (FPA)**, which uses a solid inside the auger as an extra heat conductor/carrier. A manufacture of such a reactor is the Canadian company ABRI-Tech Inc. A representation is shown in Fig. 2-6.

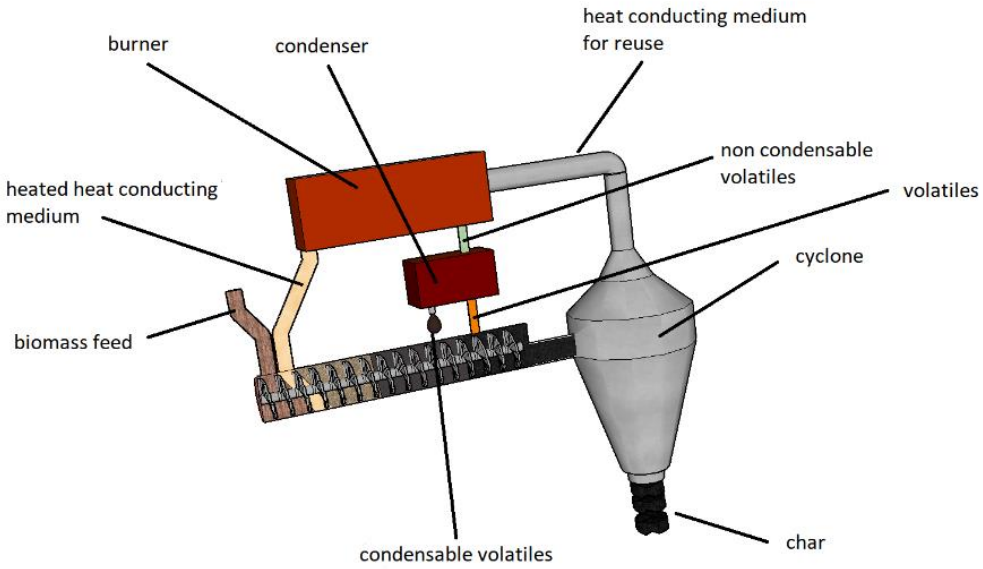

Fig. 2-6: Illustration of an FPA reactor. Drawn using the software SketchUp [32]

3. Kinetic models

There have been developed various kinetic models for describing the pyrolysis process. The models are classified into two categories. Finite rate and infinite rate kinetics. Infinite rate models assume that the decomposition occurs at a fixed temperature. Finite rate models use some form of reaction function. The 1st order Arrhenius reaction is mostly used[39]. The models used in this work are inspired from Park et. al[39] There are two models presented in this work. The first model is presented to show the basics and the second model will be used to produce the results.

The modifications done to Park's model are as follows:

(I) A simplified scheme for computing moist wood is added. This is done through a sigmoid curve fitted to experimental data collected from the literature.

(II) Internal pressure gradients are neglected. A simplified volume approach is used to calculate volatiles inside the feedstock.

(III) Radiative and convective losses are neglected. The losses is calculated in Park's model for the purpose of finding the pyrolysis temperature [39]. In this work energy and yields are the variables of interest.

(IV) For the kinetic model 2, the time volatiles stay inside the reactor is added. In most literature this variable has great impact on the yields and should be considered.[40]

3.1 Kinetic model 1.

Kinetics are described as a three-way parallel finite rate reaction. The feedstock decomposes into three products. Gas, pyrolysis oil and char. The reactions are in a competition where the temperature at a given time can favorize one reaction over another.

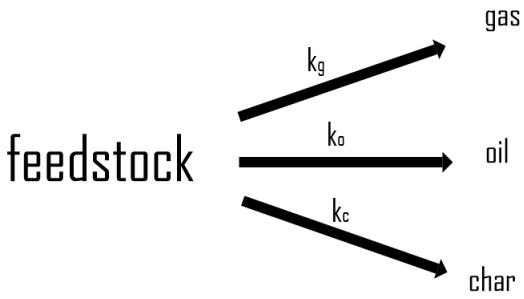

Fig. 3-1: Representation of kinetic model 1.

The reaction rate k_i is assumed to follow a 1st order Arrhenius type reaction.

$$k_i = Ae^{\frac{-E}{RT}}\rho'_f \tag{3.1}$$

Where *i* = [*gas (g), pyrolysis oil (o), char (c)*]. A is the pre-exponential constant, E is the activation energy, R is the universal gas constant, T is the temperature and ρ'_f is the relative density of the virgin feedstock. The density is in this model the relative density inside the control volume, calculated by eq. (3.2).

$$\rho'_i = \ fraction\ of\ component\ i * \ \rho_{actual\ density\ for\ i} \tag{3.2}$$

ρ'_i is the relative density and ρ is the actual density of the component.

3.1.1 Mass conservation

3.1.1.1 Moist

The moist will evaporate gradually until about 372K. The evaporation of water will be approximated as a function of temperature. This function will be constructed using values from Jankovic et. al[41].

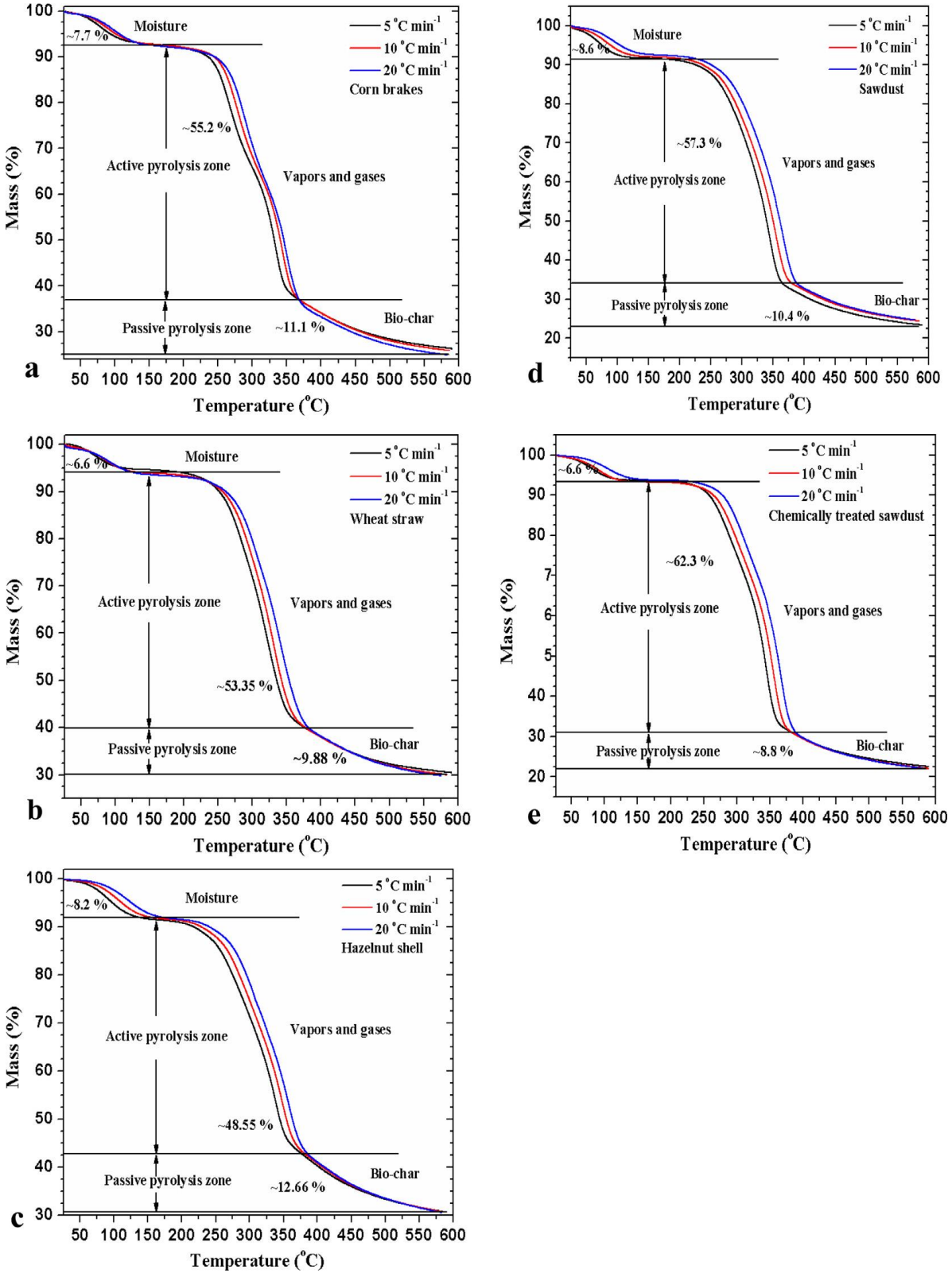

Fig. 3-2: Mass fraction as a function of temperature for different feedstocks. Adapted and reprinted with permission from Jankovic et. al[41].

The plots in Fig. 3-2 describe the fraction of solid mass as a function of temperature in the feedstock. The feedstock was heated using hot nitrogen gas. The particle weight in this experiment was in the range of 5.35 mg to 5.80 mg. The three plotted horizontal lines represents different heating rates.[41]

The curve of vaporization is indicated in the upper left corner in each subplot of Fig. 3-2. In this model the behavior is approximated using an inverse sigmoid curve, which is commonly used to describe natural phenomena[42]. The equation for the curve is shown in eq. (3.3).

$$-S(x) = \frac{-1}{1 + e^{-x}} \tag{3.3}$$

Where *S* is the value of the function and *x* is the variable of the function.

A plot of the sigmoid curve in the interval [-6,6] is represented in Fig. 3-3.

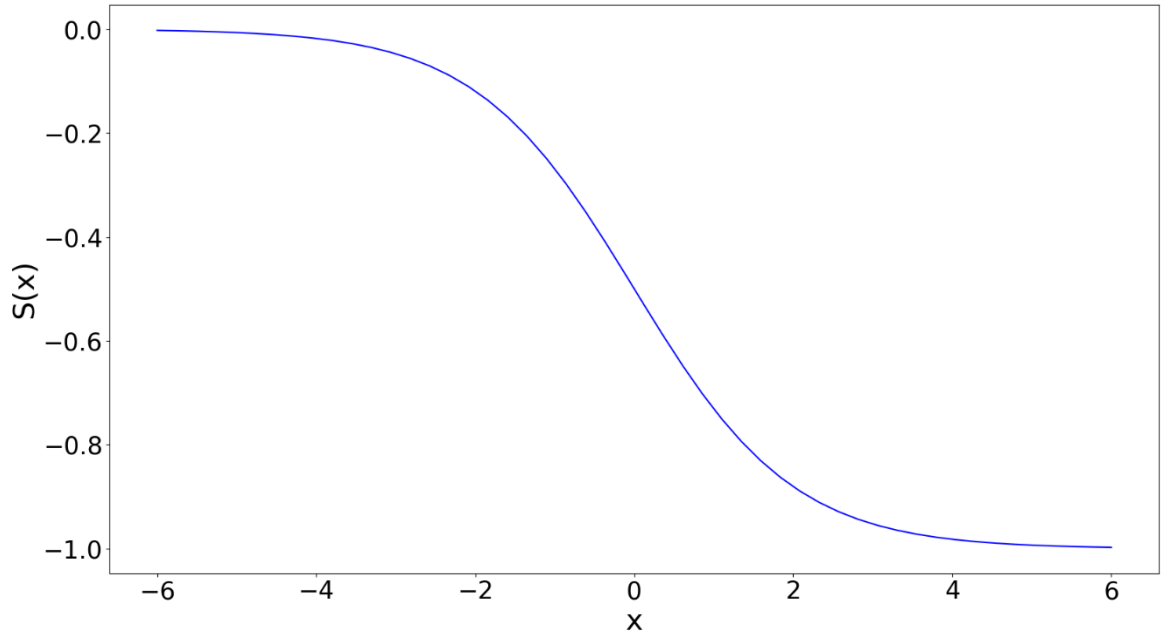

Fig. 3-3: Sigmoid curve in the interval [-6,6]. Eq. (3.3)

The sigmoid curve needs to be fitted to the values in Fig. 3-2. As shown in Fig. 3-3, the initial values for this curve is S(-6) = 0 and S(6) = -1. The initial range is 12. The range of vaporization is assumed to be 125K, from 298K to 423K. This is solved by multiplying the *x* variable in eq. (3.3) by 12/125.

The next manipulation to the equation is to set the midpoint of the curve. The initial midpoint is at S(0) = -0.5. The midpoint in the vaporization curve is assumed to be at 363K. This is solved by adding the midpoint value to the *x* variable. The complete equation is shown in eq. (3.4).

$$S(x) = \left(\frac{-1}{1 + e^{-(x-363)*{}^{12}/_{125}}}\right) \tag{3.4}$$

The range of S(*x*) in eq. (3.4) is from 0 to -1. By adding 1 to the equation the range becomes 1 to 0. Then, by multiplying the whole equation by the initial water content the final solution is obtained. Shown in eq. (3.5).

$$\rho'_w(T) = \left(\frac{-\rho_w^*}{1 + e^{-(T-363)*{}^{12}/_{125}}}\right) + \rho_w^* \tag{3.5}$$

Where ρ_w^* is the initial relative water density and ρ'_w is the relative water density at temperature *T* in K.

At two different water contents the following approximation is obtained.

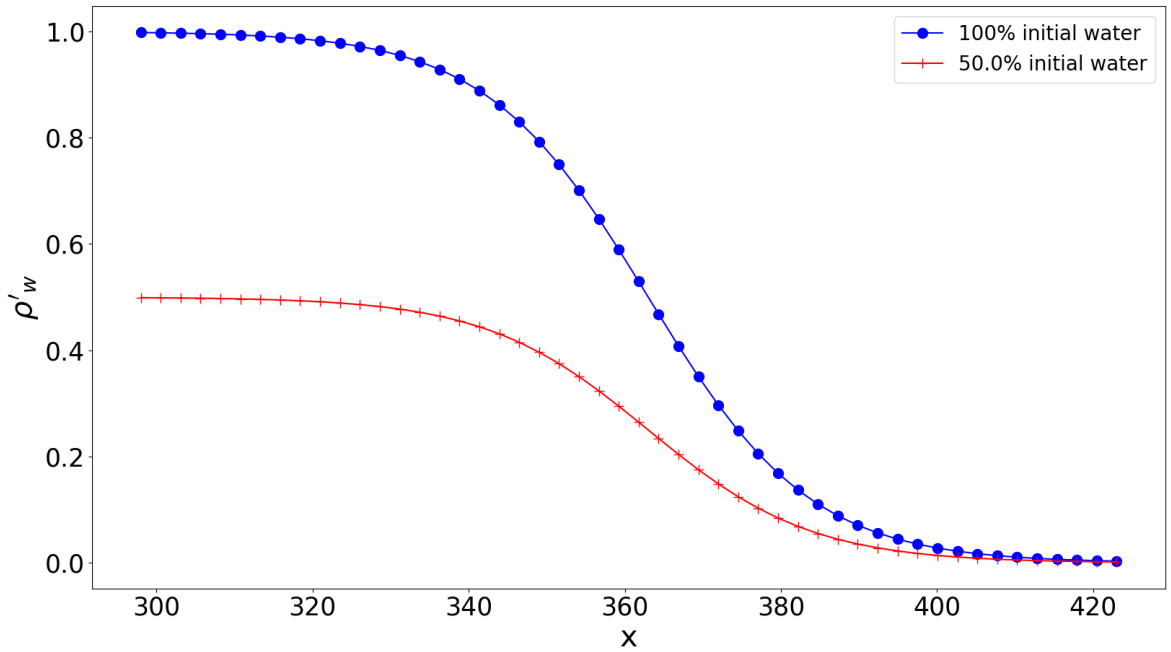

Fig. 3-4: Water content as a function of temperature. Eq. (3.5) in the interval 298K to 423K with ρ^*_w =1 and 0.5.

To convert the function from temperature domain to time domain, the functions derivative with respect to time is found.

$$\frac{\partial \rho'_w}{\partial t} = \frac{\partial \rho'_w(T(t))}{\partial t} = -\left(\frac{542.72e^{(T(t))*0.096} * \frac{\partial T(t)}{\partial t}}{(5653.33 + e^{(T(t))*0.096})^2}\right)\rho_w^* \tag{3.6}$$

In the case of this model, the heat equation is solved for the next time step before the kinetics. The notation for rate of change is shown in eq. (3.7).

$$\frac{\partial \rho'_w}{\partial t} = -k_w \rho_w^* \tag{3.7}$$

When calculating with moist feedstock, all the values will be from the virgin feedstock. Since some of the feedstock is water, the yields will fall. The equation to correct to dry mass is presented in eq. (3.8)

$$\hat{\gamma} = \frac{\gamma}{1 - \rho_w^*} \tag{3.8}$$

Where γ is an arbitrary value calculated with moist feedstock and $\hat{\gamma}$ is the same value corrected to dry mass.

3.1.1.2 Solid mass

For the solids, mass change per unit time is dependent on the pyrolysis reaction.

$$\text{Virgin feedstock:} \quad \frac{\partial \rho'_f}{\partial t} = -(k_o + k_g + k_c)\rho'_f \tag{3.9}$$

$$\text{Char:} \quad \frac{\partial \rho'_c}{\partial t} = k_c \rho'_f \tag{3.10}$$

$$\text{Water:} \quad \frac{\partial \rho'_w}{\partial t} = -k_w \rho_w^* \tag{3.11}$$

Where the subscript *f* describes the virgin feedstock. Virgin feedstock decomposes into pyrolysis oil, gas and char, this makes a negative change of mass pr. time. The mass of char is increasing with time. The subscript *w* describes liquid water and is decreasing with time.

3.1.1.3 Volatiles

The volatiles will be produced from a solid mass. The volume of a gas is much greater than the volume of a solid. To estimate the amount of gas inside the feedstock a volume approach is used.

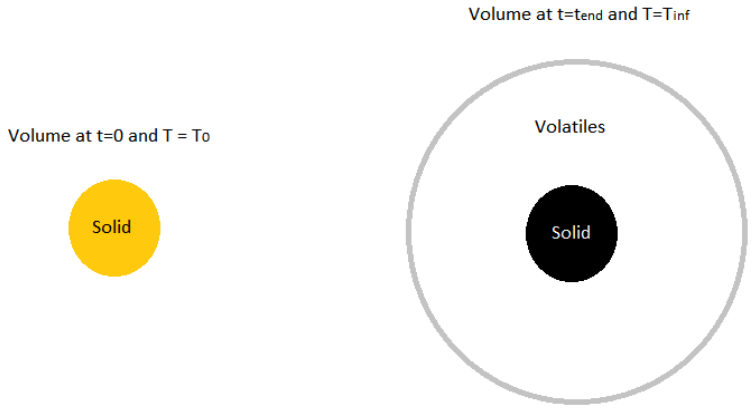

Fig. 3-5: Representation of volume before and after some of the solid has decomposed into gas.

For this purpose, two variables are introduced. *β* which is the volume factor. This factor ranges from 1, when all the feedstock is in solid phase and upwards to the value $\rho_{pure\ solid}/\rho_{pure\ gas}$ when all the feedstock is in a gaseous phase. The volume factor is described in chapter 3.1.1.3.1.

The other variable is *ε*. This is the porosity of the solid. The porosity is describing how much of the solid that is pores. Pores are empty spaces inside the solid where gas can exist. The porosity for a whole solid is described in chapter 3.1.1.3.2.

3.1.1.3.1 The volume factor

The volume factor is found by using conservation of mass and the relationship between weight, volume and density. Total mass of a body consisting of several parts are the sum of each individual part.

$$m_{0\ (pure\ solid)} = \sum m_i = m_{solids} + m_{volatiles} \tag{3.12}$$

Where m_0 is the initial mass, m_{solids} is the mass of all solid matter and $m_{volatiles}$ is the mass of all volatile matter. Volume can be described as an equation of mass and density.

$$V = m/\rho \tag{3.13}$$

By assuming the volumes don't mix, the total volume is the sum of each part.

$$V = V_{solids} + V_{volatiles} \tag{3.14}$$

The initial volume will consist of the raw feedstock and are purely a solid. To obtain a dimensionless factor, eq. (3.14) is divided by the initial volume.

$$1 = \frac{V_{solids}}{V_{pure\ solid}} + \frac{V_{volatiles}}{V_{pure\ solid}} \tag{3.15}$$

By conservation of mass (eq. 3.12) the fraction of solids and volatiles can be described as their independent mass divided by the initial mass.

$$volatiles\ wt\% = \frac{m_{volatiles}}{m_{0\ (pure\ solid)}} \quad , \quad solids\ wt\% = \frac{m_{solids}}{m_{0\ (pure\ solid)}} \tag{3.16}$$

Rearranging and combining eq. (3.13), (3.15) and (3.16) yield:

$$\beta = \frac{V_{tot}}{m_0} * \rho_0 = \left(\frac{\rho'_{solids}}{\rho_{solids}} + \frac{\rho'_{volatiles}}{\rho_{volatilies}}\right) * \rho_0 \tag{3.17}$$

It's assumed that the solids don't change density under the process, i.e. $\rho_0 = \rho_{solids}$. This assumption allows eq. (3.17) to be simplified.

$$\beta = solids\ wt.\% + \frac{(volatiles\ wt.\%)}{\rho_{volatilies}} \rho_{solids} \tag{3.18}$$

3.1.1.3.2 The porosity

The equation for the porosity is adapted from Park et. al[39] and is a function of solid phase. The porosity is describing how much of the solid mass, which is empty space, i.e. pores. The pores are filled with gaseous components.

$$\varepsilon = 1 - \frac{\rho'_{solids}}{\rho_{solids}} (1 - \varepsilon_0) \tag{3.19}$$

For a bulk material, there will be several, smaller particles that makes the whole. This can be treated as a single body, but with a much greater porosity as the particles don't stack perfectly. For a bulk material, the correction in porosity is a function of densities.

$$\varepsilon_{\text{bulk}} = \varepsilon * \frac{\rho_{bulk}}{\rho_{single\ particle}} \tag{3.20}$$

Since the change in phases causes a volume β bigger than pure solids, the volatiles inside the control volume must be divided by β in order to get the same volume. The space inside the control volume where gas can be is ε and must again be multiplied with this value. An illustration is presented in Fig. 3-6

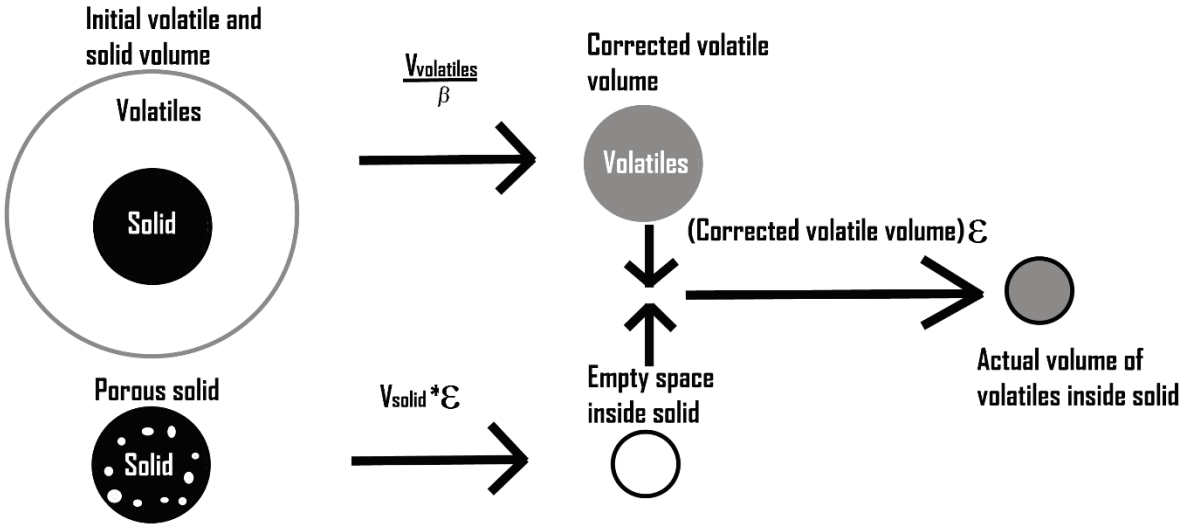

Fig. 3-6: Illustration of β's and ε's impact on the volatile volume. $V_{volatile}$ is the volume of the volatiles and V_{solid} is the volume if the solid mass.

3.1.2 Rate of changes

The rate of changes for the gaseous components are given as follows.

$$gas: \quad \frac{\partial \rho'_g}{\partial t} = k_g \rho'_f \tag{3.21}$$

$$oil: \quad \frac{\partial \rho'_o}{\partial t} = k_o \rho'_f \tag{3.22}$$

$$water\ vapor: \quad \frac{\partial \rho'_{vap}}{\partial t} = k_w \rho_w \tag{3.23}$$

Where ρ'_{vap} is the relative density of water vapor. The rate of change inside the control volume needs to be corrected as explained in chapter 3.1.1.3. The equations are given as follows.

$$gas: \quad \frac{\partial \varepsilon \rho'_g}{\partial t} = \frac{\varepsilon \rho'_g}{\beta} \tag{3.24}$$

$$oil: \quad \frac{\partial \varepsilon \rho'_o}{\partial t} = \frac{\varepsilon \rho'_o}{\beta} \tag{3.25}$$

$$vapor: \quad \frac{\partial \varepsilon \rho'_{vap}}{\partial t} = \frac{\varepsilon \rho'_{vap}}{\beta} \tag{3.26}$$

The rate of change outside the control volume is the residuals:

$$gas: \quad \frac{\partial \varepsilon \rho'^{out}_g}{\partial t} = \rho'_g \left(1 - \frac{\varepsilon}{\beta}\right) \tag{3.27}$$

$$oil: \quad \frac{\partial \varepsilon \rho_o'^{out}}{\partial t} = \rho'_o\left(1 - \frac{\varepsilon}{\beta}\right) \tag{3.28}$$

$$vapor: \quad \frac{\partial \varepsilon \rho_{vap}'^{out}}{\partial t} = \rho'_{vap}\left(1 - \frac{\varepsilon}{\beta}\right) \tag{3.29}$$

3.1.2.1 Mass balance

To confirm that the mass is conserved, the sum of each rate of change are calculated.

$$\sum \frac{\partial \rho}{\partial t} = \frac{\partial \rho'_f}{\partial t} + \frac{\partial \rho'_c}{\partial t} + \frac{\partial \rho'_g}{\partial t} + \frac{\partial \rho'_o}{\partial t} + \frac{\partial \rho_w}{\partial t} + \frac{\partial \rho'_{vap}}{\partial t}$$
$$= -\left(k_o + k_g + k_c\right)\rho'_f + k_c\rho'_f + k_g\rho'_f + k_o\rho'_f - k_w\rho_w + k_w\rho_w = 0 \tag{3.30}$$

3.1.3 Heat of reaction

It is assumed that the heat of the different pyrolysis reactions is constant with temperature. The heat of reaction is given as follows.

$$q = -(k_o\rho'_f\Delta h_o + k_g\rho'_f\Delta h_g + k_c\rho'_f\Delta h_c + k_w\rho_{w0}\Delta h_{vap}) \tag{3.31}$$

Δh is the heat of pyrolysis for the different pyrolysis reactions and heat of vaporization for water.

3.2 Kinetic model 2

This model has the same basics as model 1. The differences will be dealt with in this chapter. A new mass is added to the kinetic scheme called intermediate solid. The pyrolysis oil will also decompose into char and gas. The secondary decomposition of oil is often referred to as oil cracking[40]. A representation of the kinetics is shown in Fig. 3-7.

Antal[43] suggested a second oil component to the model, in order to prevent the pyrolysis oil yields to fully decompose which is shown to not be the case in experiments[44]. This is not added to this kinetic scheme but would probably give more reliable results.

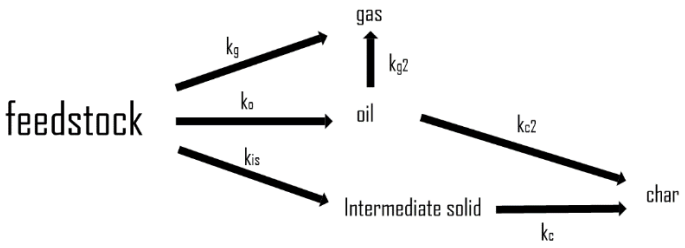

Fig. 3-7: Illustration of the kinetic model 2.

3.2.1 Mass conservation

3.2.1.1 Solid mass

Water content is calculated in the same way as kinetic model 1, chapter 3.1.1.1. The rates of changes for solid masses are given in eq. (3.32-3.35).

$$\text{Virgin feedstock:} \quad \frac{\partial \rho'_f}{\partial t} = -(k_o + k_g + k_c)\rho'_f \tag{3.32}$$

$$\text{Char:} \quad \frac{\partial \rho'_c}{\partial t} = k_c \rho'_{is} + k_{c2} * \rho'_o \tag{3.33}$$

$$\text{Water:} \quad \frac{\partial \rho'_w}{\partial t} = -k_w \rho_w \tag{3.34}$$

$$\text{Intermediate solid:} \quad \frac{\partial \rho'_{is}}{\partial t} = k_{is} \rho'_f - k_c \rho'_{is} \tag{3.35}$$

The added term, ρ'_{is} which is the relative density of intermediate solid, are produced from the virgin feedstock and decomposes to produce char. For the char, a second term is added as a result of the secondary oil cracking.

3.2.1.2 Gasses

The rate of changes for the gaseous components have two added terms. These terms take account for the secondary oil cracking as the pyrolysis oil decomposes into char and gas.

$$gas: \quad \frac{\partial \rho'_g}{\partial t} = k_g \rho'_f + k_{g2} \rho'_o - \rho'^{out}_g \tag{3.36}$$

$$oil: \quad \frac{\partial \rho'_o}{\partial t} = k_o \rho'_f - k_{g2} \rho'_o - k_{c2} * \rho'_o - \rho'^{out}_o \tag{3.37}$$

$$vapor: \quad \frac{\partial \rho'_{vap}}{\partial t} = k_w \rho_w \tag{3.38}$$

The rate of change inside the control volume are given by:

$$gas: \quad \frac{\partial \varepsilon \rho'_g}{\partial t} = \frac{\varepsilon \rho'_g}{\beta} + k_{g2} \frac{\varepsilon \rho'_o}{\beta} \tag{3.39}$$

$$oil: \quad \frac{\partial \varepsilon \rho'_o}{\partial t} = \frac{\varepsilon \rho'_o}{\beta} - k_{g2} \frac{\varepsilon \rho'_o}{\beta} - k_{c2} \frac{\varepsilon \rho'_o}{\beta} \tag{3.40}$$

$$vapor: \quad \frac{\partial \varepsilon \rho'_{vap}}{\partial t} = \frac{\varepsilon \rho'_{vap}}{\beta} \tag{3.41}$$

The rate of change outside the control volume is the residuals of the gaseous components.

$$gas: \quad \frac{\partial \rho'^{out}_g}{\partial t} = \rho'_g \left(1 - \frac{\varepsilon}{\beta}\right) + k_{g2} \rho'_o \left(1 - \frac{\varepsilon}{\beta}\right) - \rho'^{out}_g \left(1 - \frac{\varepsilon}{\beta}\right) \tag{3.42}$$

$$oil: \quad \frac{\partial \rho'^{out}_o}{\partial t} = \rho'_o \left(1 - \frac{\varepsilon}{\beta}\right) - k_{g2} \rho'_o \left(1 - \frac{\varepsilon}{\beta}\right) - k_{c2} \rho'_o \left(1 - \frac{\varepsilon}{\beta}\right) - \rho'^{out}_o \left(1 - \frac{\varepsilon}{\beta}\right) \tag{3.43}$$

$$vapor: \quad \frac{\partial \varepsilon \rho'^{out}_{vap}}{\partial t} = \rho'_{vap} (1 - \frac{\varepsilon}{\beta}) \tag{3.44}$$

The vapor that leaves the solid is not of interest in this work and is assumed to leave the reactor instantaneously. The term ρ'^{out}_i is the volatiles that are removed from the reactor and cooled down. This is calculated by the following equation:

$$\rho'^{out}_i \left(1 - \frac{\varepsilon}{\beta}\right) = \int_{t - t_{vi}}^{t} \left. \frac{\partial \rho'_i}{\partial t} \right|_{t_{vi}} dt \tag{3.45}$$

This equation keeps calculating the kinetics for the volatiles that escape the solid for the time given. t_{vi} represents the time before the volatiles gets cooled down and *t* is the current time in the calculation. An illustration is shown in Fig. 3-8.

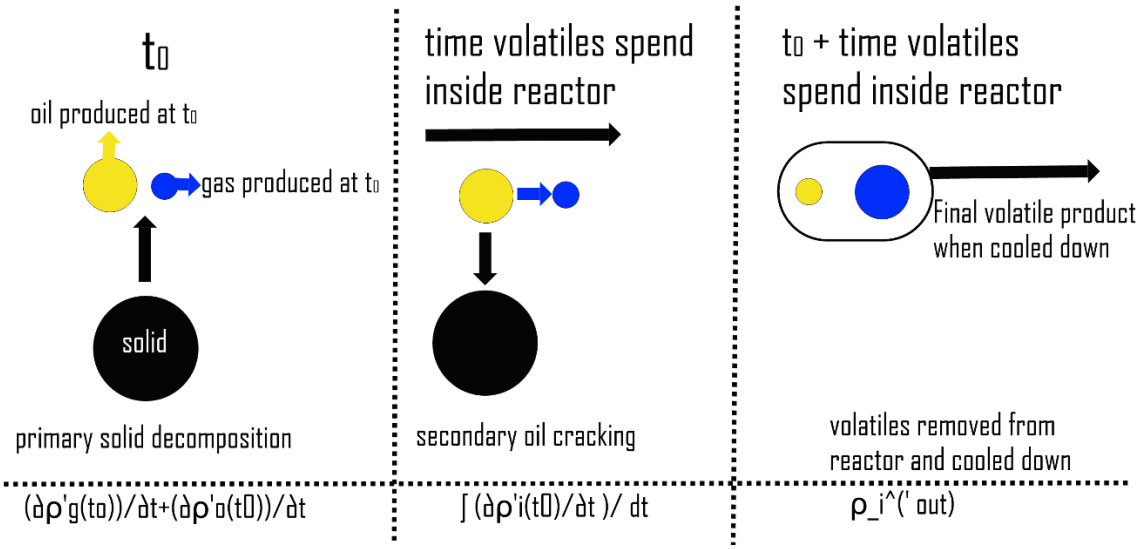

Fig. 3-8: Illustration of eq. (3.34) at *time = t_0 + time volatiles spend inside reactor*.

This modification does not affect the volume factor β, this factor is valid for the overall volume change.

3.2.1.3 Mass balance

In this model, there is a loss in mass. The mass balance is given as:

$$\sum \frac{\partial \rho}{\partial t} = \frac{\partial \rho'_f}{\partial t} + \frac{\partial \rho'_c}{\partial t} + \frac{\partial \rho'_g}{\partial t} + \frac{\partial \rho'_o}{\partial t} + \frac{\partial \rho_w}{\partial t} + \frac{\partial \rho'_{vap}}{\partial t} + \frac{\partial \rho'_{is}}{\partial t}$$

$$\begin{aligned} = &-(k_o + k_g + k_{is})\rho'_f + k_c\rho'_{is} + k_{c2} * \rho'_o + \frac{\varepsilon\rho'_g}{\beta} + k_{g2}\frac{\varepsilon\rho'_o}{\beta} + \rho'_g\left(1 - \frac{\varepsilon}{\beta}\right) \\ &+ k_{g2}\rho'_o\left(1 - \frac{\varepsilon}{\beta}\right) - \rho'^{out}_g\left(1 - \frac{\varepsilon}{\beta}\right) + \frac{\varepsilon\rho'_o}{\beta} - k_{g2}\frac{\varepsilon\rho'_o}{\beta} - k_{c2}\frac{\varepsilon\rho'_o}{\beta} \\ &+ \rho'_o\left(1 - \frac{\varepsilon}{\beta}\right) - k_{g2}\rho'_o\left(1 - \frac{\varepsilon}{\beta}\right) - k_{c2}\rho'_o\left(1 - \frac{\varepsilon}{\beta}\right) - \rho'^{out}_o\left(1 - \frac{\varepsilon}{\beta}\right) \\ &- k_w\rho_w + k_w\rho_w + k_{is}\rho'_f - k_c\rho'_{is} - \rho'_{vap}(1 - \frac{\varepsilon}{\beta}) \\ = &-\rho'^{out}_g\left(1 - \frac{\varepsilon}{\beta}\right) - \rho'^{out}_o\left(1 - \frac{\varepsilon}{\beta}\right) - \rho'_{vap}(1 - \frac{\varepsilon}{\beta}) \end{aligned} \quad (3.46)$$

The losses are due to volatiles that leaves the control volume.

3.2.2 Heat of reaction

The heat of reaction is given as follows

$$\begin{aligned} q = &-(k_o\rho'_f\Delta h_o + k_g\rho'_f\Delta h_g + k_{is}\rho'_f\Delta h_c + k_c\rho'_{is}\Delta h_c + k_{g2}\rho'_o\Delta h_{g2} + k_{c2}\rho'_o\Delta h_{c2} \\ &+ k_w\rho_{w0}\Delta h_{vap}) \end{aligned} \quad (3.47)$$

Δh is the heat of pyrolysis for the different pyrolysis reactions and heat of vaporization for water.

4. Reactor models

In this work the fixed bed (FB) and slow pyrolysis auger (SPA) reactor are chosen to be investigated. The reason for this is that these reactors are simple, suitable for small to medium scale and the technology is well known. Also, the FB reactor is a fast pyrolysis reactor and the SPA reactor is a slow pyrolysis reactor. The difference in time consumption is of interest. The main difference in the reactor models are how the heat equation is solved and the thermal energy transfer properties.

4.1 Reactor 1

Reactor 1 is the fast pyrolysis reactor. These reactors need small particles in order to heat the feedstock at a fast enough rate (See Table 2-3). The small particle size is in this work simulated by a sphere. The model will calculate the energy and yields from one single particle, assuming the exact same conditions and size for every particle inside the reactor. This approach allows the yields to be scaled up by multiplication.

4.1.1 Heat conduction.

The particle is assumed to be a sphere. It's assumed that the heat conduction is symmetric at all directions from the center and the heat equation can be solved on a single line from the outer boundary into the core.

4.1.1.1 Internal nodes.

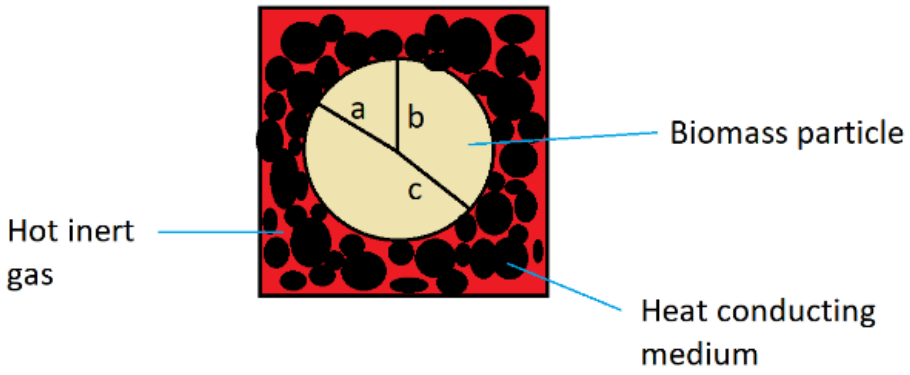

Fig. 4-1: Representation of a single particle inside a fast pyrolysis reactor with a heat conducting medium. It is assumed that the heat will be conducted symmetric from all spatial directions towards the center of the particle. The lines a, b and c represent lines where the heat will be equally distributed.

The heat equation in one spatial direction is given by:

$$\frac{\partial T}{\partial t} = \alpha \frac{\partial^2 T}{\partial x^2} + q \tag{4.1}$$

Where T is the temperature, x is the spatial location and q is the rate of temperature change due to heat added/produced by the process. α is described in eq. (4.3)

$$q = \frac{q'}{\overline{C_p} * \bar{\rho}} \tag{4.2}$$

Where q' is the energy added to the control volume [J/m^3]. $\overline{C_p}$ is the effective constant pressure heat capacity, and $\bar{\rho}$ is the effective density. Both described in chapter 4.3.

$$\alpha = \frac{\bar{\sigma}}{\overline{C_p} * \bar{\rho}} \tag{4.3}$$

Where $\overline{\sigma}$ is the effective thermal conductivity. Described in chapter 4.3. The equation will be solved using a numerical implicit scheme, i.e. the equation is solved using a backwards approximation.

$$\frac{\partial T}{\partial t} \approx \frac{T_i^{n-1} + T_i^n}{\Delta t} \tag{4.4}$$

$$\begin{aligned} t &= [0,1, \dots n-1, n, n+1, \dots t_{end}-1, t_{end}] \\ x &= [0,1, \dots, l-1, l, l+1, \dots, X-1, X] \end{aligned} \tag{4.5}$$

Where n is the time step *n*, *l* is the spatial step *l* and *Δt* is the size of the time step and X is the final spatial position.

When using the backwards approximation in time, the right side of the equation will be from the current time step, *n*. The spatial derivative will be solved by a center approximation.

$$\frac{\partial^2 T}{\partial x^2} = \frac{T_{l+1}^n - 2T_l^n + T_{l-1}^n}{\Delta x^2} \tag{4.6}$$

Where Δx is the distance between the spatial steps. Combining eq.(4.1), (4.4) and (4.6).

$$\frac{T_l^{n-1} + T_l^n}{\Delta t} = \alpha \left(\frac{T_{l+1}^n - 2T_l^n + T_{l-1}^n}{\Delta x^2} \right) + q_l^n \tag{4.7}$$

By rearranging and grouping the terms with equal time steps, the following is obtained.

$$-\lambda T_{l+1}^n + T_l^n(1 + 2\lambda) - \lambda T_{l-1}^n = T_l^{n-1} + q_l^n \, \Delta t \tag{4.8}$$

$$\lambda = \frac{\alpha \Delta t}{\Delta x^2} \tag{4.9}$$

4.1.1.2 Boundary nodes

At the center, the node will receive twice the heat from its neighbor as there is one fictional point in *i = -1*, shown in Fig 4-2.

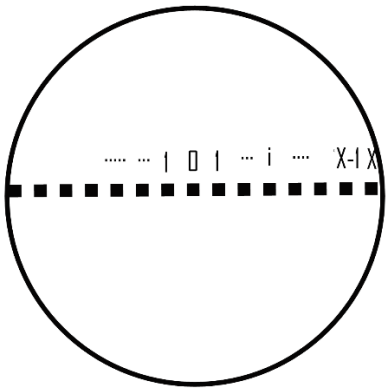

Fig. 4-2: The center node receives 2 times the heat from node 1 due to the symmetry at the center 1<->0<->1.

The equation for the center node is represented in eq. (4.11).

$$-\lambda T_1^n + T_0^n(1+2\lambda) - \lambda T_1^n = T_0^{n-1} + q_0^n \Delta t \quad (4.10)$$

$$-2 * \lambda T_1^n + T_0^n(1+2\lambda) = T_0^{n-1} + q_0^n \Delta t \quad (4.11)$$

The surface will receive heat from its surroundings. The boundary will be calculated by letting the surface node in the heat equation to be insulated, and then adding a heat flux term.

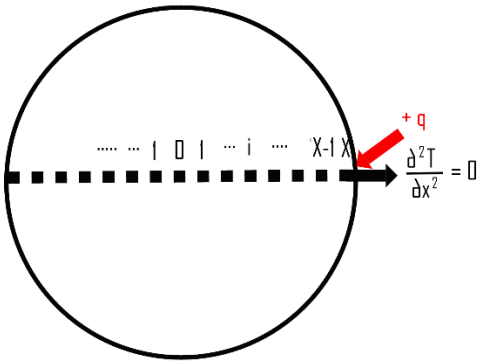

Fig. 4-3: Illustration of surface node in the 1D heat equation. Completely insulated boundary with a heat flux to the surface node.

The heat equation needs to satisfy the following conditions.

$$\frac{\partial T_X^n}{\partial t} = \begin{cases} 0 & in\ outwards\ direction \\ \alpha \dfrac{\partial^2 T}{\partial x^2} & in\ inwards\ direction \end{cases} \quad (4.12)$$

This condition is obtained by setting the outwards temperature gradient to zero.

$$\frac{\partial T}{\partial x} \approx \frac{T_{X+1}^n - T_X^n}{\Delta x} = 0 \quad (4.13)$$

$$\frac{\partial^2 T}{\partial x^2} = \frac{T_{l+1}^n - 2T_l^n + T_{l-1}^n}{\Delta x^2} \tag{4.14}$$

Inserting eq. (4.13) into eq. (4.14) yields.

$$\frac{\partial^2 T}{\partial x^2} = \frac{-T_l^n + T_{l-1}^n}{\Delta x^2} \tag{4.15}$$

For the flux term, the heat received will be a function of temperature difference, thermal contact resistance and ability to store heat.

$$q_{out} = -\frac{\sigma' A}{C_p * \rho} \frac{\partial T}{\partial x} \tag{4.16}$$

Where q is the change in temperature pr. unit time, *σ'* is the thermal contact resistivity and A is the area of contact. The term *σ'A* is converted to *h*. *h* is a value that often gets referred to as the overall heat transfer coefficient.

$$q_{out} = -\frac{h}{C_p * \rho} \frac{\partial T}{\partial x} \tag{4.17}$$

Eq. (4.17) is heat conducted in the direction from the outside of the sphere to the inside, this will on approximate form be given by:

$$q_{out} = -\frac{h}{C_p * \rho} * \frac{(T_X^n - T_{inf})}{\Delta x} \tag{4.18}$$

The full equation at the boundary are given in eq. (4.19):

$$\frac{\partial T_X^n}{\partial t} = \alpha \frac{\partial^2 T_X^n}{\partial x^2} + q_{out} + q_{reaction} \tag{4.19}$$

To find the approximate solution at the boundary, eq. (4.15) and (4.18) is inserted into eq. (4.19).

$$\frac{T_X^n - T_X^{n-1}}{\Delta t} = \alpha \frac{-T_l^n + T_{l-1}^n}{\Delta x^2} - \frac{h}{C_p * \rho} \frac{T_X^n - T_{inf}}{\Delta x} + q_{reaction} \tag{4.20}$$

After rearranging, the final equation is obtained.

$$T_X^n * \left(1 + \lambda + \frac{h * \Delta t}{\Delta x * C_p * \rho}\right) - \lambda T_{x-1}^n = +T_X^{n-1} + \frac{h * \Delta t * T_{inf}}{\Delta x * C_p * \rho} + \Delta t * q_{reaction} \tag{4.21}$$

$$\lambda = \frac{k * \Delta t}{\Delta x^2 * C_p * \rho} = \frac{\alpha * \Delta t}{\Delta x^2} \tag{4.22}$$

The complete scheme for the next time step is shown in Appendix A1.

4.2 Reactor 2.

Reactor model 2 is the SPA reactor. The reactor is simulated as a bulk of particles. The bulk will be treated as a single particle, but with a much higher porosity than the single particle. The geometry of the particle is assumed to be a cylindrical wedge illustrated in Fig. 4-4. The heat will be conducted to the feedstock at a higher rate from the steel tube than from the surrounding gas.

4.2.1 Internal nodes

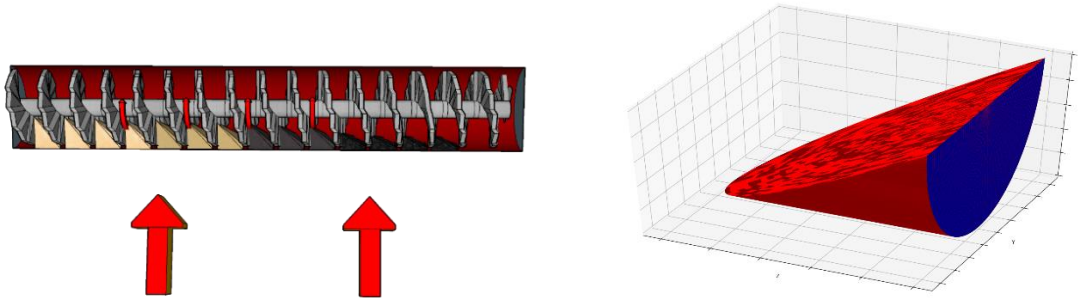

Fig. 4-4: Representation of the slow pyrolysis auger reactor and representation of assumed geometry for the feedstock inside the reactor.

The heat will mainly be conducted into the feedstock from the hot surrounding tube. The auger inside the reactor is assumed to have the same temperature as the feedstock and heat conduction along the length of the cylinder wedge in Fig.4-5 is assumed to be zero. Further, if the bulk is split into several cut circles the heat equation can be solved in 2 spatial dimensions.

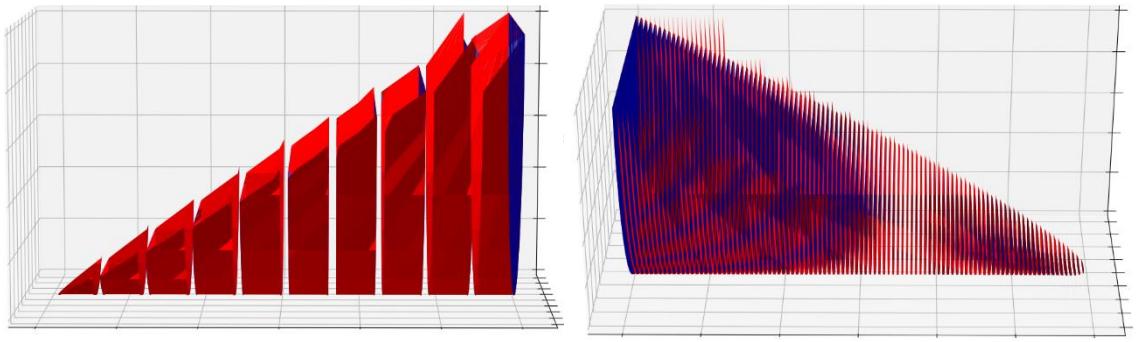

Fig. 4-5: Cylindrical wedge cut in 10 and 100 along the length.

The heat equation expanded to two spatial directions are given in eq. (4.23).

$$\frac{\partial T}{\partial t} = \alpha\left(\frac{\partial^2 T}{\partial x^2} + \frac{\partial^2 T}{\partial y^2}\right) + q \tag{4.23}$$

The full explanation for the solution in two dimensions is shown in Appendix A2. In this chapter, the geometry will be considered.

The equation for a lower half circle is given by eq. (4.24).

$$y = -\sqrt{x^2 + z^2} \tag{4.24}$$

Where x, y and z are the spatial coordinates. This equation will set the boundary along the radius. Along the length of the edge, the boundary will assume to have a 45° slope. The equation for this boundary is shown in eq. (4.25)

$$x = z \tag{4.25}$$

x is the height of the cylindrical wedge and *z* are the length along the *Z*-axis when using a Euclidean coordinate system.

4.2.1.1 Boundary nodes

There is a total of 3! different surface opportunities. The implementation of the scheme is shown in appendix A2. A figurative illustration is shown in Fig. 4-6.

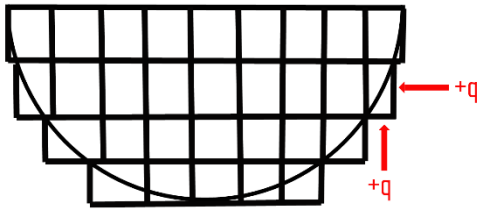

Fig. 4-6: Representation of surface point for the cut cylindrical wedge with two sides that receives heat from the surroundings.

Because the top nodes only contact the gas inside the reactor and not the hot steel that surrounds the feedstock, the boundary nodes at the top of Fig. 4-6 will have a different value of *h* than the boundary nodes at the sides and bottom.

4.3 The thermal values

The thermal values calculated in the following subsections are valid for both models.

4.3.1 Thermal conductivity

The thermal conductivity describes how heat is conducted through a material[45]. This value is an empiric value and is found through the literature. For wood, the thermal conductivity is often given as function of specific gravity, moist content and biomass[46,47]. The thermal conductivity for wood is also dependent on direction. There is a different thermal conductivity along the grains than in the radial direction.[39]. Each component inside the control volume will have a different thermal conductivity. In this work however, the average value of each thermal conductivity is used.

$$\overline{\sigma_{l,J}^{n}} = \frac{(\sum_i \sigma_i)}{n_{components}} \tag{4.26}$$

Where $n_{components}$ is the total amount of components in the control volume, [virgin biomass, gas …] and σ_i is the independent thermal conductivity for each component. For wood, the thermal conductivity is the average in each direction.

The thermal conductivity between two nodes is calculated as the average for the two.

$$\overline{\sigma_{l,J}^{n}} \leftrightarrow \overline{\sigma_{l,J+1}^{n}} = \frac{\overline{\sigma_{l,J}^{n}} + \overline{\sigma_{l,J+1}^{n}}}{2} \tag{4.27}$$

4.3.2 Heat capacity

The heat capacity describes how much energy that is needed to heat 1 kg of the material 1K[45]. The pressure is assumed to be constant, therefore the constant pressure heat capacity (C_p) is used. This is also an empiric value. This value is a function of temperature and is calculated for each time step.

$$\overline{C_p}(T) = \frac{\left(\sum_i C_{p\,i}(T)\right)}{n_{components}} \tag{4.28}$$

4.3.3 Effective density

The effective density is the actual density inside the control volume. The effective density is found by summing the products of all relative densities multiplied by the actual density. It is described in eq. (4.29)

$$\bar{\rho}(T) = \sum_i \rho'_i(T) * \rho_i \tag{4.29}$$

4.4 Energy analysis

4.4.1 Energy consumption

There are two effects that is consuming energy in the pyrolysis process.

(i) Energy needed to decompose the biomass
(ii) Energy needed to heat the biomass

The energy consumption will depend on time and temperature for both processes.

The equation for (i) is given in eq. (4.29) and the equation for (ii) is given in eq. (4.30) The sum is given in eq. (4.31)

$$E_{pyrolysis} = \int_{t_0}^{t_{decomposed}} q \, dt \tag{4.30}$$

Where $E_{pyrolysis}$ is the energy consumed by the decomposition of the biomass pr. unit volume. q is described in chapter 3.2.2.

$$E_{heat} = \int_{t_0}^{t_{decomposed}} \overline{C_p} * \bar{\rho} \frac{\partial T}{\partial t} \, dt \tag{4.31}$$

Where E_{heat} is the energy needed to heat the biomass, pr. unit volume. $\overline{C_p}$ is the effective heat capacity, $\bar{\rho}$ is the effective density and $\frac{\partial T}{\partial t}$ is the rate of temperature change pr. unit time.

$$E_{total} = \int_{t_0}^{t_{decomposed}} \left(q + \overline{C_p} * \bar{\rho} \frac{\partial T}{\partial t} \right) dt \tag{4.32}$$

Where E_{total} is the total energy consumed by the process.

4.4.2 Released heat

The total energy consumed contains information about the ambient temperature. At final time, the biomass and ambient temperature will be equal, which implies that more energy is needed to heat the biomass to a higher temperature.

The time biomass spend inside the reactor will affect the energy that leaves the reactor. Energy flows from warm to cold, if the biomass needs to be kept heated for a longer period, more energy will escape.

In this work, a simplified efficiency method is used to calculate the energy released by the process. The heat released will be calculated by two terms. An overall efficiency factor and a time dependent energy factor. The overall efficiency factor depends on the total energy consumed. The time dependent factor is dependent on both the time consumed and the total energy consumed.

$$E_{out} = \mu_o * E_{total} + \mu_t * t_{total} * E_{total} \tag{4.33}$$

Where μ_o is the overall efficiency factor and μ_t is the time dependent efficiency factor.

5. Results

Results for kinetic model 1 is not listed, as explained in chapter 3, this model was shown to work out the basics of the model. Kinetics model 2 is built upon model 1 and gives a more detailed insight to the process. Both reactor models are listed with kinetic model 2.

The results for the least and most released heat are shown for a variety of moist contents. The resultant yields at the given parameters is also shown to investigate if one main product is preferred over another when the heat energy demand changes. Values common for both models are listed below.

Table 5-1: Kinetic values used in simulation. All values are collected from Park et. al [39]

	A [s^{-1}]	E [J/mol]	Δh [kJ/kg]
k_g	$4.38*10^9$	152.7	80
k_o	$10.08*10^{10}$	148.0	80
k_{is}	$3.75*10^6$	111.7	80
K_c	$1.38*10^{10}$	161.0	-300
k_{c2}	$1.0*10^9$	108.0	-42
k_{g2}	$4.28*10^9$	108.0	-42
k_w	-	-	2256

Common material properties and thermal values is shown in Table 5-2.

Table 5-2: Common material properties and thermal values.

property	value	Ref.
Feedstock	Maple wood	Park et. al.[39]
ρ_f	630 [kg/m^3]	Park et. al.[39]
ρ_w	1000 [kg/m^3]	-
$\rho_{volatiles}$	1,4 [kg/m^3]	Estimated from [48]
$C_{p,f}$	1500 +1.0*T [J/kg*K]	Park et. al.[39]
$C_{p,w}$	4180 [J/kg*K]	-
$C_{p,c}$	4.20 + 2.09*T + 6.85*10^{-4}*T^2[J/kg*K]	Park et. al.[39]
$C_{p,g}$	770 + 0.629*T – 1.91*10^{-4}*T^2 [J/kg*K]	Park et. al.[39]
$C_{p,o}$	-100 + 4.4*T – 1.57*10^{-3}*T^2 [J/kg*K]	Park et. al.[39]
$\sigma_{f,radial}$	0.1046 [W/m*K]	Park et. al.[39]
$\sigma_{f,grain}$	0.255 [W/m*K]	Park et. al.[39]
$\sigma_{f,tangential}$	0.255 [W/m*K]	Park et. al.[39]
$\sigma_{c,radial}$	0.071 [W/m*K]	Park et. al.[39]
$\sigma_{c,grain}$	0.105 [W/m*K]	Park et. al.[39]
$\sigma_{c,tangential}$	0.105 [W/m*K]	Park et. al.[39]
ε_f	0.6	Ross [47]
R	8.314 [J/mol*K]	-

5.1 Model 1, kinetics 2.

The kinetic and thermal values used is shown in Table 5-1, every analysis is run until the residual biomass in each spatial cell falls below 0.1 %. A Table of results for a variety of parameters is shown in appendix B.1. In this chapter an overview over the different effects on the model will be given. Values for reactor and feedstock used is shown in Table 5-3. The code used to produce the results is available on github[49]. The code is inspired by Wiggins[50]

Table 5-3: Reactor dependent variables.

property	value	Ref.
d	$1*10^{-3}$ [m]	Zaman et.al.[17]
h	100 [W/m^2*K]	Estimated
Spatial nodes	99	-
Time step gap	$50*10^3$	-
Temperature range	700-1350 [K]	-
Moist values	0,25,50 %	-

5.1.1 Time consumption

The time consumed will affect both the yields and the energy consumed as explained in chapter 2.2 and 4.4.2. In this chapter, the time consumed will be investigated as a function of temperature. The effect of moist feedstock will also be presented. Time consumed before 0.1% biomass is reached is shown with three different moist values in Fig. 5-1.

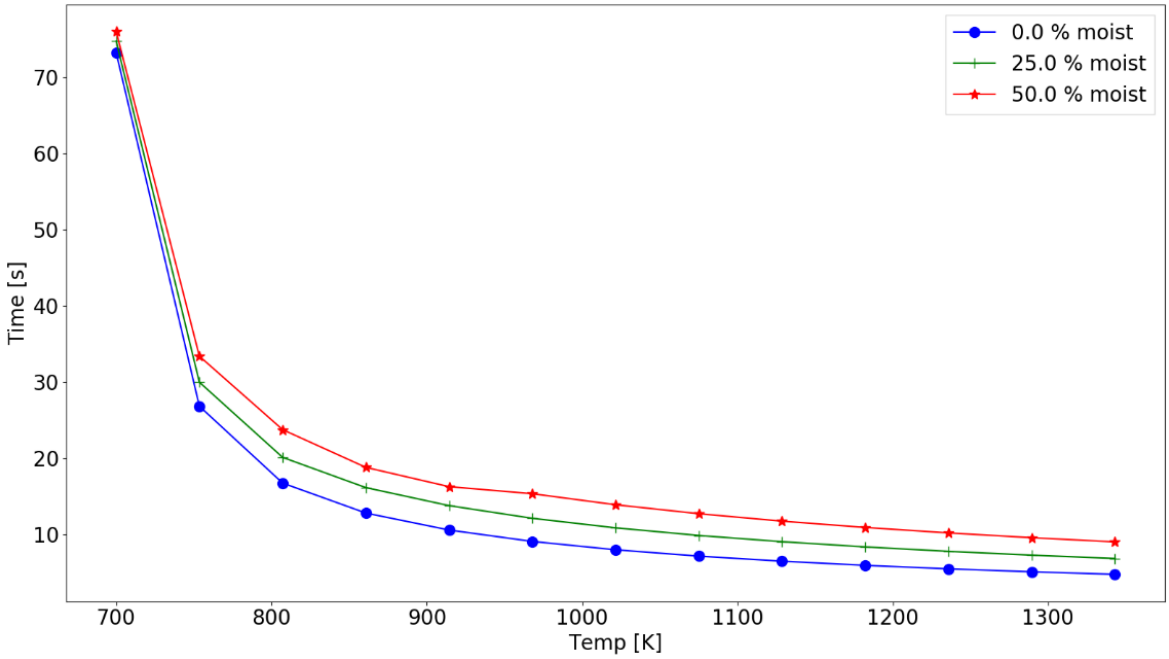

Fig. 5-1: Seconds until 0.1% biomass left as a function of temperature in the range 700K to 1350K. Three different moist contents are plotted. The plot is for virgin feedstock and with no losses.

5.1.2 Yields

The predicted yields are shown as a percentage of the dry mass. The yields are strongly dependent on the volatile cooldown time. Fig. 5-2 shows the yields with a cooldown time of 0.001 seconds and Fig. 5-3 shows a cooldown time of 1 second.

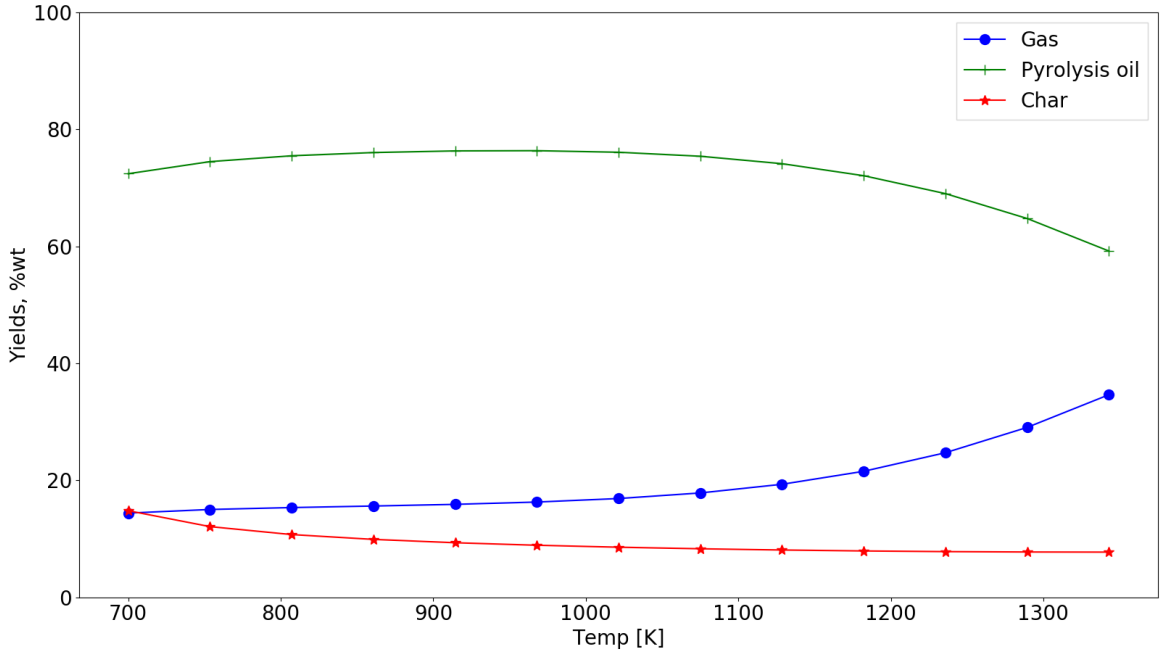

Fig. 5-2: Final yields as a % of dry feedstock weight at temperatures between 700 to 1350K. Cooldown time for the volatiles are set to 0.001s.

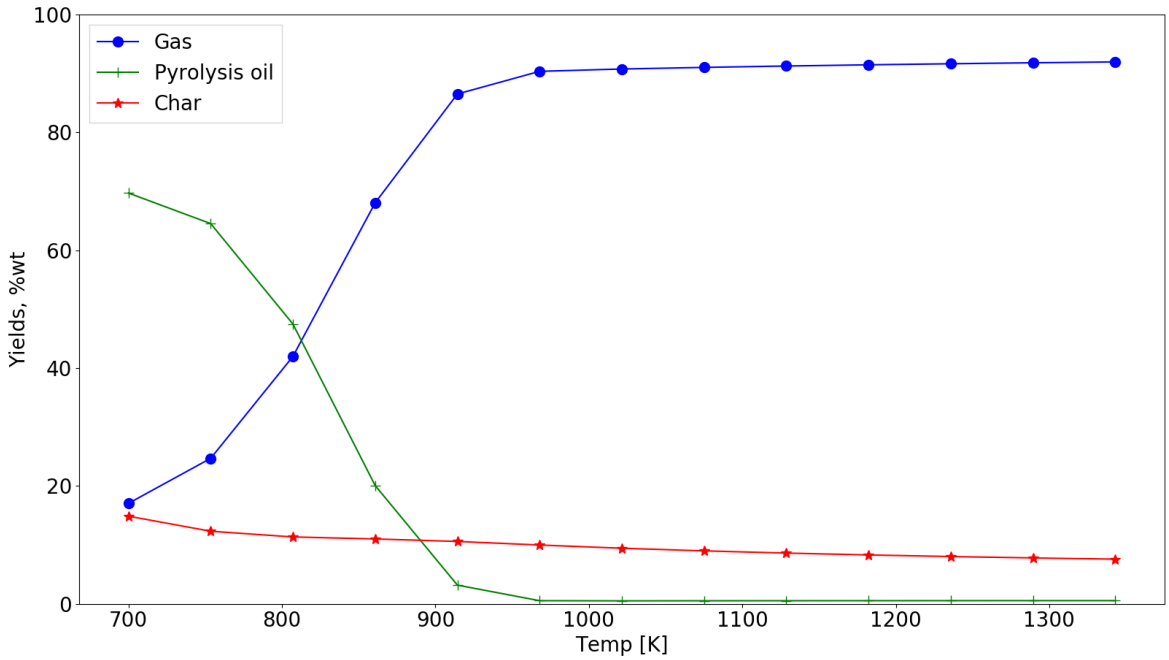

Fig. 5-3: Final yields as a % of dry feedstock weight at temperatures between 700 to 1350K. Cooldown time for the volatiles are set to 1.005s.

As the volatile cooldown time increases, the oil yield decreases at a lower temperature.

The effect on moist are shown in. Fig. 5-4.

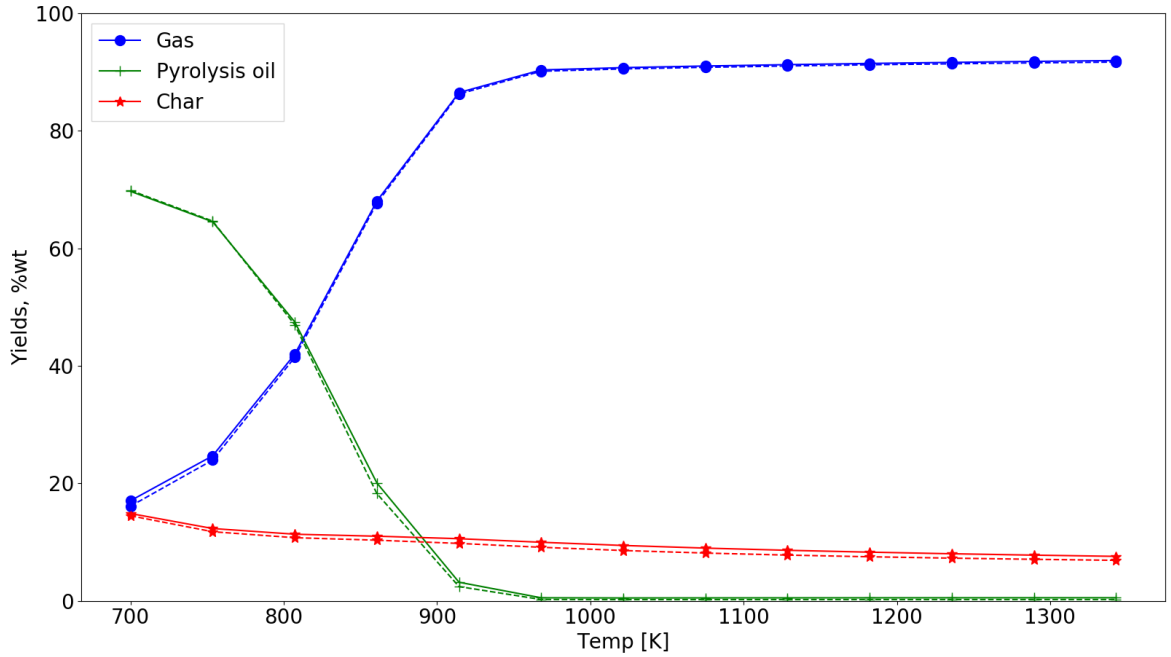

Fig. 5-4: Final yields as a % of dry feedstock weight at temperatures between 700 to 1350K. Cooldown time for the volatiles are set to 1.005s. Dashed line represents moist feedstock and solid line represents dry feedstock.

5.1.3 Energy consumption:

The energy consumed by the process is in this work is dependent on two factors. The energy required for decomposition of the feedstock and the energy required for heating the feedstock. Explained in detail in chapter 4.4. All energy analysis is shown pr. cubic meter virgin feedstock.

Without energy losses and with a cooldown time for the volatiles set to 0.001 s, the energy consumed by the process as a function of temperature is shown in Fig. 5-5. Energy consumed will have a possitive value if energy is added and negative if energy is released.

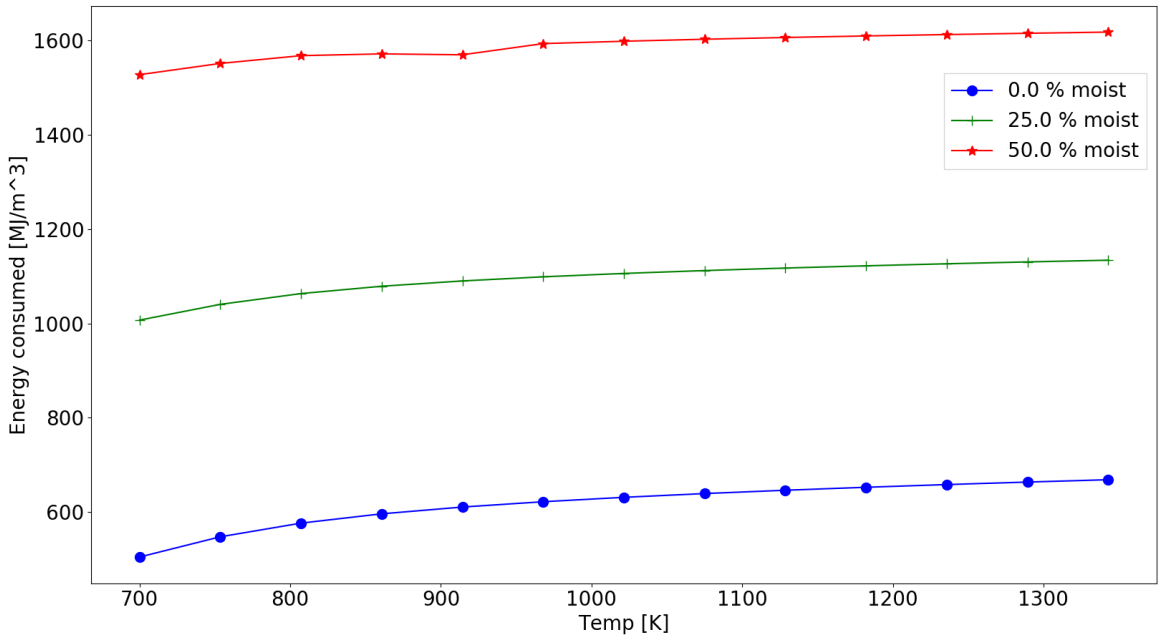

Fig. 5-5: Energy consumed as a function of temperature with three different moist values. Volatile cooldown time is set to 0.001s. The results are shown pr. cubic meter virgin feedstock.

The secondary oil cracking is assumed to be a exothermic reaction. The impact of this variable is small compared to the heat energy and other reactions. Values are listed in Appendix B and a comparison of the energy needed to heat the feedstock and the energy needed to run the process is shown in Fig. 5-8.

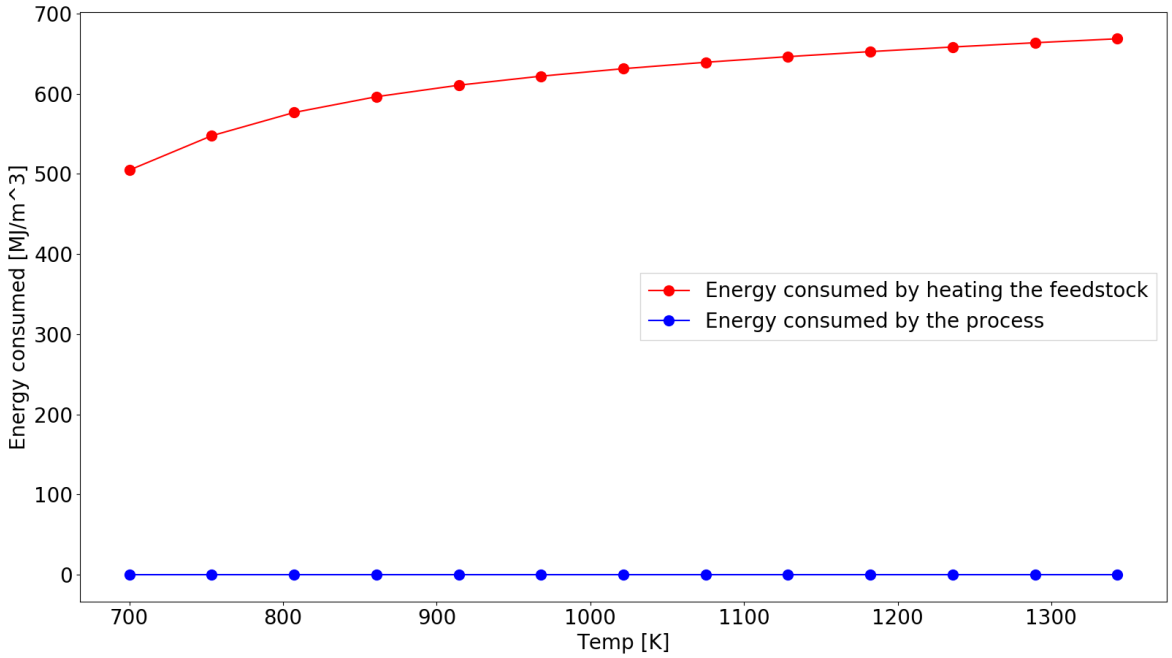

Fig. 5-6: Comparison energy consumed by the pyrolysis process and energy needed to heat the feedstock.The plot shows energy consumed as a function of temperature. The cooldown time of volatiles is set to 0.001s and the moist is set to 0%.

A closer look at the energy consumed by the pyrolysis process is shown in Fig. 5-7. A plot of the reaction energy with moist is shown in Fig. 5-8.

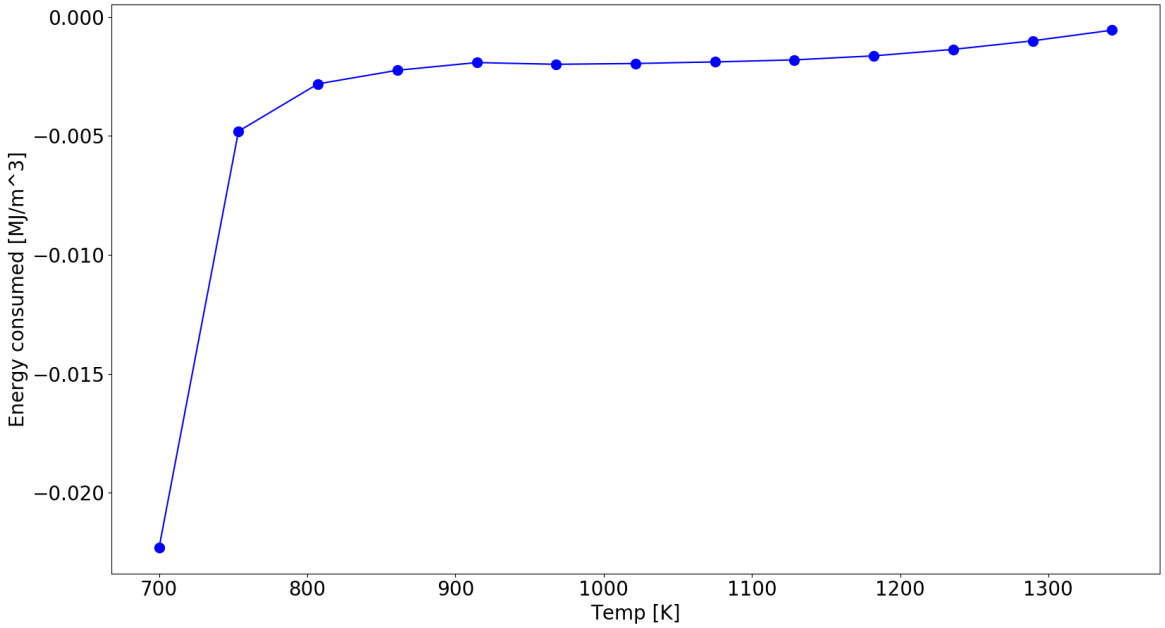

Fig. 5-7: Energy consumed by the pyrolysis process as a function of temperature. The results are shown pr. cubic meter virgin feedstock. The cooldown time of volatiles is set to 0.001s and the moist is set to 0%.

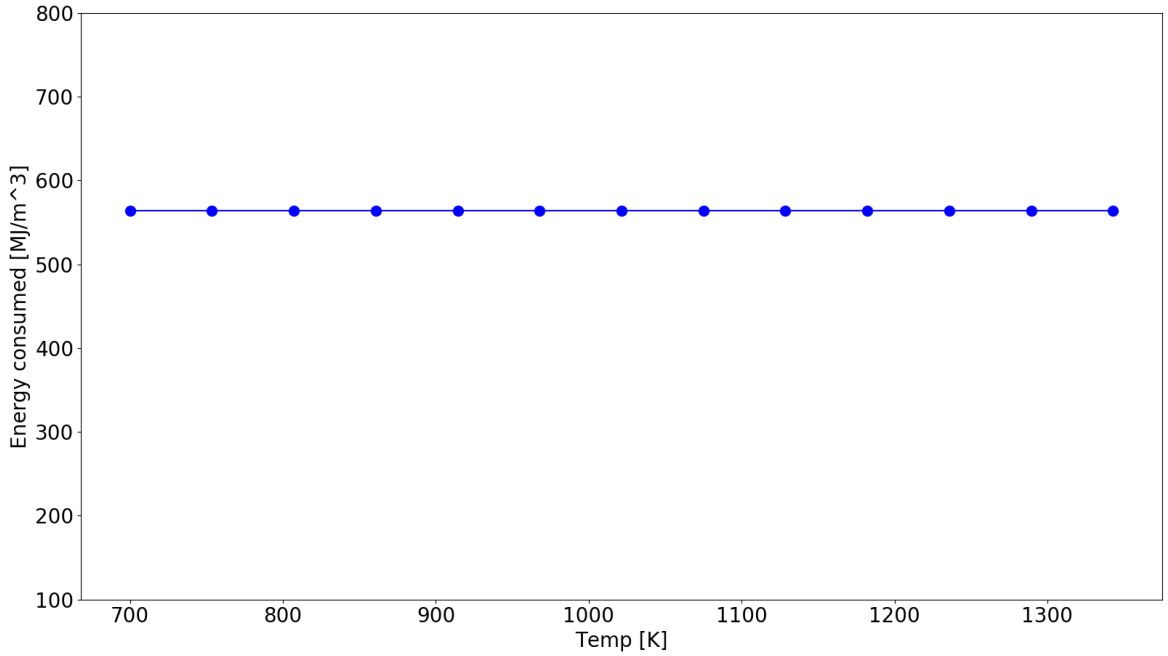

Fig. 5-8: Energy consumed by the pyrolysis process as a function of temperature. The results are shown pr. cubic meter virgin feedstock. The cooldown time of volatiles is set to 0.001s and the moist is set to 25%.

5.1.4 Released heat:

As shown in Table 2-1, the HHV of maple wood is 18.36 MJ/kg. The density of the wood is 630 Kg/m^3 which gives an energy density of 11.57GJ/m^3

By Fig. 5-5, the highest theoretical value of consumed heat is 668 MJ/m^3 for completely dry feedstock. This implies that 5.8% of the energy in the biomass needs to be consumed to run the process when there is no loss. The least theoretical value of consumed energy is 505 MJ/m^3. Which implies that 4.4% of the energy in the biomass needs to be consumed to run the process.

For moist feedstock at 25% water content. The LHV is corrected to 13,77 kJ/kg which gives an energy density at 8.68 GJ/m^3. With a proximate energy consumption of 1 GJ/m^3, 11% of the energy needs to be consumed to run the process. For 50% moist, at least 28% of the energy in the feedstock needs to be consumed to run the process. After losses, the results are shown in Fig. 5-9.

The heat released from the process are dependent on two efficiencies. On time dependent and one overall. Jaroenkhasemmeesuk et. al [25] suggested that 60% of the input energy was released from the reactor, see chapter 2.2.1. Half from the reactor walls and half from the heated feedstock. Unfortunately, the operational conditions are unknown. Nevertheless, that reactor was a fast pyrolysis reactor, and this is a fast pyrolysis model. The total amount released heat is fitted the experiment conducted by Atsonios et.al[19]. The feedstock feed will be set to 0.019kg/s, as this is the feed used in chapter 5.2.4

For the heat released, there will be presented both total released energy and energy released pr. time. The content of moist does only shift the energy consumption to a higher level. The shapes are approximately equal as shown in Fig.5-5.

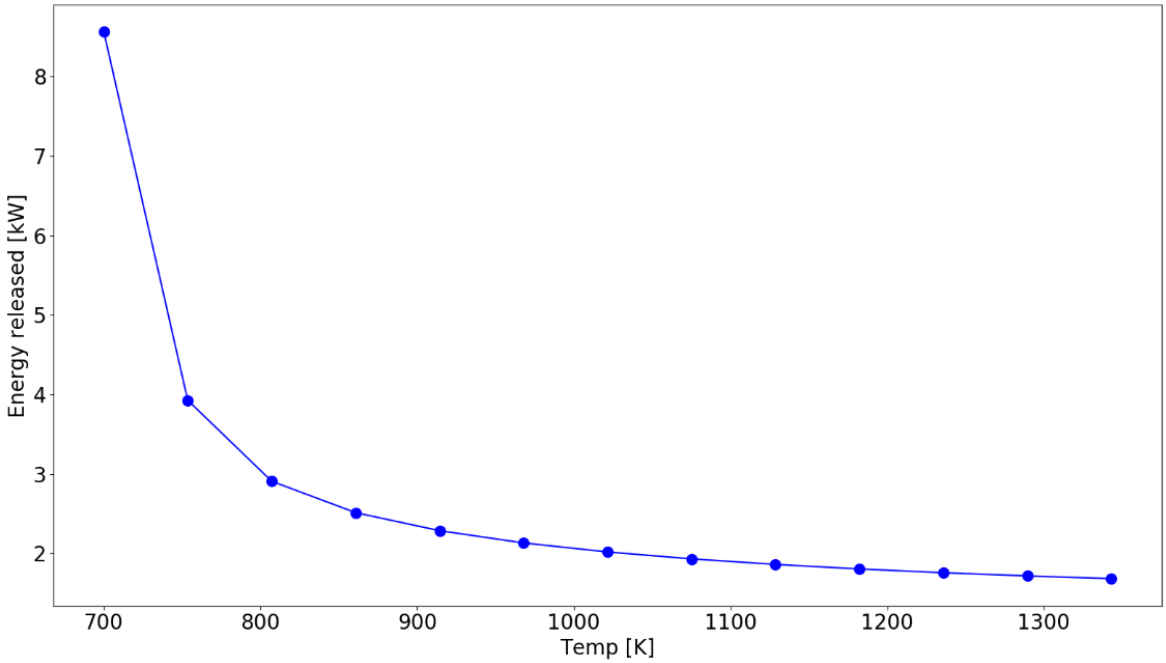

Fig. 5-9: Released heat as a function of temperature with μ_t = 0.007/s and μ_o= 0.05. both factors contribute equal at 1200K. The feedstock feed is set to 0.019kg/s and moist = 0.

Total energy consumed for this configuration are plotted in Fig. 5-10 for different moist values. This is the sum of energy consumed and energy required to run the process. Plotted as a function of percent energy consumed of the total energy in the feedstock.

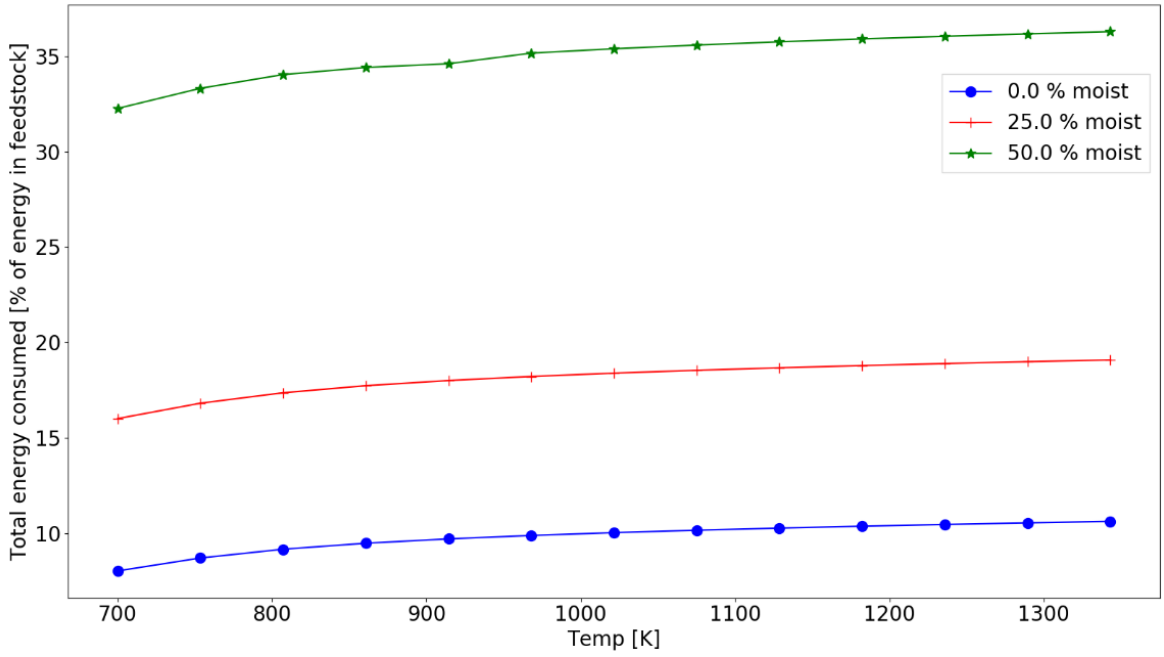

Fig. 5-10: Total consumed energy as a function of percent consumed energy of total energy in feedstock plotted against temperature. μ_t = 0.007/s and μ_o= 0.05, both factors contribute equal at 1200K.

As a function of energy consumed, the plot is shown in Fig. 5-11.

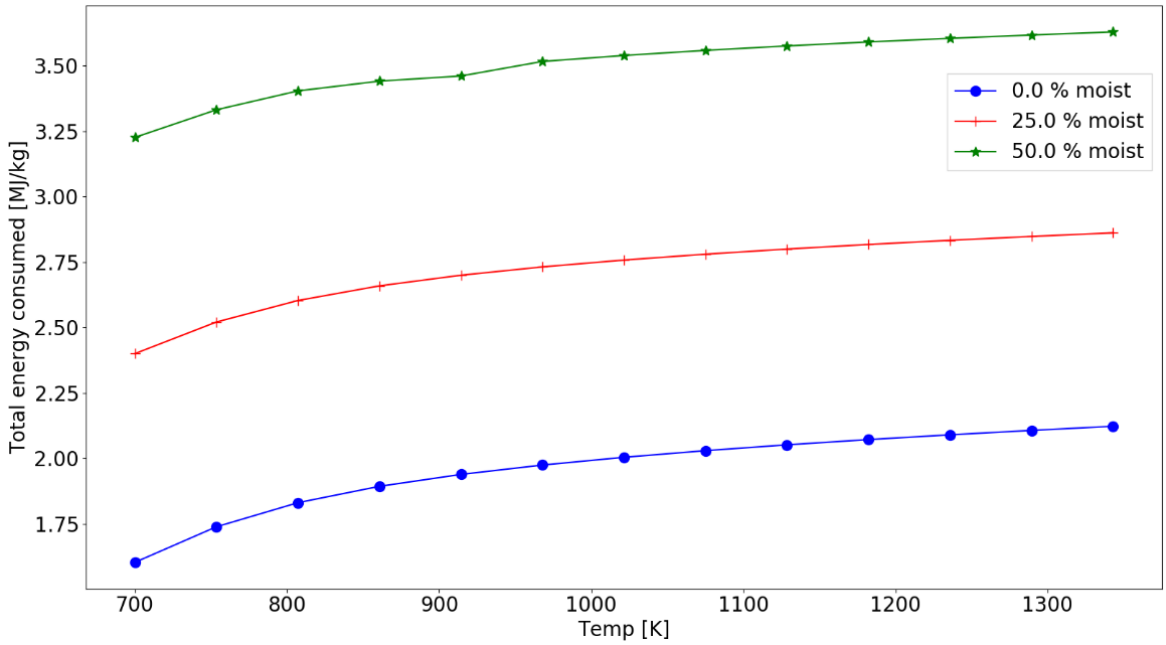

Fig. 5-11: Total consumed energy pr. kg virgin feedstock plotted against temperature. μ_t = 0.007/s and μ_o= 0.05, both factors contribute equal at 1200K.

5.2 Model 2, kinetics 2

The kinetic and thermal values used is shown in Table 5-1, every analysis is run until the residual biomass in each spatial cell falls below 0.1 %. A Table of results for a variety of parameters is shown in appendix B.2. The reactor dependent variables are shown in Table 5-4. The code used to produce the results is available on github[51]

Table 5-4: Reactor dependent variables for reactor model 2.

property	value	Ref.
Diameter of cylinder wedge	$10*10^{-3}$ [m]	-
ρ_{bulk}	200 [kg/m^3]	Kofman[52]
h gas to feedstock	1 [W/m^2*K]	Estimated
h steel to feedstock	5 [W/m^2*K]	Estimated
Spatial steps sideways	14	-
Spatial steps upwards	7	-
Spatial steps along length	3	-
Time step gap	$10.9*10^5$	-
Temperature range	700-1350 [K]	-
Moist values	0,15,30 %	-

5.2.1 Time consumption:

The time consumed is dependent on temperature and moist. A plot of time consumed as a function of temperature is shown in Fig. 5-12. The time consumed ranges from 1838s to 343s on a dry feedstock basis. Moist content shifts the time consumption to a higher rate.

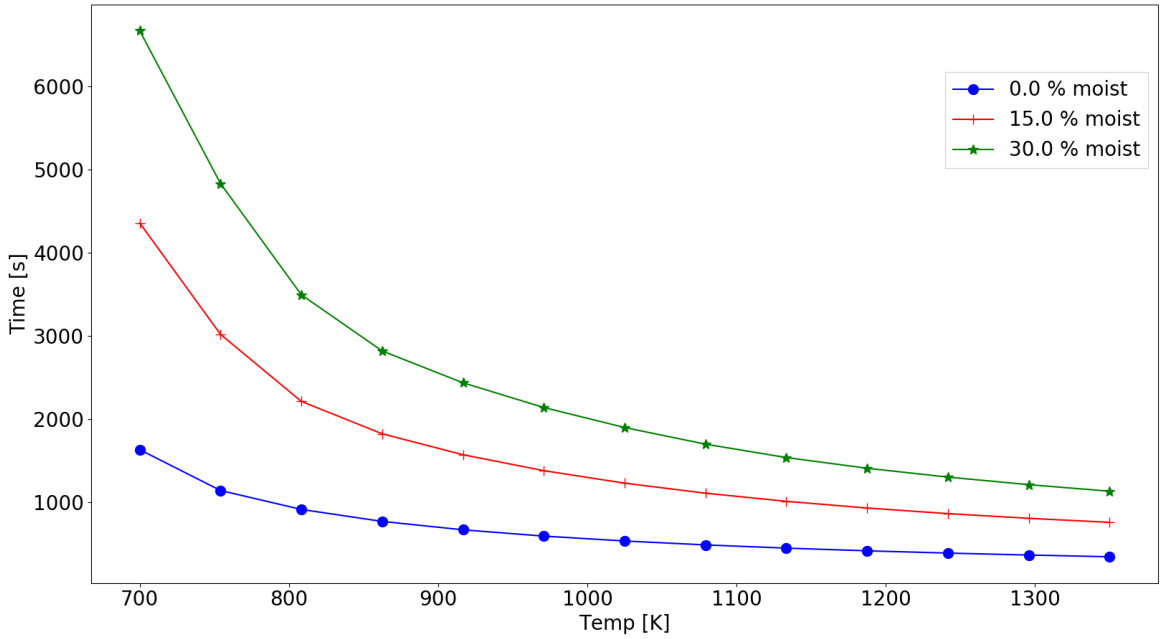

Fig. 5-12: Seconds until 0.1% biomass left as a function of temperature in the range 700K to 1350K. Three different moist contents are plotted. The plot is for virgin feedstock and with no losses.

5.2.2 Yields

The predicted yields are shown as a percentage of the dry mass. Fig. 5-13 shows the yields with a cooldown time of 0.001 seconds.

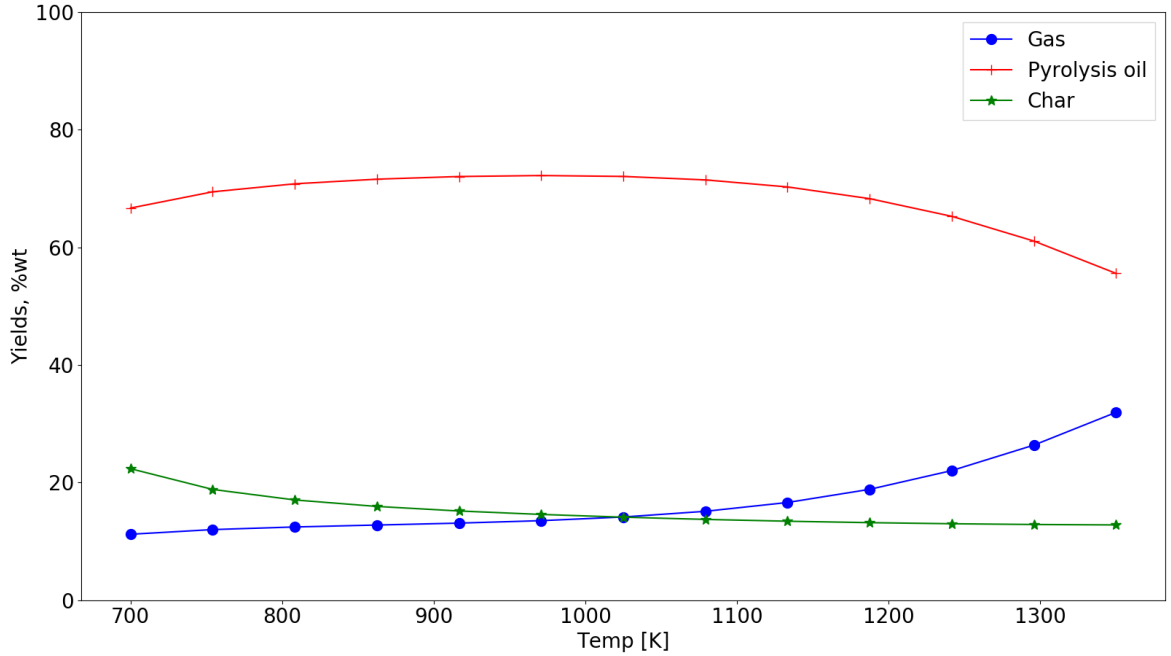

Fig. 5-13: Final yields as a percent of dry feedstock weight at temperatures between 700 to 1350K. Cooldown time for the volatiles are set to 0.001s.

For a volatile cooldown time of 1s, the plot is shown in Fig. 5-14

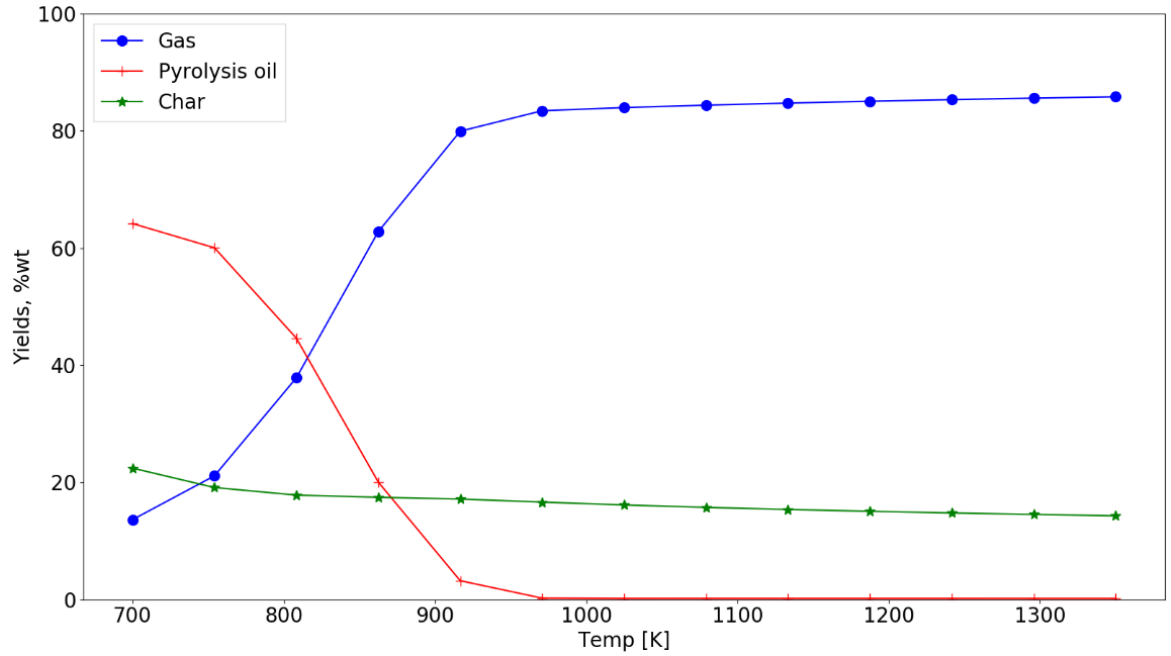

Fig. 5-14: Final yields as a % of dry feedstock weight at temperatures between 700 to 1350K. Cooldown time for the volatiles are set to 1.005s.

As the volatile cooldown time increases, the pyrolysis oil yield decreases at a lower temperature.

The effect on moist are shown in. Fig. 5-15.

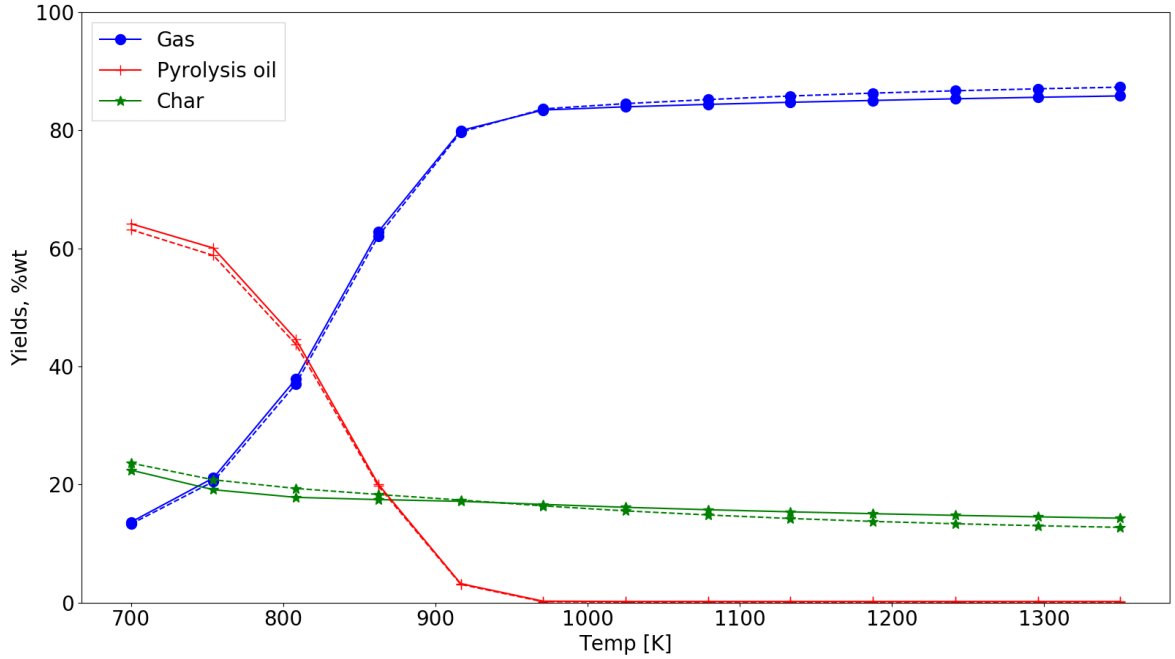

Fig. 5-15: Final yields as a % of dry feedstock weight at temperatures between 700 to 1350K. Cooldown time for the volatiles are set to 1.005s. Dashed line represents feedstock with 30% moist and solid line represents dry feedstock.

5.2.3 Energy consumption:

The energy consumed by the process is in this work dependent on two factors. The energy required for decomposition of the feedstock and the energy required for heating the feedstock. Explained in detail in chapter 4.4. Without energy losses and with a cooldown time for the volatiles = 0.001 s, the energy consumed by the process as a function of temperature is shown in Fig. 5-16. Energy consumed will have a possitive value if energy is added and negative if energy is released.

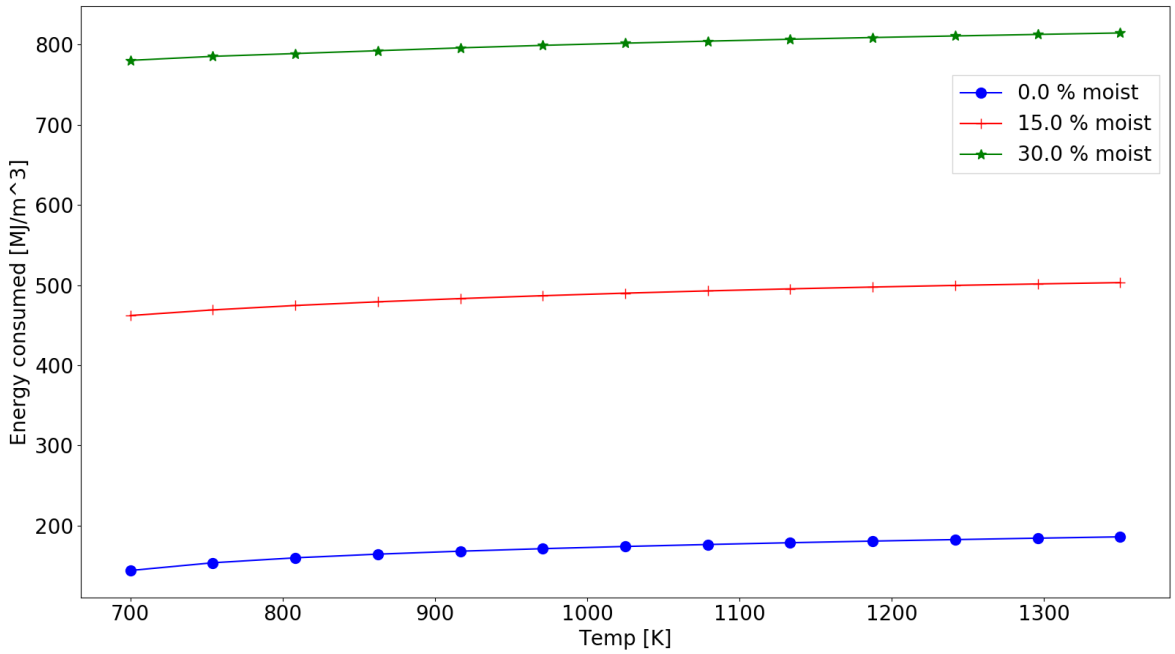

Fig. 5-16: Energy consumed as a function of temperature with three different moist values. The results are shown pr. cubic meter virgin feedstock.

A closer look on the dry biomass line (i.e. 0% moist) is shown in Fig. 5-17.

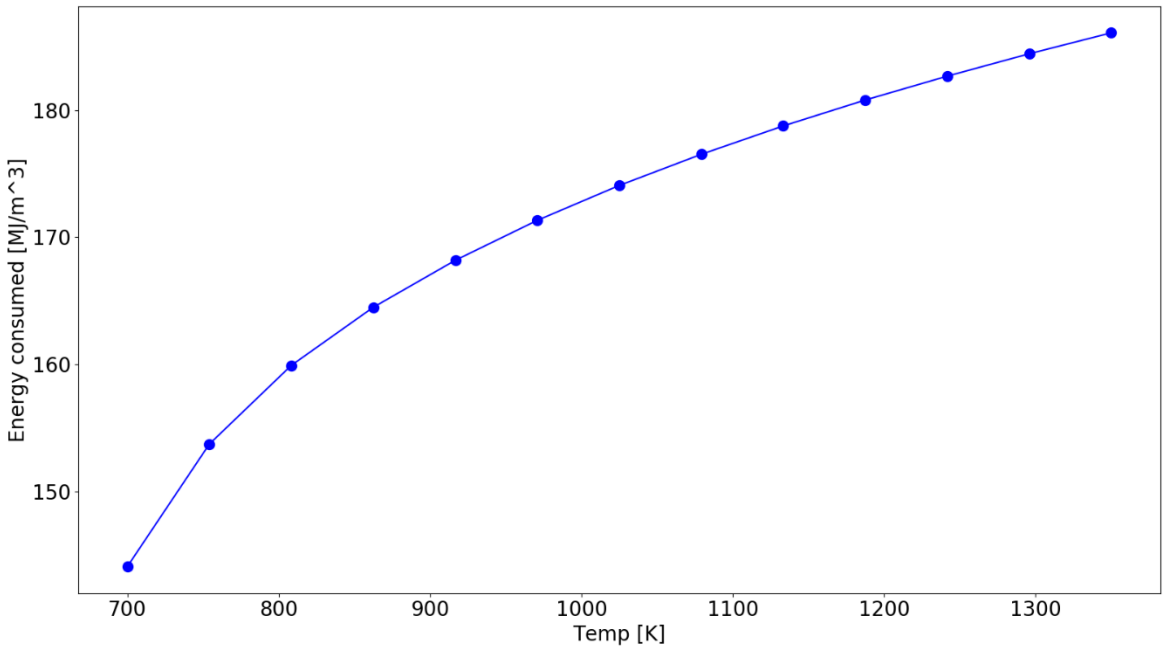

Fig. 5-17: Energy consumed as a function of temperature. The moist is 0% and the results are shown pr. cubic meter virgin feedstock.

For the secondary oil craking and the overall heat of reaction, the results are the same as reactor model 1. The effect is neglectable compared to the other energy consuming factors. See Fig. 5-8

A closer look at the energy consumed by the pyrolysis process is shown in Fig. 5-17. A plot of the reaction energy with moist is shown in Fig. 5-18.

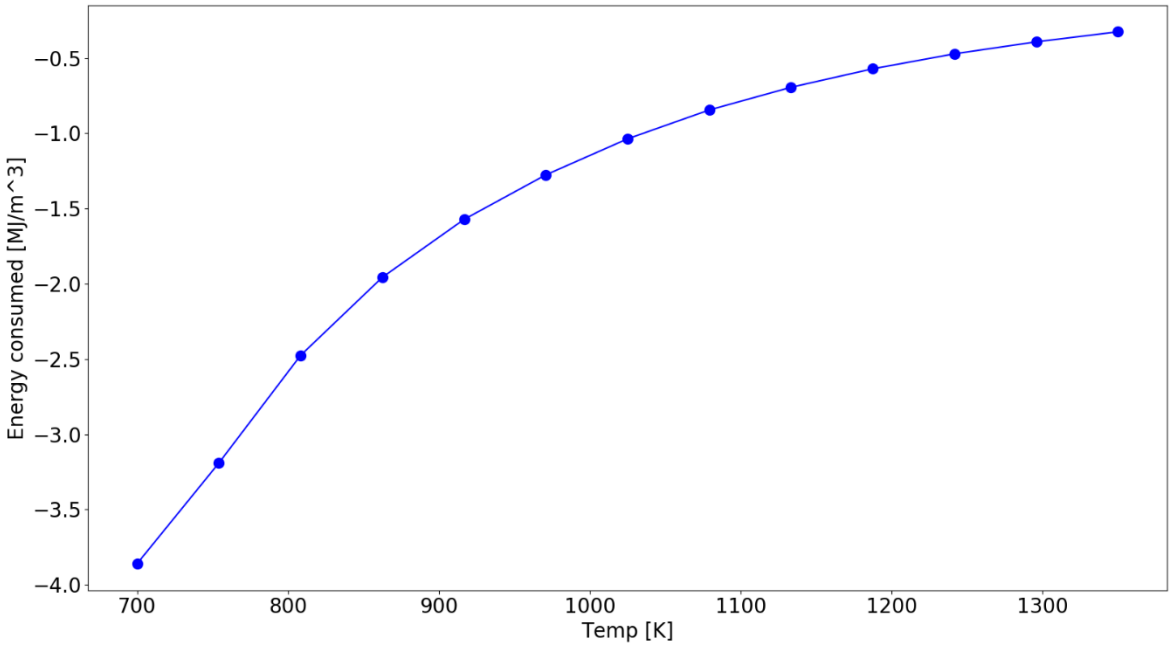

Fig. 5-18: Energy consumed by the pyrolysis process as a function of temperature. The results are shown pr. cubic meter virgin feedstock.

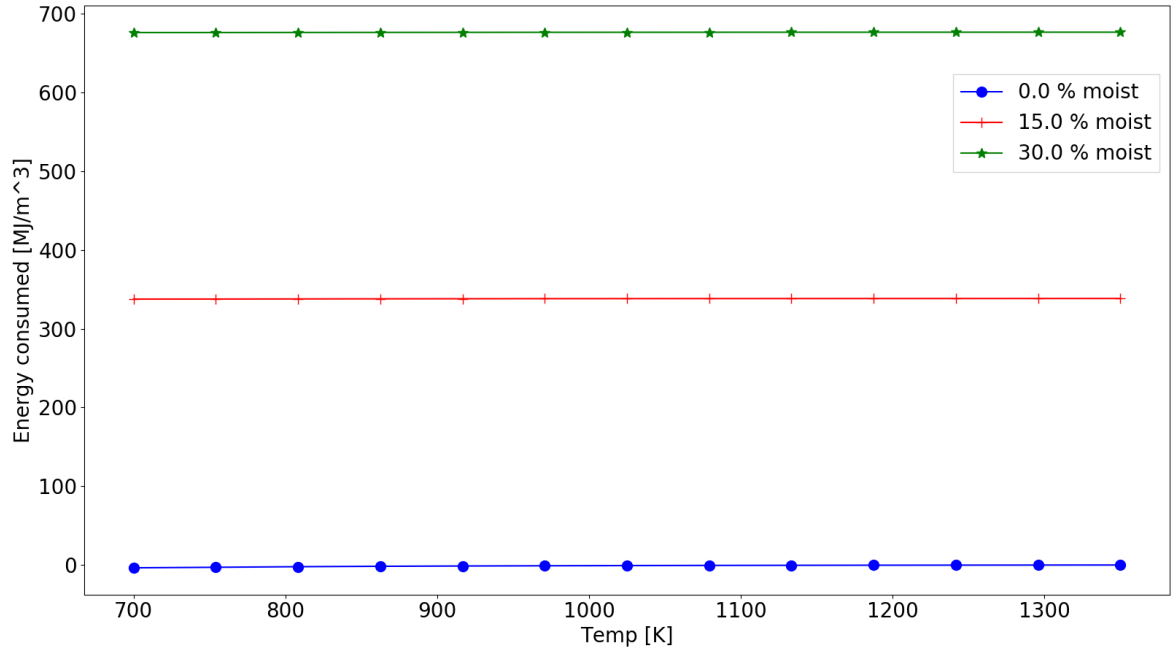

Fig. 5-19: Energy consumed by the pyrolysis process as a function of temperature. The results are shown pr. cubic meter virgin feedstock and with three different values of moist.

5.2.4 Released heat:

For the moist, the results are the same as for model 1. The same amount of energy is required to run the process at different moist levels. The feedstock, kinetic and thermal values are the same for both reactor models. For this model, the released heat is calculated from the reactor described in chapter 2.3.3

It is important to notice that the density of the feedstock is different in this model as the feedstock is simulated as a bulk material. The LHV of the dry feedstock is 18.36MJ/kg from Table 2-2 and the density is 200kg/m^3 from Table 5-4. This gives an energy density of 3,67GJ/m^3. For values over this number, the energy balance is negative.

As mentioned in chapter 2.3.3 one such reactor has an output of 50-100kW and yields 20 %wt. of char. The feedstock has a residence time of 2 hours inside the reactor. Operational temperature is in the range of 800K-1000K. The char yield is stated to be 13.8kg/hour at full capacity.

When assuming the upper heat output is obtained for completely dry mass and at full capacity, 13.8kg/hour is divided by 20% to obtain the feedstock feed. This means that 69kg/hour or 0.019kg/s is the amount of feedstock fed to the reactor pr. unit time. Three different scenarios are shown in Fig. 5-20 for heat outputs around 100kW.

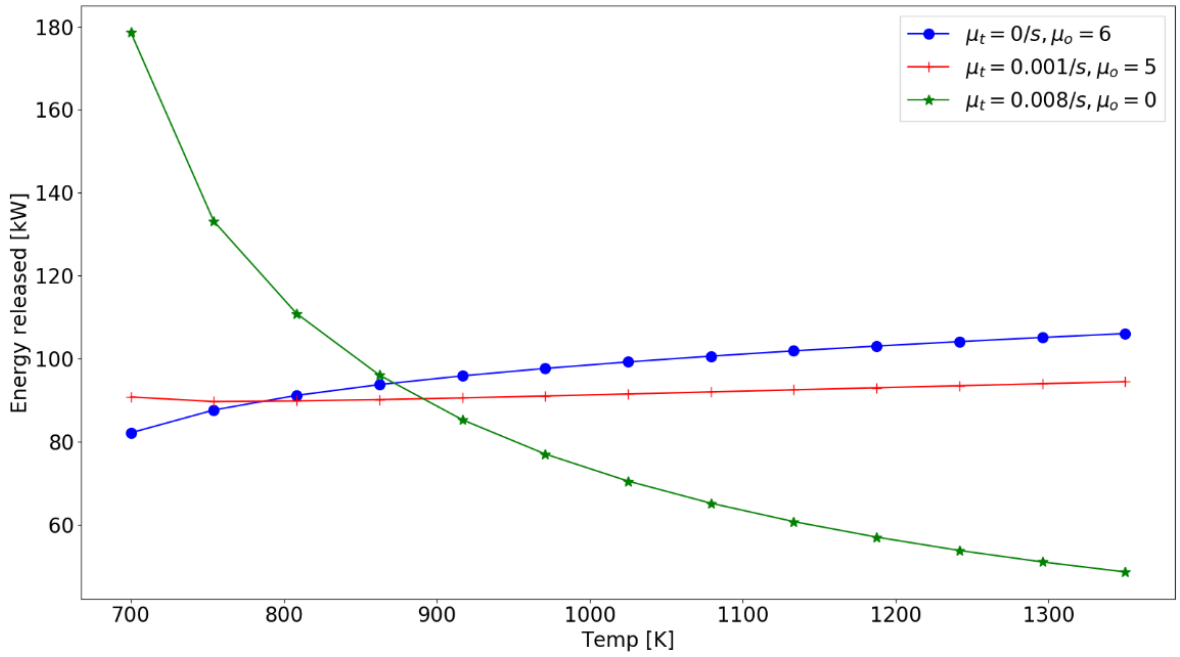

Fig. 5-20: Released heat pr. unit time as a function of temperature with μ_t = 0, 0.001 and 0.008 and μ_o = 6,5,0. The plot is describing energy released with a feedstock feed of 0.019kg/s dry feedstock.

Energy consumed pr. cubic meter dry feedstock is presented in Fig. 5-21.

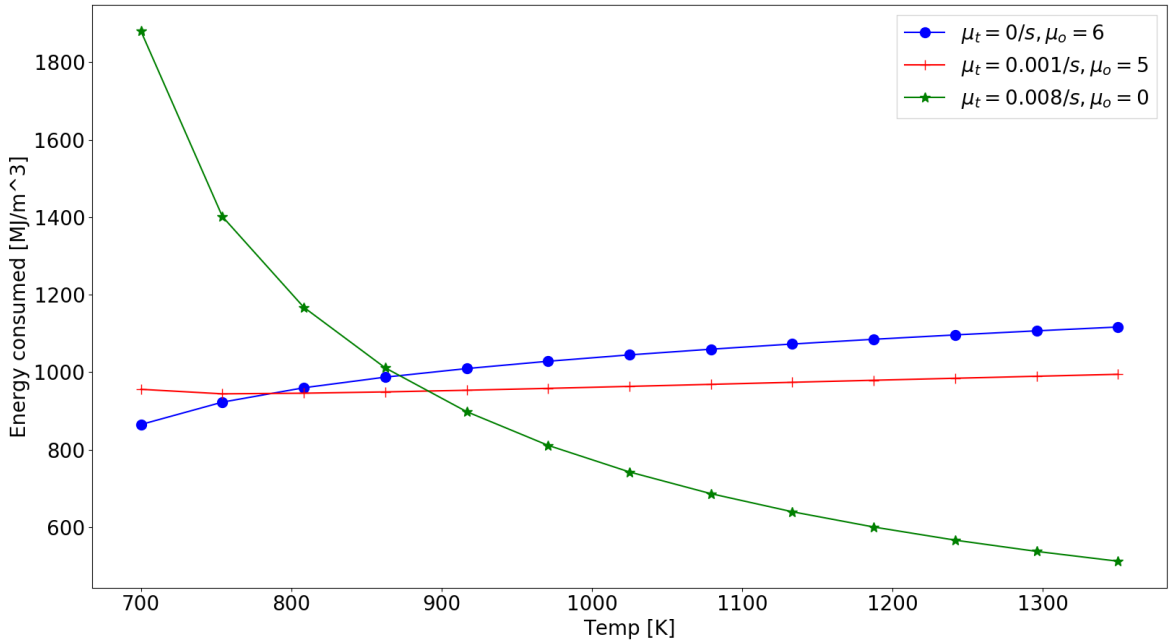

Fig. 5-21: Released heat pr. unit time as a function of temperature with μ_t = 0, 0.001 and 0.008 and μ_o = 6,5 and 0. The plot is describing energy consumed pr. cubic meter dry feedstock with a feedstock feed of 0.019kg/s.

For the same amount of feedstock fed into the reactor, the effect of moist on released heat is shown in Fig. 5-22 with efficiency factors μ_t = 0.001 and μ_o = 5 .

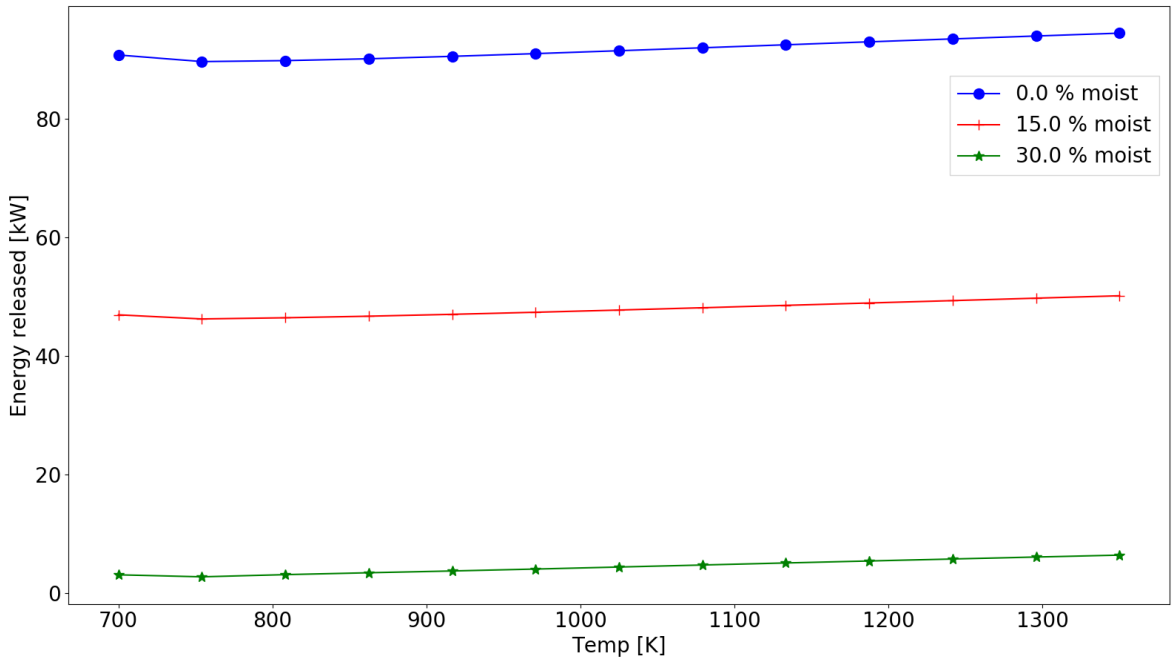

Fig. 5-22: Released heat pr. unit time as a function of temperature with μ_t = 0.001 and μ_o =5. Feeding rate is 0.019kg/s. The plot shows three different values for moist.

6. Discussion

6.1 Reactor model 1:

This model is supposed to represent a fast pyrolysis reactor. The time consumed by the process ranges from 76s to 5s. At temperatures above 1100K, this model falls in the range of the category 'fast' as listed in Table 2-3. The chosen temperature range is below what is listed in Table 2-3 to compare the slow and fast pyrolysis reactor models.

6.1.1 Time consumed and moist

The temperature has a logarithmic effect on the time consumption. For temperatures below 800K the time consumed is rapidly decreasing as temperatures increase. Above 800K, the time consumption is decreasing slower. This effect is due to the values in the kinetics. At low temperatures, decomposition of feedstock into intermediate solid is favorized as this has the lowest activation energy. The pre exponential factor of this reaction is in an order of 10^3 – 10^4 smaller than the other reactions and this is the factor that is describing the rate at which the process runs in this model. This result agrees with the literature as the expected time consumed and char yield are shown to be highest at low temperatures, see Table 2-3.

The rapid evaporation of the water in this model is likely due to the small particle size and high heat transfer coefficient. At lower temperatures, more energy is transferred between the surroundings and the biomass. Water in the feedstock keeps the particle at a low temperature, where the heat transfer is faster, until the water is evaporated.

The neglectable effect on the yields with moist feedstock, shown in Fig. 5-4, could be a result of the low temperature required to evaporate water compared to the temperature of the pyrolysis processes. The feedstock does not decompose as long there is moist present, and the reaction takes place after the moist is evaporated.

A much higher energy consumption is shown to be the case for moist feedstock. When doing a theoretical analysis on energy consumed to run the process, 28% of the feedstock needs to be burned to process feedstock with 50% moist compared to 4.4% on a dry feedstock basis. This energy consumption is 6,36 times higher than dry feedstock.

As mentioned in chapter 2.2.4, the temperature inside the reactor is decreasing along the reactor. This effect is not calculated in this model and the effect on moist may show a different result for the yields as the energy consumed is much higher with moist present and would cause an even bigger decrease in temperature along the reactor.

6.1.2 Yields and energy

The energy consumption with no losses is mainly dominated by the energy required to heat the feedstock to the required temperature. This implies that at lower temperatures, less energy is needed to run the process. For both short and long volatile cooldown times, the main yield is pyrolysis oil at 700K. The biochar yield is also at its highest at these temperatures.

As shown in Table 2-3, the expected product yields under 'fast' pyrolysis conditions are 50% pyrolysis oil, 30% gas and 20% char. With a volatile cooldown time of 0.001 s, this model predicts yields of 59-74% pyrolysis oil, 19-35% gas and 8% char. For a volatile cooldown time of 2s, the yields are about 1% pyrolysis oil, 8% char and 91% gas. The numbers are about the same for 1s volatile cooldown time as shown in appendix B.1. These results do not directly agree with the expected values. The reason for this inconsistency is mostly due to the low char yield. As mentioned in chapter 2.2, the product yields are dependent on several factors and the given parameters could be advantaged for pyrolysis oil over char,

but the char yield is even lower than what is expected even for flash pyrolysis and may be a miscalculation in the model. The miscalculation can be corrected by tuning the kinetic values for intermediate solid.

For the energy released pr. unit time, see Fig. 5-9, the curve is steadily decreasing with temperature. This is a result of the constant feedstock feed and high time consumption in the reactor which gives more time for heat loss through the walls of the reactor.

6.2 Reactor model 1, kinetics 2

This model is simulating a slow pyrolysis auger reactor. The time consumed for 99.9% of the feedstock to decompose is in the range of 1838s to 343s. This model falls into the category 'slow' from Table 2-3, but with a higher time consumption, still lower according to the reactor mentioned in chapter 2.3.3. The temperature range is set to a higher value than usual for slow pyrolysis. This is done to compare the two models. The moist content is chosen to be at a lower rate for this reactor. This is due to the computational load that is required for high moist contents. The high energy required to evaporate water can result in temperature decrease in the model. To avoid this, a high number of time steps is required, and more is needed if the moist is higher.

6.2.1 Time consumed and moist

The time consumed is steadily decreasing with temperature. The slope of the curve is steeper at temperatures below 900K and smoothens thereafter. For this model, the heat transfer is low, and the feedstock is at a low temperature for a long period of time before it gets heated to temperatures where the fast reactions takes place.

The time consumed to process feedstock with 30% moist is almost 4 times higher than dry feedstock on a virgin feedstock basis. The long evaporation time is due to the big body that is treated and the low heat transfer. When the size of the body increases, the outer layers insulate the core, and more time needs to pass before the core gets to a high enough temperature to evaporate the water. This in combination with a low heat transfer gives a long residence time for the feedstock.

As with model 1, the energy consumed is much greater with moist feedstock. See chapter 6.1.1

The gas yield becomes higher with a higher content of moist, and the char yield becomes smaller. The difference is minor but becomes greater with higher temperatures. The reason for this effect could be that the temperature gradient inside the bulk material becomes greater when moist is presented. The moist keeps the solid cooled down. The high heat capacity and heat of evaporation lets the outer layer reach a higher temperature before the water evaporates in the inner layer. The difference at 1350K is about 2 %wt. lower yield for char and higher for gas.

6.2.2 Yields and energy

The yields of this model are mainly dependent on the volatile cooldown time for temperatures above 750K. If the volatile cooldown time is small, the pyrolysis oil yield is increasing to about 1050K and decreasing at higher temperatures. The gas yield is increasing, and the char yield is decreasing for the whole temperature range.

For higher volatile cooldown times, the pyrolysis oil yield will decrease at lower temperatures and the slope of the decrease will be steeper, see Fig. 5-17. The pyrolysis oil does mainly crack into gas as expected from the low activation energy and high pre exponential factor. Only a small fraction becomes char as the pre exponential factor is about 4 time lower

The main yields under the 'slow' pyrolysis conditions, i.e. temperatures under 1100K, see Table 2-3 are either pyrolysis oil and char or gas and char dependent on the volatile cooldown time.

The energy consumption is increasing with temperature, Fig. 5-19. The main energy consumed is energy needed to heat the feedstock and more energy is needed when the temperature is higher.

The predicted heat released from the reactor is tuned into the reactor as explained in chapter 2.3.3. Released heat is calculated to be about 1GJ/m^3 when both μ_t and μ_o contributes to the model and the unused energy stored in the char is calculated to be 4.9MJ/kg or 0.98 GJ/m^3 (from Table 2-3 and 6-1). The energy density in the feedstock is 3,67GJ/m^3 on a dry feedstock basis which leaves about 46.1% of the energy in the feedstock to losses. The reason for the low efficiency could be that the assumption about the highest heat output was obtained with 0% moist is wrong. As calculated in model 1, chapter 5.1.4, an increase of 23,6% of the energy in the feedstock is required to run the process at 50% moist. This shows that even at high levels of moist, there will be a positive energy balance (i.e more energy in the feedstock than what is consumed). The char yield predicted in this model is also low, higher char yields would cause more energy stored and less losses would be predicted. However, the model predicts that an increase in moist with a constant amount of losses results in major decrease in released heat as a result of the increase in energy consumption.

Energy released by the process is almost a straight line when plotted against temperature, but with a small minimum at 800K. See Fig. 5-26 where μ_o = 5 and μ_t = 0.001. The yields for the process at 800K are shown with two different volatile cooldown times in Table 6-1.

Table 6-1: Yields at 800K with long and short volatile cooldown time.

Cooldown time for volatiles [s]	Gas %wt.	Pyrolysis oil %wt.	Char %wt.
0.001	13.1	72	15
1.005	82	0.3	17

As the temperature raises, the char yield decreases for both volatile cooldown times. For a volatile cooldown time of 0.001s, the gas yield increases and oil yield decreases. As this is a slow pyrolysis reactor, the volatiles will be in the reactor for a longer period. In this reactor system, the volatile leaves the reactor as a result of the expanding volume when solids decompose into gas. The long solid residence time inside the reactor implies that a small amount of gas is produced at every instant and stays for longer periods before it escapes.

6.3 Comparing the models

Both models predict the pyrolysis process in a similar way. The effects of moist and energy without losses are similar in both models. The main difference is the time consumed, char yield and released heat. The time consumed in reactor model 2 is much greater than reactor model 1 which causes a higher char yield in model 2.

For both models, the oil yield approaches zero as the temperature and cooldown time of volatiles increases. This prediction disagrees with the literature and is probably caused by the kinetics for the pyrolysis oil. With a secondary oil component introduced, the predicted oil yield would fall into an asymptotic value like the char yields and result in a more accurate prediction. This was not added to the model as the number of variables to fit would increase and the time available for the thesis was limited.

There is less energy released from model 1 than model 2. The parameters μ_t and μ_o are also different for the two. This is caused by the fact that model 2 is supposed to represent a reactor where released heat is wanted and model 1 represents a reactor where the released heat is considered as waste. The fact that

the overall heat transferring constant is much higher in reactor model 1 also implies that the overall efficiency factor is smaller as the heat is transferred to the feedstock more efficiently i.e. higher *h* value.

When calculating the released heat pr. unit time, a constant feedstock feed is used, and the time consumed is not considered. When the feedstock requires less time inside the reactor, a higher feed could be obtained. As a result, higher temperatures would give an even higher amount of released heat as more feedstock is processed.

The heat of reaction is a factor of 10^2 smaller for model 2 compared to model 1 at low temperatures. This is caused by the high char yield, the reaction from intermediate solid to char releases energy and the decomposition into gas and pyrolysis oil consumes energy. As more char is produced, less pyrolysis oil and gas get produced and the overall energy consumption of the reaction decreases fast. The inequality reduces at higher temperatures.

The efficiency factor method that is used for calculating the released heat is shown to produce accurate results but needs to be fitted for a specific temperature range. For temperatures outside the specific range, this method does not hold.

7. Conclusion

The main goal of this study was to construct two mathematical models for optimizing different energy outputs and yields. The effect of moist feedstock and cooldown time for the volatiles were also investigated.

The models predict lower char yields than the literature and zero oil yield at high temperatures with a long volatile cooldown time. This could be a result of wrong estimates in the kinetic values.

For the fast pyrolysis reactor model, the highest heat released pr. unit time was obtained at low temperatures. The model predicted high char and pyrolysis oil yields at these temperatures. The slow pyrolysis reactor released more energy pr. unit time and the energy released was slowly increasing with temperature. The main yields under such conditions are char and pyrolysis oil. As a result of this, the most released heat pr. unit time is obtained when the temperature is high, and gas is the main yield.

From these results, there could be an option to use a slow pyrolysis reactor instead of conventional biomass burners. For this reactor, oil and char could be produced during periods with low energy demand. The char would lead to a negative CO_2 balance if spread on the soil and the oil could be stored and burned under conditions where more heat is needed. Under high energy demand, the temperature in the reactor could be adjusted up which would result in more released energy and high gas yields. Both the pyrolysis oil and char yield are estimated to decrease at temperatures over 1100K.

The fast pyrolysis reactor released most heat pr. unit time at low temperatures. Char and pyrolysis oil are the main yields under these conditions. For the least heat produced pr. unit time, gas is the main yield and due to the nature of gas, storage is difficult and such reactors does not stand as a valid option to a conventional biomass burner.

The cooldown time for the volatiles strongly affected the yields at higher temperatures. For the highest possible oil yield, this work predicts that temperatures around 1100K, low cooldown time of volatiles and fast pyrolysis is the preferred configuration. The highest possible char yield is obtained by low temperatures and slow pyrolysis. For high gas yields, high temperature, fast pyrolysis and long cooldown time of volatiles is preferred.

Moist have a minor effect on the yields, but a major effect on the energy consumed by the process. The energy consumed for feedstock with 50%wt. moist is 5,75 times higher than on a dry feedstock basis. The released heat is shown to fall almost 100% if the moist content is increased with 30% from the initial heat output estimate with a constant amount of losses

7.1 Further work

The models could be tested in experiments. The values that are used are mainly collected from Park et. al (22). Simplifications and changes are done to Park's model and should be verified. This is also the case for data collected regarding the different pyrolysis reactors where feeding rates of feedstock, effects of moist and other values should be investigated to both validate the model and, if needed, tune the values in the model to predict more accurate.

The effect of different feedstock is not considered in this model. A machine learning algorithm could be used to predict the kinetic values in the model to best fit different feedstock. Further, a study on using machine learning for the whole process could be done by collecting experimental data and fill in missing values using sophisticated mathematical models.

A new kinetic reaction should also be investigated. This feature should describe an intermediate pyrolysis oil phase, where the intermediate oil would decompose into gas, char and permanent pyrolysis oil.

Other features added to the models that could be investigated further are particle size of the feedstock and heating rates.

References

1. Smil, V. (2016). *Energy transitions: global and national perspectives*: ABC-CLIO.
2. Laboratory, E. S. R. (2019). *Trends in Atmospheric Carbon Dioxide*. Available at: https://www.esrl.noaa.gov/gmd/ccgg/trends/global.html (accessed: 22.02.2019).
3. Ledenko, M., Velić, J. & Sedlar, D. K. J. R.-G.-N. Z. (2018). Analysis of oil reserves, production and oil price trends in 1995, 2005, 2015. 33 (4): 105.
4. Oreskes, N. J. S. (2004). The scientific consensus on climate change. 306 (5702): 1686-1686.
5. Hunt, J., DuPonte, M., Sato, D., Kawabata, A. J. S. & Management, C. (2010). The basics of biochar: A natural soil amendment. 30 (7): 1-6.
6. DeLuca, T. H., Gundale, M. J., MacKenzie, M. D., Jones, D. L. J. B. f. e. m. s., technology & implementation. (2015). Biochar effects on soil nutrient transformations. 2: 421-454.
7. O'toole, A. & Spindler, K. J. B. R. (2012). Biokull: vurdering og formidling av flere feltforsøk i Norge for å optimalisere biokull som jordforbedringsmiddel og karbonlagringstiltak.
8. Enviroment, N. M. o. C. a. (2015). *New emission commitment for Norway for 2030 – towards joint fulfilment with the EU*. Enviroment, N. M. o. C. a.: Norwegian Ministry of Climate and Enviroment.
9. Maria Kollberg Thomassen, A. O. T., Erik Joner, Roman Tschentscher, Pia Otte, Jostein Vik, Jostein Brobakk, Svein Horn, Lars Vik, Trond Halvorsen (2017). *Utvikling og implementering av biokull som klimatiltak i Norge*. Sintef: Sintef.
10. Biederman, L. A. & Harpole, W. S. J. G. b. (2013). Biochar and its effects on plant productivity and nutrient cycling: a meta-analysis. 5 (2): 202-214.
11. Lang, Å. (2018). *Biobasert gårdsvarme økte med 15 % i fjor*: Norges Skogeierforbund. Available at: https://www.skog.no/nyheter/biobasert-gardsvarme-okte-med-15-i-fjor/ (accessed: 26.02).
12. Kjuus, L. (2016). *Vurder verdien av biovarme*. Norsk Landbruksrådgining Øst: Norsk Landbruksrådgivning. Available at: https://ost.nlr.no/fagartikler/vurder-verdien-av-biovarme/ (accessed: 26.02).
13. Klass, D. L. (1998). *Biomass for renewable energy, fuels, and chemicals*: Elsevier.
14. McKendry, P. J. B. t. (2002). Energy production from biomass (part 1): overview of biomass. 83 (1): 37-46.
15. Basu, P. (2010). *Biomass gasification and pyrolysis: practical design and theory*: Academic press.
16. Sims, R., Taylor, M., Saddler, J., Mabee, W. J. P. I. E. A., Co-Operation, O. f. E. & Development. (2008). From 1st-to 2nd-generation biofuel technologies.
17. © 2017 Zaman CZ, P. K., Yehye WA, Sagadevan S, Shah ST, Adebisi GA, Marliana E, Rafique RF, Bin Johan R. Published in IntechOpen under CC BY 3.0 license. Available from: http://dx.doi.org/10.5772/intechopen.69036.
18. Phyllis2. (2019). *database for biomass and waste*. Available at: https://phyllis.nl/Browse/Standard/ECN-Phyllis (accessed: 11.03).
19. Atsonios, K., Panopoulos, K. D., Bridgwater, T. & Kakaras, E. (2015). Biomass fast pyrolysis energy balance of a 1kg/h test rig.
20. Jahirul, M., Rasul, M., Chowdhury, A. & Ashwath, N. J. E. (2012). Biofuels production through biomass pyrolysis—a technological review. 5 (12): 4952-5001.
21. Diebold, J., Bridgwater, A., Czernik, S., Diebold, J., Meier, D., Oasmaa, A., Peacocke, C., Piskorz, J. & Radlein, D. J. F. p. o. b. A. h. (1999). Overview of fast pyrolysis of biomass for the production of liquid fuels. 1: 14-32.
22. Venderbosch, R., Prins, W. J. B., bioproducts & biorefining. (2010). Fast pyrolysis technology development. 4 (2): 178-208.

23. Mohan, D., Pittman, C. U., Steele, P. H. J. E. & fuels. (2006). Pyrolysis of wood/biomass for bio-oil: a critical review. 20 (3): 848-889.
24. Demirbas, A. J. E. E. S. T. (2000). Recent advances in biomass conversion technologies. 6: 19-41.
25. Jaroenkhasemmeesuk, C. & Tippayawong, N. (2015). Technical and economic analysis of a biomass pyrolysis plant. *Energy Procedia*, 79: 950-955.
26. Jesus, M. S., Napoli, A., Trugilho, P. F., Abreu Júnior, Á. A., Martinez, C. L. M. & Freitas, T. P. (2018). ENERGY AND MASS BALANCE IN THE PYROLYSIS PROCESS OF Eucalyptus WOOD. *CERNE*, 24 (3): 288-294.
27. Heggdal, Ø. (2018). Tester ut biokull produksjon. *Norsk Landbruk*, 20: 40-44.
28. GmbH, P. (2019). *PYROLYSIS GMBH*. Available at: http://pyrolysis.ch/home-2/ (accessed: 26.02).
29. Nygård, H. S. & Olsen, E. J. I. J. o. L.-C. T. (2012). Review of thermal processing of biomass and waste in molten salts for production of renewable fuels and chemicals. 7 (4): 318-324.
30. Sadaka, S. & Boateng, A. A. (2009). *Pyrolysis and bio-oil*: [Cooperative Extension Service], University of Arkansas, US Department of ….
31. Cheng, Y., Wei, F. & Jin, Y. (2017). *Multiphase Reactor Engineering for Clean and Low-carbon Energy Applications*: John Wiley & Sons.
32. Inc., T. (2019). Available at: https://www.sketchup.com/ (accessed: 29.04).
33. Valmet. (2014). *Bio-refining* Available at: https://www.valmet.com/globalassets/media/downloads/white-papers/power-and-recovery/biorefining_whitepaper.pdf (accessed: 27.03).
34. Fortum. (2013). *Joensuu CHP plant*: fortum. Available at: https://www.fortum.com/about-us/our-company/our-energy-production/our-power-plants/joensuu-chp-plant (accessed: 27.03).
35. Arne Bardalen, S. R., Anders Aune, Adam O' Toole, Finn Walland, Hanna Silvennoinen, Ievina Sturite, Fredrik Bøe, Daniel Rasse, Ivar Pettersen, Lillian Øygarden. (2018). *Utslippsreduksjoner i norsk jordbruk Kunnskapsstatus og tiltaksmuligheter* Nibio Rapport.
36. stulz, e. (2019). *PYREG*. Available at: https://www.eliquostulz.com/en/pyreg.html (accessed: 27.03).
37. GmbH, P. (2019). *P-500*. Available at: https://www.pyreg.de/p500-biomasse/ (accessed: 04.03).
38. gmbH, P. (2019). *HOME PAGE*. Available at: https://www.pyreg.de/ (accessed: 04.03).
39. Park, W. C., Atreya, A., Baum, H. R. J. C. & Flame. (2010). Experimental and theoretical investigation of heat and mass transfer processes during wood pyrolysis. 157 (3): 481-494.
40. Yuming Zhang, R. L., Lei Huang, Liang Zhang, Guogang Sun and Shu Zhang. (2018). Effects of Secondary reaction of Primary Volatiles on Oil/gas Yield and Quality from Oil Shale Pyrolysis. *InternationalJournal of Petrochemistry and Research* 2(2): 11.
41. Janković, B., Manić, N., Stojiljković, D. & Jovanović, V. (2018). TSA-MS characterization and kinetic study of the pyrolysis process of various types of biomass based on the Gaussian multi-peak fitting and peak-to-peak approaches. *Fuel*, 234: 447-463. doi: https://doi.org/10.1016/j.fuel.2018.07.051.
42. Kyurkchiev, N. & Markov, S. J. S. M. i. P. E. M., ISBN. (2015). Sigmoid functions: some approximation and modelling aspects. 978-3.
43. Antal, M. J. (1983). Effects of reactor severity on the gas-phase pyrolysis of cellulose- and kraft lignin-derived volatile matter. *Industrial & Engineering Chemistry Product Research and Development*, 22 (2): 366-375. doi: 10.1021/i300010a039.
44. Rasul, M. & Jahirul, M. I. (2012). Recent developments in biomass pyrolysis for bio-fuel production: Its potential for commercial applications. *Central Queensland University, Centre for Plant and Water Science, Faculty of Sciences, Engineering and Health*.

45. Schroeder, D. V. (2014). *An Introduction to Thermal Physics*, vol. First Edition. Edinburgh Gate, Harlow, Essex CM20 2JE: Pearson Education Limitied.
46. MacLean, J. J. H., piping & air conditioning. Madison, U. (1941). Thermal conductivity of wood.
47. Ross, R. J. J. U. F. S., Forest Products Laboratory, General Technical Report FPL-GTR-190, : 509 p. 1 v. (2010). Wood handbook: wood as an engineering material. 190.
48. *Engineering ToolBox, (2003). Gases - Densities. [online] Available at: https://www.engineeringtoolbox.com/gas-density-d_158.html, cited: [01.05.2019].* .
49. Aschjem, C. (2019). *Code, model 1*. GitHub. Available at: https://github.com/cwsa/Master/blob/master/model1 (accessed: 06.05).
50. Wiggins, G. (2016). *Copyright (c) 2016 Computational Pyrolysis Consortium, CSTR modeling approach for fluidized bed reactors*. GitHub. Available at: https://github.com/ccpcode/low-order-reactor (accessed: 15.12).
51. Aschjem, C. (2019). *Code, model 2*. GitHub. Available at: https://github.com/cwsa/Master/blob/master/Model2 (accessed: 06.05).
52. Kofman, P. D. (2006). Quality wood chip fuel. *Danish Forestry Extension. Accessed*, 22.

Appendix A, scheme for heat equation

A.1 Scheme for 1D heat equation

Next time step is solved by setting up the set of equations.

$$\begin{aligned}
-\lambda T_{X+1}^{n} + T_X^n(1+2\lambda) - \lambda T_{X-1}^{n} &= T_X^{n-1} + q_X^n\,\Delta t \\
&\dots\dots\dots \\
-\lambda T_{l+2}^{n} + T_{l+1}^n(1+2\lambda) - \lambda T_l^{n} &= T_{l+1}^{n-1} + q_{l+1}^n\,\Delta t \\
-\lambda T_{l+1}^{n} + T_l^n(1+2\lambda) - \lambda T_{l-1}^{n} &= T_l^{n-1} + q_l^n\,\Delta t \\
-\lambda T_{l}^{n} + T_{l-1}^n(1+2\lambda) - \lambda T_{l-2}^{n} &= T_{l-1}^{n-1} + q_{l-1}^n\,\Delta t \\
&\dots\dots\dots \\
-\lambda T_{-1}^{n} + T_0^n(1+2\lambda) - \lambda T_1^{n} &= T_0^{n-1} + q_0^n\,\Delta t
\end{aligned} \tag{A - 1}$$

This can be represented in matrix form

$$Ax = b \tag{A - 2}$$

Where A, x and b are shown in eq. (A - 3)-(A - 5).

$$A = \begin{bmatrix}
(1+2\lambda) & -2*\lambda & 0 & 0 & \cdots & 0 & 0 \\
-\lambda & (1+2\lambda) & -\lambda & 0 & \cdots & 0 & 0 \\
0 & -\lambda & (1+2\lambda) & \ddots & \ddots & \vdots & \vdots \\
0 & 0 & \ddots & \ddots & -\lambda & 0 & 0 \\
\vdots & \vdots & \ddots & -\lambda & (1+2\lambda) & -\lambda & 0 \\
0 & 0 & \cdots & 0 & -\lambda & (1+2\lambda) & -\lambda \\
0 & 0 & \cdots & 0 & 0 & -\lambda & 1+\lambda(1+\frac{h*\Delta x}{k})
\end{bmatrix} \tag{A - 3}$$

$$x = \begin{bmatrix} T_0^n \\ \vdots \\ T_j^n \\ \vdots \\ T_X^n \end{bmatrix} \tag{A - 4}$$

$$b = \begin{bmatrix}
T_0^{n-1} + q_0^n \dfrac{\Delta t}{\overline{Cp_0^n} * \overline{\rho_0^n}} \\
\vdots \\
T_l^{n-1} + q_l^n \dfrac{\Delta t}{\overline{Cp_l^n} * \overline{\rho_l^n}} \\
\vdots \\
T_X^{n-1} + q_X^n \dfrac{\Delta t}{\overline{Cp_X^n} * \overline{\rho_X^n}} + \dfrac{h*\Delta x}{k} * Tinf
\end{bmatrix} \tag{A - 5}$$

Each time step will then be calculated by solving eq.(A - 2) for x. This is done by inverting A and do a dot multiplication of b with A^{-1}.

$$x = b \cdot A^{-1} \tag{A - 6}$$

A.2 Scheme for 2D heat equation

The heat equation in two dimensions:

$$\frac{\partial T}{\partial t} = \alpha\left(\frac{\partial^2 T}{\partial x^2} + \frac{\partial^2 T}{\partial y^2}\right) + q \tag{A - 7}$$

On approximate form:

$$\frac{(T_{l,j}^{n-1} - T_{l,j}^{n})}{\Delta t} \approx \alpha\left(\frac{(T_{l+1,j}^{n} - 2T_{l,j}^{n} + T_{l-1,j}^{n})}{\Delta x^2} + \frac{(T_{l,j+1}^{n} - 2T_{l,j}^{n} + T_{l,j-1}^{n})}{\Delta y^2}\right) + q_{l,j}^{n} \tag{A - 8}$$

Rearranging

$$T_{l,j}^{n} + \lambda_x\left(T_{l+1,j}^{n} - 2T_{l,j}^{n} + T_{l-1,j}^{n}\right) + \lambda_y(T_{l+1,j}^{n} - 2T_{l,j}^{n} + T_{l-1,j}^{n}) \approx T_{l,j}^{n-1} + q_{l,j}^{n} * \Delta t \tag{A - 9}$$

$$\lambda_x = \frac{k*\Delta t}{\Delta x^2 * C_p * \rho} = \frac{\alpha*\Delta t}{\Delta x^2} \tag{A - 10}$$

$$\lambda_y = \frac{k*\Delta t}{\Delta y^2 * C_p * \rho} = \frac{\alpha*\Delta t}{\Delta y^2} \tag{A - 11}$$

This set of equations can be represented in matrix form.

$$Ax = b \tag{A - 12}$$

To obtain this, the matrix containing the temperatures needs to be reshaped. A representation of x and b is shown in eq.

(A - 14), (A - 15) respectively. Here the matrixes are reshaped column vise, i.e. each column vector in the matrix is set under the previous.

$$x = \begin{bmatrix} T_{0,0}^{n} & T_{0,1}^{n} & \dots & T_{0,j}^{n} & \dots & T_{0,Y}^{n} \\ T_{1,0}^{n} & T_{1,1}^{n} & \dots & T_{1,j}^{n} & \dots & T_{1,Y}^{n} \\ \vdots & \vdots & \dots & \vdots & \dots & \vdots \\ T_{l,0}^{n} & T_{l,1}^{n} & \dots & T_{l,j}^{n} & \dots & T_{l,Y}^{n} \\ \vdots & \vdots & \dots & \vdots & \dots & \vdots \\ T_{X-1,0}^{n} & T_{X-1,1}^{n} & \dots & T_{X-1,j}^{n} & \dots & T_{X-1,Y}^{n} \\ T_{X,0}^{n} & T_{X,1}^{n} & \dots & T_{X,j}^{n} & \dots & T_{X,Y}^{n} \end{bmatrix} \tag{A - 13}$$

$$x = \begin{bmatrix} T_{0,0}^{n} \\ \vdots \\ T_{l,0}^{n} \\ \vdots \\ T_{X,0}^{n} \\ - - - \\ T_{0,1}^{n} \\ \vdots \\ - - - \\ T_{0,j}^{n} \\ \vdots \\ T_{X-1,Y}^{n} \\ T_{X,Y}^{n} \end{bmatrix} \tag{A - 14}$$

$$b = \begin{bmatrix} T_{0,0}^{n-1} + 2q_{surface} + \Delta t * q_{reaction} \\ \vdots \\ T_{l,0}^{n-1} + 1q_{surface} + \Delta t * q_{reaction} \\ \vdots \\ T_{X,0}^{n-1} + 2q_{surface} + \Delta t * q_{reaction} \\ - - - \\ T_{0,1}^{n-1} + 1q_{surface} + \Delta t * q_{reaction} \\ T_{1,1}^{n-1} + \Delta t * q_{reaction} \\ \vdots \\ - - - \\ T_{0,j}^{n-1} + 1q_{surface} + \Delta t * q_{reaction} \\ \vdots \\ T_{X-1,Y}^{n-1} + 1q_{surface} + \Delta t * q_{reaction} \\ T_{X,Y}^{n-1} + 2q_{surface} + \Delta t * q_{reaction} \end{bmatrix} \tag{A - 15}$$

For each row vector there is a loading matrix. The matrix A will be a block matrix, where each block is represented as the loading matrix for each row vector

$$A = \begin{bmatrix} B & -\lambda_y I & 0 & 0 & \cdots & 0 \\ -\lambda_y I & B & -\lambda_y I & 0 & \cdots & 0 \\ \vdots & & \ddots & & \vdots & \\ 0 & 0 & -\lambda_y I & B & -\lambda_y I & 0 \\ 0 & 0 & \cdots & -\lambda_y I & B & -\lambda_y I \\ 0 & 0 & \cdots & 0 & -\lambda_y I & B \end{bmatrix} \tag{A - 16}$$

Here *I* is the identity matrix, and *B* is the loading matrix for each row vector. Given in eq.(A - 17).

$$B = \begin{bmatrix} 1 + \lambda_y + \lambda_x + q_{out-x}^{n} + q_{out-y}^{n} & -\lambda_x & 0 & 0 & \cdots & 0 \\ -\lambda_x & 1 + \lambda_y + 2\lambda_x + q_{out-y}^{n} & -\lambda_x & 0 & \cdots & 0 \\ \vdots & & \ddots & & \vdots & \\ 0 & 0 & -\lambda_x & 1 + 1\lambda_y + 2\lambda_x + q_{out-y}^{n} & -\lambda_x & 0 \\ 0 & 0 & \cdots & -\lambda_x & 1 + 1\lambda_y + 2\lambda_x + q_{out-y}^{n} & -\lambda_2 \\ 0 & 0 & \cdots & 0 & -\lambda_x & 1 + \lambda_1 + \lambda_2 + q_{out-x}^{n} + q_{out-y}^{n} \end{bmatrix} \tag{A - 17}$$

Notice that at the boundaries are having the additional terms q^{n}_{out} for both spatial directions, for 1 surface node, the boundary are solved in eq.(4.21) for two, the solution is given in eq.(A - 18).

$$T_{X,Y}^{n} * \left(1 + \ \lambda_x + \lambda_y \ + \frac{h_X * \Delta t}{\Delta x * C_p * \rho} + \frac{h_Y * \Delta t}{\Delta y * C_p * \rho}\right) - \lambda T_{X-1}^{n} - \lambda T_{Y-1}^{n} = +T_X^{n-1} + \frac{h_Y * \Delta t * T_{inf}}{\Delta y * C_p * \rho} + \frac{h * \Delta t * T_{inf}}{\Delta x * C_p * \rho} + \Delta t * q_{reaction} \quad \text{(A - 18)}$$

This equation looks messy but are just eq. (4.21) expanded to two dimensions and a second surface flux is added. If there are three surface areas at a node, one of the λ's is changed to a surface flux.

The scheme for the surface nodes is represented below.

For an internal node, with the matrix containing the λ value for each node restacked column wise. The following is obtained:

$$A_{l,l} = 1 - (1 \quad 1 \quad 1 \quad 1) \cdot \begin{pmatrix} -\frac{\lambda_{l-1}}{dx^2} \\ -\frac{\lambda_{l+1}}{dx^2} \\ -\frac{\lambda_{l-1*nx}}{dy^2} \\ -\frac{\lambda_{l+nx}}{dy^2} \end{pmatrix} \quad \text{(A - 19)}$$

$$A_{l-1,l} = (1 \quad 0 \quad 0 \quad 0) \cdot \begin{pmatrix} -\frac{\lambda_{l-1}}{dx^2} \\ -\frac{\lambda_{l+1}}{dx^2} \\ -\frac{\lambda_{l-1*nx}}{dy^2} \\ -\frac{\lambda_{l+nx}}{dy^2} \end{pmatrix} \quad \text{(A - 20)}$$

$$A_{l+1,l} = (0 \quad 1 \quad 0 \quad 0) \cdot \begin{pmatrix} -\frac{\lambda_{l-1}}{dx^2} \\ -\frac{\lambda_{l+1}}{dx^2} \\ -\frac{\lambda_{l-1*nx}}{dy^2} \\ -\frac{\lambda_{l+nx}}{dy^2} \end{pmatrix} \quad \text{(A - 21)}$$

$$A_{l,l-nx} = (0 \quad 0 \quad 1 \quad 0) \cdot \begin{pmatrix} -\frac{\lambda_{l-1}}{dx^2} \\ -\frac{\lambda_{l+1}}{dx^2} \\ -\frac{\lambda_{l-1*nx}}{dy^2} \\ -\frac{\lambda_{l+nx}}{dy^2} \end{pmatrix} \quad \text{(A - 22)}$$

$$A_{l,l+nx} = \begin{pmatrix} 0 & 0 & 0 & 1 \end{pmatrix} \cdot \begin{pmatrix} -\frac{\lambda_{l-1}}{dx^2} \\ -\frac{\lambda_{l+1}}{dx^2} \\ -\frac{\lambda_{l-1*nx}}{dy^2} \\ -\frac{\lambda_{l+nx}}{dy^2} \end{pmatrix} \quad \text{(A - 23)}$$

If there is a surface node, ex. To the upper right the scheme will be:

$$A_{l,l} = 1 - \begin{pmatrix} 1 & 1 & 1 & 1 \end{pmatrix} \cdot \begin{pmatrix} -\frac{dt}{Cp_i * \rho_i * dx} * h \\ -\frac{\lambda_{l+1}}{dx^2} \\ -\frac{\lambda_{l-1*nx}}{dy^2} \\ -\frac{\lambda_{l+nx}}{dy^2} \end{pmatrix} \quad \text{(A - 24)}$$

$$A_{l-1,l} = -\begin{pmatrix} 0 & 0 & 0 & 0 \end{pmatrix} \cdot \begin{pmatrix} -\frac{\lambda_{l-1}}{dx^2} \\ -\frac{\lambda_{l+1}}{dx^2} \\ -\frac{\lambda_{l-1*nx}}{dy^2} \\ -\frac{\lambda_{l+nx}}{dy^2} \end{pmatrix} \quad \text{(A - 25)}$$

The rest of the block matrix is shown in eq.(A - 21)-

(A - 23). Vector b is shown in eq. (A - 26).

$$b = \begin{pmatrix} \vdots \\ T^{n-1}{}_{nx-1,j-1} + q_{nx-1,j-1} \\ - - - - - - - - - \\ T_{0,j}^{n-1} + T_{inf} \frac{dt}{Cp_i * \rho_i * dx} h + q_{0,j} \\ T_{1,j}^{n-1} + q_{1,j} \\ \vdots \end{pmatrix} \quad \text{(A - 26)}$$

The equation for the next time step is given by:

$$x = A^{-1} b \quad \text{(A - 27)}$$

A.3 Scheme for kinetic models.

This will be solved using an explicit method.

First, the initial values are initiated.

$$\rho'^{c,0} = [\rho_{init}^{c,0}, 0 \dots, 0] \quad \text{(A - 28)}$$

Where c is the component. Followed by the actual densities, fractions and thermal values.

$$\rho^{*c,0} = \rho'^{c,0} * \rho^{c,0} \quad \text{(A - 29)}$$

$$Y_l^0 = \frac{\rho^{*c,0}}{\sum \rho^{*l,0}} \quad \text{(A - 30)}$$

$$e^0 = \frac{Y_{virgin\ feedstock}}{Y_s} \quad \text{(A - 31)}$$

$$\beta = Y_s^0 + \frac{Y_v^0}{\rho_{volatilies}} \rho_{solids} \quad \text{(A - 32)}$$

$$C_{p_l}^{\ 0} = C_{p_l}(T^0) \quad \text{(A - 33)}$$

$$\overline{C_p^0}(T) = \frac{\left(\sum_l C_{p_l}^0(T)\right)}{n_{comp}} \quad \text{(A - 34)}$$

$$\overline{\sigma_{i,j}^n} = \frac{\left(\sum_{comp\ l} k_l\right)}{n_{comp}} \quad \text{(A - 35)}$$

Where Y is the wt.% of the component of interest, and $\rho^{*c,0}$ is the partial density of the component inside the control volume.

Next, the kinetic rate is calculated.

$$\sigma_{i,j}^{c,0} = A_C * e^{-\frac{E_c}{R * T_{i,j}^0}} \quad \text{(A - 36)}$$

The rate pr. time are given by:

$$\frac{c_{i,j}^1 - c_{i,j}^0}{dt} = k_{c,i,j}^0 * c_{i,j}^0 \quad \text{(A - 37)}$$

And the new fraction of each component is then:

$$c_{i,j}^1 = k * c_{i,j}^0 * dt + c_{i,j}^0 \quad \text{(A - 38)}$$

The heat of reaction:

$$q_{i,j}^0 = \sum (c_{i,j}^1 - c_{i,j}^0) * \Delta h_c * \rho^c \quad \text{(A - 39)}$$

Effective density:

$$\bar{\rho} = \sum \rho^{*i,0} \quad \text{(A - 40)}$$

Heat energy consumed:

$$E' = \overline{C_p^0}(T) * \bar{\rho} * \Delta T^0 \quad \text{(A - 41)}$$

Finally, the heat equation is solved as shown in Appendix A.1 or A.2. After that, this scheme is repeated for the next time step until the final time is reached.

The total energy consumed is calculated by using the trapezoid method on *E'* and *q* with the vector containing time and summing the values.

Appendix B. Raw data results.

B.1 Results reactor model 1, kinetics 2.

The Table over all the data collected from reactor model 2 are shown in Table B-1. The code used to produce the results is available on github[49]

Table B-1: All data collected from model 1.

Vol inside time [s]	Moist %wt	Temperature [K]	Char %wt	Final Gas %wt	Final Oil %wt	Heat of reaction [J/m³]	Heat Energy [J/m³]	Time to 0,1% Biomass [s]
0,00	0,00	700	0,15	0,14	0,72	$-2{,}23*10^{4}$	$5{,}05*10^{8}$	73,18
1,00	0,00	700	0,15	0,17	0,70	$1{,}91*10^{4}$	$-5{,}05*10^{8}$	73,19
2,00	0,00	700	0,15	0,20	0,67	$1{,}62*10^{4}$	$-5{,}05*10^{8}$	73,18
0,00	25,00	700	0,11	0,10	0,54	$-5{,}64*10^{8}$	$-4{,}43*10^{8}$	74,70
1,00	25,00	700	0,11	0,12	0,52	$-5{,}64*10^{8}$	$-4{,}43*10^{8}$	74,70
2,00	25,00	700	0,11	0,14	0,50	$-5{,}64*10^{8}$	$-4{,}43*10^{8}$	74,70
0,00	50,00	700	0,07	0,07	0,36	$-1{,}13*10^{9}$	$-3{,}99*10^{8}$	75,96
1,00	50,00	700	0,07	0,08	0,35	$-1{,}13*10^{9}$	$-3{,}99*10^{8}$	75,96
2,00	50,00	700	0,07	0,09	0,34	$-1{,}13*10^{9}$	$-3{,}99*10^{8}$	75,96
0,00	0,00	754	0,12	0,15	0,74	$4{,}80*10^{3}$	$-5{,}48*10^{8}$	26,83
1,00	0,00	754	0,12	0,25	0,65	$2{,}63*10^{3}$	$-5{,}48*10^{8}$	26,84
2,00	0,00	754	0,13	0,33	0,56	$7{,}79*10^{2}$	$-5{,}48*10^{8}$	26,84
0,00	25,00	754	0,09	0,11	0,56	$-5{,}64*10^{8}$	$-4{,}76*10^{8}$	29,98
1,00	25,00	754	0,09	0,18	0,48	$-5{,}64*10^{8}$	$-4{,}77*10^{8}$	29,99
2,00	25,00	754	0,09	0,24	0,42	$-5{,}64*10^{8}$	$-4{,}77*10^{8}$	29,99
0,00	50,00	754	0,05	0,07	0,38	$-1{,}13*10^{9}$	$-4{,}23*10^{8}$	33,39
1,00	50,00	754	0,06	0,12	0,32	$-1{,}13*10^{9}$	$-4{,}23*10^{8}$	33,40
2,00	50,00	754	0,06	0,16	0,28	$-1{,}13*10^{9}$	$-4{,}23*10^{8}$	33,40
0,00	0,00	807	0,11	0,15	0,75	$2{,}81*10^{3}$	$-5{,}77*10^{8}$	16,76
1,00	0,00	807	0,11	0,42	0,47	$-4{,}28*10^{2}$	$-5{,}77*10^{8}$	16,78
2,00	0,00	807	0,12	0,59	0,27	$-2{,}0*10^{3}$	$-5{,}77*10^{8}$	16,79
0,00	25,00	807	0,08	0,11	0,57	$-5{,}64*10^{8}$	$-4{,}99*10^{8}$	20,13
1,00	25,00	807	0,08	0,31	0,35	$-5{,}64*10^{8}$	$-5{,}0*10^{8}$	20,15
2,00	25,00	807	0,08	0,44	0,19	$-5{,}64*10^{8}$	$-5{,}0*10^{8}$	20,15
0,00	50,00	807	0,05	0,07	0,38	$-1{,}13*10^{9}$	$-4{,}40*10^{8}$	23,77
1,00	50,00	807	0,05	0,21	0,23	$-1{,}13*10^{9}$	$-4{,}40*10^{8}$	23,77
2,00	50,00	807	0,05	0,29	0,11	$-1{,}13*10^{9}$	$-4{,}40*10^{8}$	23,77
0,00	0,00	861	0,10	0,16	0,76	$2{,}24*10^{3}$	$-5{,}96*10^{8}$	12,84
1,00	0,00	861	0,11	0,68	0,20	$-2{,}31*10^{3}$	$-5{,}97*10^{8}$	12,87
2,00	0,00	861	0,11	0,83	0,04	$-1{,}57*10^{3}$	$-5{,}97*10^{8}$	12,86
0,00	25,00	861	0,07	0,11	0,57	$-5{,}64*10^{8}$	$-5{,}15*10^{8}$	16,17
1,00	25,00	861	0,08	0,51	0,14	$-5{,}64*10^{8}$	$-5{,}15*10^{8}$	16,19
2,00	25,00	861	0,07	0,62	0,02	$-5{,}64*10^{8}$	$-5{,}15*10^{8}$	16,18
0,00	50,00	861	0,03	0,05	0,27	$-1{,}13*10^{9}$	$-4{,}44*10^{8}$	18,82
1,00	50,00	861	0,03	0,23	0,02	$-1{,}13*10^{9}$	$-4{,}42*10^{8}$	18,74
2,00	50,00	861	0,04	0,32	0,00	$-1{,}13*10^{9}$	$-4{,}45*10^{8}$	18,93
0,00	0,00	914	0,09	0,16	0,76	$1{,}92*10^{3}$	$-6{,}11*10^{8}$	10,60
1,00	0,00	914	0,11	0,86	0,03	$-2{,}49*10^{3}$	$-6{,}11*10^{8}$	10,63

2,00	0,00	914	0,10	0,90	0,01	$-2,40*10^{2}$	$-6,11*10^{8}$	10,62
0,00	25,00	914	0,07	0,11	0,57	$-5,64*10^{8}$	$-5,26*10^{8}$	13,81
1,00	25,00	914	0,07	0,65	0,02	$-5,64*10^{8}$	$-5,27*10^{8}$	13,82
2,00	25,00	914	0,07	0,67	0,00	$-5,64*10^{8}$	$-5,26*10^{8}$	13,81
0,00	50,00	914	0,02	0,03	0,18	$-1,13*10^{9}$	$-4,42*10^{8}$	16,29
1,00	50,00	914	0,03	0,25	0,00	$-1,13*10^{9}$	$-4,46*10^{8}$	16,47
2,00	50,00	914	0,02	0,19	0,00	$-1,13*10^{9}$	$-4,40*10^{8}$	16,24
0,00	0,00	968	0,09	0,16	0,76	$1,99*10^{3}$	$-6,22*10^{8}$	9,11
1,00	0,00	968	0,10	0,90	0,01	$-1,91*10^{3}$	$-6,23*10^{8}$	9,13
2,00	0,00	968	0,09	0,90	0,00	$6,51*10^{2}$	$-6,22*10^{8}$	9,12
0,00	25,00	968	0,06	0,12	0,57	$-5,64*10^{8}$	$-5,35*10^{8}$	12,15
1,00	25,00	968	0,07	0,68	0,00	$-5,64*10^{8}$	$-5,35*10^{8}$	12,16
2,00	25,00	968	0,06	0,68	0,00	$-5,64*10^{8}$	$-5,35*10^{8}$	12,15
0,00	50,00	968	0,04	0,08	0,38	$-1,13*10^{9}$	$-4,65*10^{8}$	15,37
1,00	50,00	968	0,04	0,45	0,00	$-1,13*10^{9}$	$-4,65*10^{8}$	15,37
2,00	50,00	968	0,04	0,45	0,00	$-1,13*10^{9}$	$-4,65*10^{8}$	15,37
0,00	0,00	1022	0,09	0,17	0,76	$1,96*10^{3}$	$-6,31*10^{8}$	8,02
1,00	0,00	1022	0,09	0,91	0,01	$-1,17*10^{3}$	$-6,32*10^{8}$	8,03
2,00	0,00	1022	0,09	0,91	0,01	$1,19*10^{3}$	$-6,31*10^{8}$	8,02
0,00	25,00	1022	0,06	0,12	0,57	$-5,64*10^{8}$	$-5,42*10^{8}$	10,89
1,00	25,00	1022	0,06	0,68	0,00	$-5,64*10^{8}$	$-5,42*10^{8}$	10,90
2,00	25,00	1022	0,06	0,68	0,00	$-5,64*10^{8}$	$-5,42*10^{8}$	10,89
0,00	50,00	1022	0,04	0,08	0,38	$-1,13*10^{9}$	$-4,70*10^{8}$	13,92
1,00	50,00	1022	0,04	0,46	0,00	$-1,13*10^{9}$	$-4,70*10^{8}$	13,93
2,00	50,00	1022	0,04	0,46	0,00	$-1,13*10^{9}$	$-4,70*10^{8}$	13,92
0,00	0,00	1075	0,08	0,18	0,75	$1,89*10^{3}$	$-6,39*10^{8}$	7,18
1,00	0,00	1075	0,09	0,91	0,01	$-5,63*10^{2}$	$-6,40*10^{8}$	7,19
2,00	0,00	1075	0,08	0,91	0,01	$1,53*10^{3}$	$-6,39*10^{8}$	7,18
0,00	25,00	1075	0,06	0,13	0,57	$-5,64*10^{8}$	$-5,48*10^{8}$	9,89
1,00	25,00	1075	0,06	0,68	0,00	$-5,64*10^{8}$	$-5,48*10^{8}$	9,90
2,00	25,00	1075	0,06	0,68	0,00	$-5,64*10^{8}$	$-5,48*10^{8}$	9,89
0,00	50,00	1075	0,04	0,09	0,38	$-1,13*10^{9}$	$-4,75*10^{8}$	12,75
1,00	50,00	1075	0,04	0,46	0,00	$-1,13*10^{9}$	$-4,75*10^{8}$	12,75
2,00	50,00	1075	0,04	0,46	0,00	$-1,13*10^{9}$	$-4,75*10^{8}$	12,75
0,00	0,00	1129	0,08	0,19	0,74	$1,80*10^{3}$	$-6,46*10^{8}$	6,52
1,00	0,00	1129	0,09	0,91	0,01	$-8,87*10^{1}$	$-6,47*10^{8}$	6,52
2,00	0,00	1129	0,08	0,91	0,01	$1,76*10^{3}$	$-6,46*10^{8}$	6,52
0,00	25,00	1129	0,06	0,14	0,56	$-5,64*10^{8}$	$-5,53*10^{8}$	9,08
1,00	25,00	1129	0,06	0,68	0,00	$-5,64*10^{8}$	$-5,54*10^{8}$	9,08
2,00	25,00	1129	0,06	0,68	0,00	$-5,64*10^{8}$	$-5,53*10^{8}$	9,08
0,00	50,00	1129	0,03	0,09	0,37	$-1,13*10^{9}$	$-4,78*10^{8}$	11,77
1,00	50,00	1129	0,03	0,46	0,00	$-1,13*10^{9}$	$-4,78*10^{8}$	11,77
2,00	50,00	1129	0,03	0,46	0,00	$-1,13*10^{9}$	$-4,78*10^{8}$	11,77
0,00	0,00	1182	0,08	0,22	0,72	$1,63*10^{3}$	$-6,53*10^{8}$	5,97
1,00	0,00	1182	0,08	0,91	0,01	$3,06*10^{2}$	$-6,53*10^{8}$	5,98
2,00	0,00	1182	0,08	0,91	0,01	$1,94*10^{3}$	$-6,53*10^{8}$	5,97

0,00	25,00	1182	0,06	0,16	0,54	$-5,64*10^{8}$	$-5,58*10^{8}$	8,40
1,00	25,00	1182	0,06	0,68	0,00	$-5,64*10^{8}$	$-5,58*10^{8}$	8,40
2,00	25,00	1182	0,05	0,68	0,00	$-5,64*10^{8}$	$-5,58*10^{8}$	8,39
0,00	50,00	1182	0,03	0,11	0,36	$-1,13*10^{9}$	$-4,82*10^{8}$	10,94
1,00	50,00	1182	0,03	0,46	0,00	$-1,13*10^{9}$	$-4,82*10^{8}$	10,94
2,00	50,00	1182	0,03	0,46	0,00	$-1,13*10^{9}$	$-4,82*10^{8}$	10,94
0,00	0,00	1236	0,08	0,25	0,69	$1,36*10^{3}$	$-6,58*10^{8}$	5,52
1,00	0,00	1236	0,08	0,92	0,01	$5,95*10^{2}$	$-6,58*10^{8}$	5,52
2,00	0,00	1236	0,08	0,92	0,01	$1,95*10^{3}$	$-6,58*10^{8}$	5,51
0,00	25,00	1236	0,05	0,18	0,52	$-5,64*10^{8}$	$-5,63*10^{8}$	7,81
1,00	25,00	1236	0,05	0,69	0,00	$-5,64*10^{8}$	$-5,62*10^{8}$	7,81
2,00	25,00	1236	0,05	0,69	0,00	$-5,64*10^{8}$	$-5,62*10^{8}$	7,81
0,00	50,00	1236	0,03	0,12	0,35	$-1,13*10^{9}$	$-4,85*10^{8}$	10,23
1,00	50,00	1236	0,03	0,46	0,00	$-1,13*10^{9}$	$-4,84*10^{8}$	10,22
2,00	50,00	1236	0,03	0,46	0,00	$-1,13*10^{9}$	$-4,84*10^{8}$	10,22
0,00	0,00	1289	0,08	0,29	0,65	$1,0*10^{3}$	$-6,64*10^{8}$	5,13
1,00	0,00	1289	0,08	0,92	0,01	$8,82*10^{2}$	$-6,64*10^{8}$	5,13
2,00	0,00	1289	0,07	0,92	0,01	$2,02*10^{3}$	$-6,63*10^{8}$	5,13
0,00	25,00	1289	0,05	0,21	0,48	$-5,64*10^{8}$	$-5,66*10^{8}$	7,31
1,00	25,00	1289	0,05	0,69	0,00	$-5,64*10^{8}$	$-5,66*10^{8}$	7,31
2,00	25,00	1289	0,05	0,69	0,00	$-5,64*10^{8}$	$-5,66*10^{8}$	7,31
0,00	50,00	1289	0,03	0,14	0,32	$-1,13*10^{9}$	$-4,87*10^{8}$	9,60
1,00	50,00	1289	0,03	0,46	0,00	$-1,13*10^{9}$	$-4,87*10^{8}$	9,60
2,00	50,00	1289	0,03	0,46	0,00	$-1,13*10^{9}$	$-4,87*10^{8}$	9,60
0,00	0,00	1343	0,08	0,35	0,59	$5,56*10^{2}$	$-6,69*10^{8}$	4,80
1,00	0,00	1343	0,08	0,92	0,01	$1,10*10^{3}$	$-6,68*10^{8}$	4,80
2,00	0,00	1343	0,07	0,92	0,01	$2,05*10^{3}$	$-6,68*10^{8}$	4,79
0,00	25,00	1343	0,05	0,26	0,44	$-5,64*10^{8}$	$-5,70*10^{8}$	6,88
1,00	25,00	1343	0,05	0,69	0,00	$-5,64*10^{8}$	$-5,70*10^{8}$	6,87
2,00	25,00	1343	0,05	0,69	0,00	$-5,64*10^{8}$	$-5,70*10^{8}$	6,87
0,00	50,00	1343	0,03	0,17	0,30	$-1,13*10^{9}$	$-4,90*10^{8}$	9,05
1,00	50,00	1343	0,03	0,46	0,00	$-1,13*10^{9}$	$-4,90*10^{8}$	9,05
2,00	50,00	1343	0,03	0,46	0,00	$-1,13*10^{9}$	$-4,90*10^{8}$	9,05

B.2 Results reactor model 2, kinetics 2.

The Table over all the data collected from reactor model 2 are shown in Table B-1. The code used to produce the results is available on github[51]

Table B-2: All data collected from model 1.

Vol inside time [s]	Moist %wt	Temperature [K]	Char %wt	Final Gas %wt	Final Oil %wt	Heat of reaction [J/m³]	Heat Energy [J/m³]	Time to 0,1% Biomass [s]
0.001	0,00	700,00	0,22	0,11	0,67	$3,86*10^{6}$	$-1,48*10^{8}$	1630,69
1.0005	0,00	700,00	0,22	0,14	0,64	$3,98*10^{6}$	$-1,48*10^{8}$	1633,66
2.0	0,00	700,00	0,23	0,16	0,62	$4,09*10^{6}$	$-1,48*10^{8}$	1636,62
0.001	0,15	700,00	0,20	0,09	0,56	$-3,38*10^{8}$	$-1,24*10^{8}$	4355,29
1.0005	0,15	700,00	0,20	0,11	0,54	$-3,38*10^{8}$	$-1,24*10^{8}$	4358,98
2.0	0,15	700,00	0,20	0,13	0,52	$-3,38*10^{8}$	$-1,24*10^{8}$	4362,51
0.001	0,30	700,00	0,16	0,08	0,46	$-6,76*10^{8}$	$-1,04*10^{8}$	6665,25
1.0005	0,30	700,00	0,17	0,09	0,44	$-6,76*10^{8}$	$-1,04*10^{8}$	6669,55
2.0	0,30	700,00	0,17	0,11	0,43	$-6,76*10^{8}$	$-1,04*10^{8}$	6673,97
0.001	0,00	754,00	0,19	0,12	0,69	$3,19*10^{6}$	$-1,57*10^{8}$	1139,55
1.0005	0,00	754,00	0,19	0,21	0,60	$3,59*10^{6}$	$-1,57*10^{8}$	1143,55
2.0	0,00	754,00	0,19	0,29	0,52	$3,94*10^{6}$	$-1,57*10^{8}$	1147,55
0.001	0,15	754,00	0,17	0,10	0,58	$-3,38*10^{8}$	$-1,31*10^{8}$	3015,79
1.0005	0,15	754,00	0,17	0,18	0,50	$-3,38*10^{8}$	$-1,31*10^{8}$	3032,01
2.0	0,15	754,00	0,17	0,24	0,44	$-3,37*10^{8}$	$-1,31*10^{8}$	3046,07
0.001	0,30	754,00	0,14	0,08	0,48	$-6,76*10^{8}$	$-1,09*10^{8}$	4829,08
1.0005	0,30	754,00	0,15	0,14	0,41	$-6,76*10^{8}$	$-1,09*10^{8}$	4849,92
2.0	0,30	754,00	0,15	0,20	0,36	$-6,76*10^{8}$	$-1,09*10^{8}$	4867,75
0.001	0,00	807,00	0,17	0,12	0,71	$2,48*10^{6}$	$-1,62*10^{8}$	912,34
1.0005	0,00	807,00	0,18	0,38	0,45	$3,42*10^{6}$	$-1,62*10^{8}$	922,44
2.0	0,00	807,00	0,18	0,54	0,28	$3,99*10^{6}$	$-1,62*10^{8}$	928,76
0.001	0,15	807,00	0,15	0,10	0,60	$-3,38*10^{8}$	$-1,37*10^{8}$	2210,33
1.0005	0,15	807,00	0,16	0,32	0,38	$-3,38*10^{8}$	$-1,37*10^{8}$	2252,81
2.0	0,15	807,00	0,16	0,45	0,24	$-3,37*10^{8}$	$-1,36*10^{8}$	2279,35
0.001	0,30	807,00	0,13	0,08	0,49	$-6,76*10^{8}$	$-1,12*10^{8}$	3492,06
1.0005	0,30	807,00	0,14	0,26	0,31	$-6,76*10^{8}$	$-1,12*10^{8}$	3551,60
2.0	0,30	807,00	0,14	0,37	0,19	$-6,76*10^{8}$	$-1,12*10^{8}$	3588,67
0.001	0,00	861,00	0,16	0,13	0,72	$1,96*10^{6}$	$-1,66*10^{8}$	768,19
1.0005	0,00	861,00	0,17	0,63	0,20	$3,49*10^{6}$	$-1,66*10^{8}$	785,89
2.0	0,00	861,00	0,18	0,77	0,06	$3,87*10^{6}$	$-1,66*10^{8}$	790,50
0.001	0,15	861,00	0,14	0,11	0,61	$-3,38*10^{8}$	$-1,41*10^{8}$	1821,09
1.0005	0,15	861,00	0,15	0,53	0,17	$-3,38*10^{8}$	$-1,41*10^{8}$	1852,31
2.0	0,15	861,00	0,15	0,65	0,05	$-3,37*10^{8}$	$-1,41*10^{8}$	1860,93
0.001	0,30	861,00	0,12	0,09	0,50	$-6,76*10^{8}$	$-1,16*10^{8}$	2816,88
1.0005	0,30	861,00	0,13	0,43	0,14	$-6,76*10^{8}$	$-1,16*10^{8}$	2857,46
2.0	0,30	861,00	0,13	0,53	0,04	$-6,76*10^{8}$	$-1,15*10^{8}$	2868,65
0.001	0,00	914,00	0,15	0,13	0,72	$1,57*10^{6}$	$-1,70*10^{8}$	667,29
1.0005	0,00	914,00	0,17	0,80	0,03	$3,22*10^{6}$	$-1,69*10^{8}$	688,06

2.0	0,00	914,00	0,17	0,83	0,00	$3,18*10^{6}$	$-1,69*10^{8}$	688,95
0.001	0,15	914,00	0,13	0,11	0,61	$-3,38*10^{8}$	$-1,45*10^{8}$	1569,50
1.0005	0,15	914,00	0,14	0,68	0,03	$-3,38*10^{8}$	$-1,44*10^{8}$	1607,86
2.0	0,15	914,00	0,15	0,70	0,00	$-3,38*10^{8}$	$-1,44*10^{8}$	1609,31
0.001	0,30	914,00	0,11	0,09	0,50	$-6,77*10^{8}$	$-1,19*10^{8}$	2434,08
1.0005	0,30	914,00	0,12	0,56	0,02	$-6,76*10^{8}$	$-1,19*10^{8}$	2485,43
2.0	0,30	914,00	0,12	0,58	0,00	$-6,76*10^{8}$	$-1,19*10^{8}$	2487,46
0.001	0,00	968,00	0,15	0,14	0,72	$1,28*10^{6}$	$-1,73*10^{8}$	591,62
1.0005	0,00	968,00	0,17	0,83	0,00	$2,60*10^{6}$	$-1,72*10^{8}$	611,92
2.0	0,00	968,00	0,17	0,83	0,00	$2,40*10^{6}$	$-1,72*10^{8}$	611,92
0.001	0,15	968,00	0,12	0,12	0,62	$-3,38*10^{8}$	$-1,49*10^{8}$	1378,13
1.0005	0,15	968,00	0,14	0,71	0,00	$-3,38*10^{8}$	$-1,48*10^{8}$	1415,56
2.0	0,15	968,00	0,14	0,71	0,00	$-3,38*10^{8}$	$-1,48*10^{8}$	1415,42
0.001	0,30	968,00	0,10	0,10	0,51	$-6,77*10^{8}$	$-1,22*10^{8}$	2137,02
1.0005	0,30	968,00	0,11	0,59	0,00	$-6,76*10^{8}$	$-1,22*10^{8}$	2187,19
2.0	0,30	968,00	0,11	0,59	0,00	$-6,76*10^{8}$	$-1,22*10^{8}$	2187,09
0.001	0,00	1022,00	0,14	0,14	0,72	$1,04*10^{6}$	$-1,75*10^{8}$	532,94
1.0005	0,00	1022,00	0,16	0,84	0,00	$1,96*10^{6}$	$-1,74*10^{8}$	551,62
2.0	0,00	1022,00	0,16	0,84	0,00	$1,61*10^{6}$	$-1,74*10^{8}$	551,62
0.001	0,15	1022,00	0,11	0,12	0,62	$-3,38*10^{8}$	$-1,52*10^{8}$	1227,78
1.0005	0,15	1022,00	0,13	0,72	0,00	$-3,38*10^{8}$	$-1,51*10^{8}$	1262,48
2.0	0,15	1022,00	0,13	0,72	0,00	$-3,38*10^{8}$	$-1,51*10^{8}$	1262,37
0.001	0,30	1022,00	0,09	0,10	0,51	$-6,77*10^{8}$	$-1,25*10^{8}$	1896,78
1.0005	0,30	1022,00	0,11	0,59	0,00	$-6,77*10^{8}$	$-1,25*10^{8}$	1942,69
2.0	0,30	1022,00	0,11	0,59	0,00	$-6,77*10^{8}$	$-1,25*10^{8}$	1942,49
0.001	0,00	1075,00	0,14	0,15	0,71	$8,45*10^{5}$	$-1,77*10^{8}$	485,87
1.0005	0,00	1075,00	0,16	0,84	0,00	$1,34*10^{6}$	$-1,77*10^{8}$	503,11
2.0	0,00	1075,00	0,16	0,84	0,00	$8,61*10^{5}$	$-1,77*10^{8}$	503,11
0.001	0,15	1075,00	0,11	0,13	0,61	$-3,38*10^{8}$	$-1,55*10^{8}$	1107,46
1.0005	0,15	1075,00	0,13	0,72	0,00	$-3,38*10^{8}$	$-1,54*10^{8}$	1139,55
2.0	0,15	1075,00	0,13	0,72	0,00	$-3,38*10^{8}$	$-1,54*10^{8}$	1139,37
0.001	0,30	1075,00	0,09	0,11	0,50	$-6,77*10^{8}$	$-1,28*10^{8}$	1696,70
1.0005	0,30	1075,00	0,10	0,60	0,00	$-6,77*10^{8}$	$-1,27*10^{8}$	1739,57
2.0	0,30	1075,00	0,10	0,60	0,00	$-6,77*10^{8}$	$-1,27*10^{8}$	1739,33
0.001	0,00	1129,00	0,13	0,17	0,70	$6,94*10^{5}$	$-1,79*10^{8}$	447,17
1.0005	0,00	1129,00	0,15	0,85	0,00	$7,40*10^{5}$	$-1,79*10^{8}$	463,16
2.0	0,00	1129,00	0,15	0,85	0,00	$6,95*10^{5}$	$-1,79*10^{8}$	463,16
0.001	0,15	1129,00	0,11	0,14	0,60	$-3,38*10^{8}$	$-1,57*10^{8}$	1009,62
1.0005	0,15	1129,00	0,12	0,73	0,00	$-3,38*10^{8}$	$-1,56*10^{8}$	1039,27
2.0	0,15	1129,00	0,12	0,73	0,00	$-3,38*10^{8}$	$-1,56*10^{8}$	1039,12
0.001	0,30	1129,00	0,09	0,12	0,50	$-6,77*10^{8}$	$-1,30*10^{8}$	1535,85
1.0005	0,30	1129,00	0,10	0,60	0,00	$-6,77*10^{8}$	$-1,30*10^{8}$	1575,52
2.0	0,30	1129,00	0,10	0,60	0,00	$-6,77*10^{8}$	$-1,30*10^{8}$	1575,30
0.001	0,00	1182,00	0,13	0,19	0,68	$5,71*10^{5}$	$-1,81*10^{8}$	414,90
1.0005	0,00	1182,00	0,15	0,85	0,00	$5,54*10^{5}$	$-1,81*10^{8}$	429,59
2.0	0,00	1182,00	0,15	0,85	0,00	$5,52*10^{5}$	$-1,81*10^{8}$	429,48

0.001	0,15	1182,00	0,10	0,16	0,59	$-3,38*10^{8}$	$-1,59*10^{8}$	929,05
1.0005	0,15	1182,00	0,12	0,73	0,00	$-3,38*10^{8}$	$-1,59*10^{8}$	956,37
2.0	0,15	1182,00	0,12	0,73	0,00	$-3,38*10^{8}$	$-1,59*10^{8}$	956,19
0.001	0,30	1182,00	0,08	0,14	0,48	$-6,77*10^{8}$	$-1,32*10^{8}$	1407,08
1.0005	0,30	1182,00	0,10	0,60	0,00	$-6,77*10^{8}$	$-1,32*10^{8}$	1443,84
2.0	0,30	1182,00	0,10	0,60	0,00	$-6,77*10^{8}$	$-1,32*10^{8}$	1443,64
0.001	0,00	1236,00	0,13	0,22	0,65	$4,72*10^{5}$	$-1,83*10^{8}$	387,43
1.0005	0,00	1236,00	0,15	0,85	0,00	$4,30*10^{5}$	$-1,83*10^{8}$	400,75
2.0	0,00	1236,00	0,15	0,85	0,00	$4,32*10^{5}$	$-1,83*10^{8}$	400,66
0.001	0,15	1236,00	0,10	0,19	0,56	$-3,38*10^{8}$	$-1,61*10^{8}$	861,99
1.0005	0,15	1236,00	0,12	0,73	0,00	$-3,38*10^{8}$	$-1,61*10^{8}$	886,84
2.0	0,15	1236,00	0,12	0,73	0,00	$-3,38*10^{8}$	$-1,61*10^{8}$	886,60
0.001	0,30	1236,00	0,08	0,16	0,46	$-6,77*10^{8}$	$-1,34*10^{8}$	1300,75
1.0005	0,30	1236,00	0,09	0,61	0,00	$-6,77*10^{8}$	$-1,34*10^{8}$	1334,70
2.0	0,30	1236,00	0,09	0,61	0,00	$-6,77*10^{8}$	$-1,34*10^{8}$	1334,50
0.001	0,00	1289,00	0,13	0,26	0,61	$3,92*10^{5}$	$-1,85*10^{8}$	364,06
1.0005	0,00	1289,00	0,15	0,86	0,00	$3,35*10^{5}$	$-1,85*10^{8}$	375,86
2.0	0,00	1289,00	0,15	0,86	0,00	$3,34*10^{5}$	$-1,84*10^{8}$	375,72
0.001	0,15	1289,00	0,10	0,23	0,52	$-3,38*10^{8}$	$-1,63*10^{8}$	805,37
1.0005	0,15	1289,00	0,11	0,74	0,00	$-3,38*10^{8}$	$-1,63*10^{8}$	827,62
2.0	0,15	1289,00	0,11	0,74	0,00	$-3,38*10^{8}$	$-1,63*10^{8}$	827,35
0.001	0,30	1289,00	0,08	0,19	0,43	$-6,77*10^{8}$	$-1,36*10^{8}$	1210,06
1.0005	0,30	1289,00	0,09	0,61	0,00	$-6,77*10^{8}$	$-1,36*10^{8}$	1241,35
2.0	0,30	1289,00	0,09	0,61	0,00	$-6,77*10^{8}$	$-1,36*10^{8}$	1241,05
0.001	0,00	1343,00	0,13	0,32	0,56	$3,26*10^{5}$	$-1,86*10^{8}$	343,79
1.0005	0,00	1343,00	0,14	0,86	0,00	$2,54*10^{5}$	$-1,86*10^{8}$	354,02
2.0	0,00	1343,00	0,14	0,86	0,00	$2,55*10^{5}$	$-1,86*10^{8}$	353,91
0.001	0,15	1343,00	0,10	0,28	0,48	$-3,38*10^{8}$	$-1,65*10^{8}$	757,00
1.0005	0,15	1343,00	0,11	0,74	0,00	$-3,38*10^{8}$	$-1,64*10^{8}$	776,41
2.0	0,15	1343,00	0,11	0,74	0,00	$-3,38*10^{8}$	$-1,64*10^{8}$	776,12
0.001	0,30	1343,00	0,08	0,23	0,39	$-6,77*10^{8}$	$-1,38*10^{8}$	1131,26
1.0005	0,30	1343,00	0,09	0,61	0,00	$-6,77*10^{8}$	$-1,37*10^{8}$	1159,39
2.0	0,30	1343,00	0,09	0,61	0,00	$-6,77*10^{8}$	$-1,37*10^{8}$	1159,02

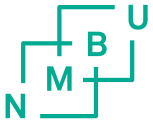

Norges miljø- og biovitenskapelige universitet
Noregs miljø- og biovitskapelege universitet
Norwegian University of Life Sciences

Postboks 5003
NO-1432 Ås
Norway